ISSN 1580-2949
UDK 669+666+678+53 MTAEC9, 41(5)197–253(2007)

MATER. TEHNOL.	LETNIK VOLUME 41	ŠTEV. NO. 5	STR. P. 197–253	LJUBLJANA SLOVENIJA	SEP.-OKT. 2007

VSEBINA – CONTENTS

ŠESTDESET LET PROF. DR. VASILIJA PREŠERNA

LAUDATION IN HONOUR OF PROFESSOR DR. VASILIJ PREŠERN ON THE OCCASION OF HIS 60th BIRTHDAY

Rodil se je 4. julija 1947 v Mariboru. Osnovno šolo in prvi letnik gimnazije je obiskoval na Jesenicah. Po preselitvi v Ljubljano je leta 1966 z odliko maturiral na Gimnaziji Vič v Ljubljani. Vpisal je študij metalurgije na Univerzi v Ljubljani, kjer je leta 1971 kot prvi iz letnika tudi diplomiral. Naziv magistra znanosti je pridobil leta 1974, naziv doktorja metalurških znanosti pa že leta 1978. Leta 1992 je bil habilitiran za izrednega profesorja.

Po diplomi se je zaposlil na Metalurškem inštitutu v Ljubljani (danes IMT – Inštitut za kovinske materiale in tehnologije), kjer je ostal do leta 1991.

Na inštitutu se je ukvarjal z raziskavami termodinamike procesov rafinacije z dodatkom kalcija v z aluminijem pomirjenem tekočem jeklu in s formiranjem nekovinskih vključkov, z raziskavo reakcije kalcija v sistemu talina-vključki-žlindra. Področje raziskav je že takrat zahtevalo tesno sodelovanje s slovensko oziroma jugoslovansko kot tudi z avstrijsko jeklarsko industrijo. Študij termodinamičnih reakcij v talini pri dodajanju Ca je bilo izredno pomembno tako z raziskovalnega vidika kot tudi s proizvodnega, zato so ga povabili k sodelovanju strokovnjaki z National Standardization and Technology – NIST, Gaithersburg, ZDA. V večletnem bilateralnem projektu YU-USA je bil pojasnjen vpliv CaO in Al_2O_3 v talini, dobljeni rezultati pa so bistveno

Professor Dr. Vasilij Prešern, scientific councillor and former general director of the Acroni steelworks, is celebrating his 60th birthday. This provides us with an excellent opportunity to look at the background and the development of this well-known scientist – and even more successful economist – and his influence on research and economics in the field of steelmaking in Slovenia and abroad.

Vasilij Prešern was born in Maribor, on the 4th of July 1947. After completing his secondary-school education in Ljubljana with a distinction, he studied metallurgy at the University of Ljubljana and finished in 1971, as the first in his class. He joined the Metallurgical Institute, now the Institute of Metals and Technology (IMT), Ljubljana, where he worked until 1991. In 1974 he finished his master's degree. He then went on to his doctoral thesis and graduated in 1978 at the University of Ljubljana. In 1992 he was habilitated at the university as a professor.

In 1981 he received a six-month scholarship from the Confederation of British Industry (CIB) to develop subsidiary steelmaking agents for molten steel treatment at Foseco in Birmingham, UK.

Vasilij Prešern is an enthusiastic developer, with creative ideas and tremendous energy. During his time at IMT he worked on the thermodynamic conditions for the modification of inclusions in calcium-treated aluminium-killed molten steel. The topic of his research was very innovative and he was invited to take part in a

pripomogli k proizvodnji jekla z manjšo vsebnostjo žvepla in nekovinskih vključkov.

V želji, da bi svoje bogato teoretično znanje in poznanje svetovne metalurgije čim bolj povezal s prakso, se je leta 1991 zaposlil v takratnem Holdingu Slovenske železarne (danes SIJ – Slovenska industrija jekla).

Leta 1998 je sprejel zelo zahtevno nalogo sanacije največje slovenske jeklarske družbe Acroni. Kot glavni direktor Acronija je bil postavljen pred zahteven izziv sestaviti skupino ključnih sodelavcev, ki bo sposobna prenoviti in usposobiti podjetje za konkurenčni boj na zahtevnih svetovnih trgih.

Z dobrim poznanjem svetovnega jeklarskega trga in konkurence ter s svojo širino in pozitivnim načinom je Prešernu uspelo prepričati lastnika, da je jeklarstvo panoga, ki ima dolgoročno prihodnost tudi v Sloveniji in ji je vredno zagotoviti vso podporo za uspešno sanacijo in tudi nadaljnji razvoj Acronija. Tako so z večletnim investiranjem v spremembo in optimizacijo proizvodnih poti, v odpravljanje ozkih grl in v naprave, ki omogočajo večjo proizvodnjo izdelkov z visoko dodano vrednostjo, uspeli sanirati Acroni, in leto 2005 je bilo v vseh pogledih najuspešnejše, saj je postal največji proizvajalec specialnega jekla v Sloveniji z dodano vrednostjo več kot 38 000 EUR na zaposlenega.

Za uspešno saniranje Acronija je bil prof. dr. Prešern prejemnik nagrade GZS za leto 2006. V utemeljitvi so navedli:

"ACRONI je družba z eno največjih hitrosti v rasti dodane vrednosti na zaposlenega in hitre rasti produktivnosti! Ima močno izraženo razvojno komponento, dolgoročno in moderno, atraktivno strategijo, rekordno izpolnjevanje tržnih, razvojnih, R&D in splošnih meril za nagrado GZS ter tudi meril internacionalizacije. Velja podobno kot za Krko: model nagrad GZS najbolj ustreza prav takšnim družbam.

Zelo dobri poslovno-finančni rezultati, tudi če se jih zaradi razmeroma velikega tržnega deleža in majhnega števila primerljivih konkurentov primerja na osnovi celotne panoge 27 – Proizvodnja kovin.

Predsednik uprave prof. dr.Vasilj Prešern je opravljal funkcijo od leta 1998 do 2007 in je mednarodno priznan strokovnjak na svojem področju ter optimističen, nadvse uspešen gospodarstvenik.

Ves čas je prof. dr. Vasilij Prešern skrbel tudi za prenos znanja, saj je sodelovanje med Inštitutom za kovinske materiale in tehnologije vzor za sodelovanje med akademsko sfero in industrijo. Mladi raziskovalci so se usposabljali od pol do 1 leta v Acroniju in delali skupaj s strokovnjaki iz prakse ter si tako pridobili izredne izkušnje, in stkale so se prijateljske vezi, ki zagotavljajo dolgotrajno sodelovanje.

Po prodaji večinskega deleža SIJ je prof. Vasilij Prešern prepustil mesto glavnega direktorja mlajšim

Yugoslav-USA bilateral project, where he worked together with world-recognized experts from the National Institute of Standards and Technology in Gaithersburg, USA. He investigated the thermodynamic relations between calcium-treated aluminium-killed molten steel and non-metallic inclusions and demonstrated the importance of having the right Ca content. The results of this research were also very important for the steelmaking industry. The influence of CaO and Al_2O_3 in molten steel was explained during the course of the bilateral project, and the results were very helpful for the production of cleaner steels containing smaller amounts of sulphur and non-metallic inclusions.

During his time at IMT he published more than 50 papers in leading scientific journals and had more than 50 invited lectures at the most important international conferences. He has also been involved in more than 250 projects with industry.

Because of his wish to combine his deep theoretical expertise and his knowledge of world metallurgy with industrial work, in 1991 he joined the then Holding of Slovenian Steelworks (presently, the SIJ, the Slovenian Steelwork Industry)

In 1998 he accepted the very difficult task of reorganizing the biggest Slovenian steelworks company, Acroni. As the general manager he faced a great challenge: to form a highly qualified group of leading co-workers, qualified to modernize and reposition the company to be competitive on the global market.

His expertise in the global steelmaking market and competition and his positive approach enabled him to persuade the owners that the steelmaking branch had great promise – also in Slovenia – and was worth supporting during the successful reorganization and further development of Acroni.

The investments over several years led to the modification and optimisation of the production lines and equipment; this enabled increased production levels with a higher added value and made possible the successful reorganization of Acroni. The year 2005 was, in all respects, the most successful year for Acroni, which produced special steels in Slovenia with an added value of € 38,000/employee.

In 2006 Vasilij Prešern was the winner of an award from the Chamber of the Economy of the Republic of Slovenia (GZS-gospodarska zbornica RS) for his successful reorganization of Acroni. At the awards ceremony Acroni was recognised as a company with a rapid growth in added value per employee and increasing production levels. The company was described as having a strong development component, long-range and advanced strategies, a record of satisfying the market, and good R&D standards.

Vasilij Prešern took great care of the knowledge transfer and cooperation involving on of Slovenia's leading research institutes, IMT, representing an ideal model of cooperation between the academic sphere and industry in Slovenia. IMT's young researchers were able to work together with Acroni's experts for six months to one year at the Acroni plant, where they gained

sodelavcem, ki jih je vzgojil in ki jim zaupa, da bodo tako zagnani in uspešni, kot je bil sam.

Prof. dr. Vasilij se privaja na novo odgovornost v okviru SIJ kot direktor za investicije in razvoj celotnega SIJ-a. Tako mu ostaja čas, ki ga je vsak dan porabil za vožnjo na Jesenice, da ga preživlja s svojo vnukinjo Julijo.

Vendar pa še vedno najde čas za stroko, saj v okviru Mednarodne podiplomske šole Jožefa Stefana prenaša svoje bogate izkušnje na mlade podiplomce.

Dragi kolega in prijatelj Vasilij! Ob 60-letnici ti iskreno čestitamo za vse dosežke in ti želimo tudi v prihodnje veliko uspehov, sreče, predvsem pa osebnega zadovoljstva v krogu svoje družine in prijateljev.

invaluable experience. Friendly links were formed and these links have ensured the long-lasting cooperation between these two partners

After a takeover of the majority share of the Slovenian Steel Industry, Vasilij Prešern left his position as Acroni's general manager to younger co-workers, who he brought up in previous years and who he has trusted to be even more successful than he was.

Professor Vasilij Prešern is getting accustomed to his new position in the SIJ – as the director responsible for investments and the development of the whole SIJ. This means he now has the time, which he previously used for a daily commute to Jesenice, to spend with his grand-daughter Julija.

Dear colleague and friend, Vasilij, on the occasion of this 60th anniversary we congratulate you on your excellent results and we wish you and your family many years of successes and happiness in good health.

Monika Jenko

UDK 669.18:669.14.018.8
Reviewed scientific article/Pregledni znanstveni članek

ISSN 1580-2949
MTAEC9, 41(5)203(2007)

THE OXIDATION AND REDUCTION OF CHROMIUM DURING THE ELABORATION OF STAINLESS STEELS IN AN ELECTRIC ARC FURNACE

OKSIDACIJA IN REDUKCIJA KROMA IZ ŽLINDRE MED IZDELAVO NERJAVNIH JEKEL V ELEKTROOBLOČNI PEČI

Boštjan Arh, Franc Tehovnik

Institute of Metals and Technology, Lepi pot 11, 1000 Ljubljana, Slovenia
bostjan.arh@imt.si

Prejem rokopisa – received: 2007-07-13; sprejem za objavo – accepted for publication: 2007-08-30

The oxidation of chromium during the elaboration of stainless steels occurs with oxygen in solution blown in the melt and with oxides in the slag. The loss of chromium during the steel bath processing increases the production costs and generates problems because of the high content of chromium oxide in the slag. A higher content of silicon in the furnace charge decreases the extent of the oxidation of chromium; however, the efficient reduction of chromium from the slag is very important for a minimal loss of chromium. In this survey, the theory of the oxidation of chromium, its reduction from the slag and the conditions for the formation of foaming slag are discussed.

Key words: electric arc furnace, chromium oxidation, foaming slag, slag reduction, stainless steel

Oksidacija kroma med izdelavo nerjavnih jekel poteka zaradi topnega kisika v talini, vpihanega kisika in zaradi oksidov v žlindri. Izguba kroma med izdelavo nerjavnega jekla v EOP nima za posledico samo višji materialni strošek, ampak tudi določene operativne posege zaradi prekomerne količine kromovega oksida v žlindri. Večja vsebnost silicija v založenem legiranem vložku zadrži oksidacijo kroma med njegovim taljenjem, vendar je le učinkovita redukcija žlindre po oksidaciji taline ključnega pomena za minimalno izgubo kroma. V prispevku bomo predstavili predvsem teoretične osnove oksidacije kroma, redukcijo kroma iz žlindre in pogoje za tvorbo peneče se žlindre pri izdelavi nerjavnih jekel v elektrooblučni peči.

Ključne besede: elektrooblučna peč, oksidacija kroma, peneča se žlindra, redukcija žlindre, nerjavna jekla

1 INTRODUCTION

The content of chromium in austenite stainless steels is generally in the range from 16 % to 24 %. More than 97 % of the chromium is lost during the melting of steels from scrap in an electric arc furnace (EAF). The oxidation of chromium occurs during the melting, and to an even greater extent it occurs during the blowing in of oxygen, aimed at decreasing the content of carbon in the bath. A smaller part of chromium is also oxidised while discharging the melt from the EAF. A high content of chromium increases the crusting of the slag, decreases its reactivity and impairs the formation of the foaming slag and the slag reduction during the process of steel elaboration. Stainless slags with a high content of chromium oxide cannot be recycled or used, and are for this reason also an ecological problem.

2 OXIDATION OF CHROMIUM IN THE MELT

The oxidation of chromium with oxygen in solution in the melt occurs in parallel with the oxidation of other elements, e.g., carbon, aluminium, silicon and manganese, and it depends on the temperature and the activity of these elements and the oxygen. The standard free energy of oxidation ($\Delta G°$) for these elements is given by the following relations[1]:

$$3[Cr] + 4[O] = (Cr_3O_4) \quad \Delta G° = -244.800 + 109.6\,T \quad (1)$$

$$[C] + [O] = CO_{(g)} \quad \Delta G° = -5.600 - 9.37\,T \quad (2)$$

$$[Si] + 2[O] = (SiO_2) \quad \Delta G° = -139.070 + 53.09\,T \quad (3)$$

$$2[Al] + 3[O] = (Al_2O_3) \quad \Delta G° = -286.900 + 89.05\,T \quad (4)$$

$$[Mn] + [O] = (MnO) \quad \Delta G° = -57.530 + 24.73\,T \quad (5)$$

The equilibrium constant is deduced for every one of these reactions from the change in the standard free energy, and it is written for the oxidation of chromium as:

$$\lg K_1 = \frac{53521}{T} - 23.96 \quad (6)$$

and

$$K_1 = \frac{a_{Cr3O4}}{a_{Cr}^3 \cdot a_O^4} = \frac{a_{Cr3O4}}{f_{Cr}^3 \cdot f_O^4 \cdot w_{Cr}^3 \cdot w_O^4} \quad (7)$$

with a_{Cr2O3}, a_{Cr}, a_O being the activity of (Cr_2O_3), [Cr], [O]; f_{Cr}, f_O being the activity coefficient for Cr and O, and w_{Cr}/%, w_o/% being the mass fractions of Cr and O in the steel melt.

The equation giving the content of oxygen in solution in the steel bath of known composition (T304L) as a function of the temperature and the activity of chromium oxide is:

$$w_o/\% = \left[\frac{a_{Cr3O4}}{K_1 \cdot f_{Cr}^3 \cdot f_O^4 \cdot w_{Cr}^3} \right]^{1/4} \quad (8)$$

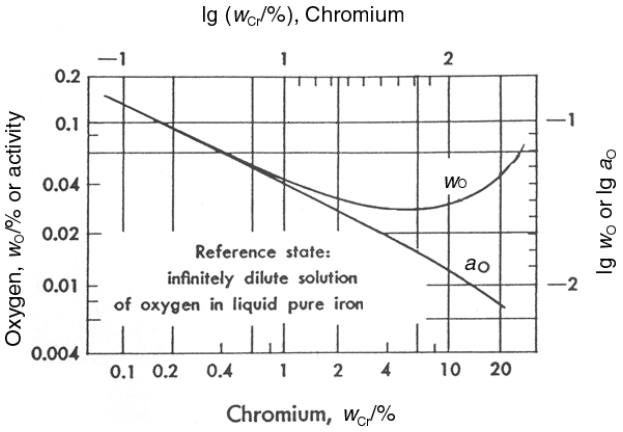

Figure 1: Effect of chromium on the activity and the content of oxygen in the system Fe-Cr at 1873 K [2]

Slika 1: Vpliv kroma na aktivnost in vsebnost kisika v sistemu Fe-Cr pri 1873 K [2]

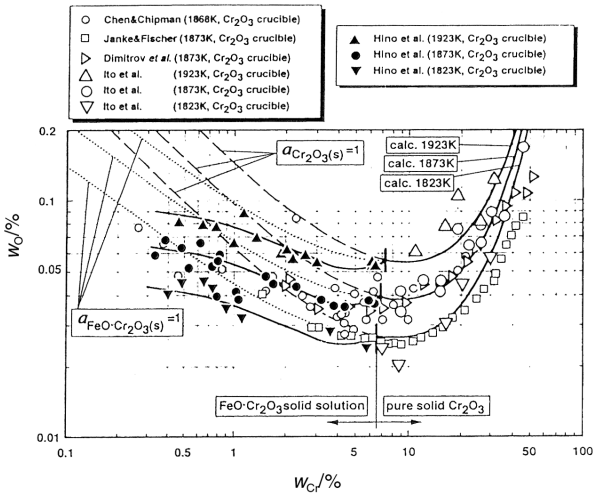

Figure 2: Equilibrium between chromium and oxygen in the steel melt saturated with pure solid Cr_2O_3 and $FeO\cdot Cr_2O_3$ [4]

Slika 2: Ravnotežje med kromom in kisikom v tekočem železu, nasičenem s čistim trdnim Cr_2O_3 in $FeO\cdot Cr_2O_3$ [4]

For a high content of chromium in the melt the activity of the oxygen and of the carbon is lower, as both interaction coefficients are negative. The effect of chromium on the content and the activity of the oxygen in the melt at 1600 °C is shown in **Figure 1**[2].

The dependences were calculated using an equation valid for a content of 9 % chromium and more in the steel bath (eq. 9)[2,3]. It is evident that for a high content of chromium the solubility of oxygen in the melt is greater (**Figure 1**). For this reason, and with an equal content of carbon, the content of oxygen is higher in the bath with chromium than in the bath without this element.

$$\lg[w_{Cr}^{3/4} \cdot (f_O \cdot w_O)] = -13380/T + 5{,}99 \qquad (9)$$

Chromium is a relatively strong deoxidiser. With a higher content of chromium, the oxidation products consist of iron-chromium spinels of the type $FeO\cdot Cr_2O_3$. The transition from spinel to the saturation with Cr_2O_3 in the system Fe–O–Cr occurs when the critical content of chromium is exceeded[4].

$$Fe(s) + \tfrac{1}{2}\, O_2\,(g) + Cr_2O_3(s) = \\ = FeO\cdot Cr_2O_3(s)\ \Delta G^\circ = -307.600 + 66.82\ T \qquad (10)$$

In **Figure 2** the equilibrium between $FeO.Cr_2O_3$ and oxygen is shown for both a low and a high content of chromium in the bath. The critical content of chromium is shown for different temperatures when the equilibrium oxide phase changes from $FeO\cdot Cr_2O_3$ to Cr_2O_3. The phase $FeO\cdot Cr_2O_3$ in equilibrium with the Fe–Cr melt is changed to Cr_2O_3 when the actual content of chromium in the bath increases above the critical content. Pure Cr_2O_3 is the phase in equilibrium with the Fe–Cr bath for more than 7 % Cr in the bath.

The activity of Cr_2O_3 and of $FeO\cdot Cr_2O_3$ in the $FeO\cdot Cr_2O_3$ solid solution in equilibrium with the Fe–Cr melt decreases when decreasing the content of chromium below the $w_{Cr\ critical}$.

In addition to the thermodynamic activity of different elements in the melt, the connection temperature-activity of chromium oxide in the slag is of great importance, since this effect is significantly greater at lower temperatures. The activity of Cr_2O_3 depends on the alkalinity of the slag and on the content of CaO and SiO_2. The dependence of the free enthalpy of oxidation of chromium, silicon and carbon on the temperature shows that, according to the affinity for oxygen in solution, silicon lies between carbon and chromium and, for this reason, it is oxidised first and its oxidation delays the oxidation of chromium.

The deoxidation of the Fe-Cr melt with silicon is shown in **Figure 3**[5] as the equilibrium of the contents of chromium and oxygen in the bath at 1600 °C in dependence of the silicon content. The initial content of oxygen in the Fe-Cr melt before the addition of silicon is shown by the upper dashed line, which represents the equilibrium Fe-Cr/Cr_2O_3 or Fe-Cr/$FeO\cdot Cr_2O_3$ for the content of w_{Si}/% = 0. The addition of silicon lowers the content of oxygen by a constant amount of chromium.

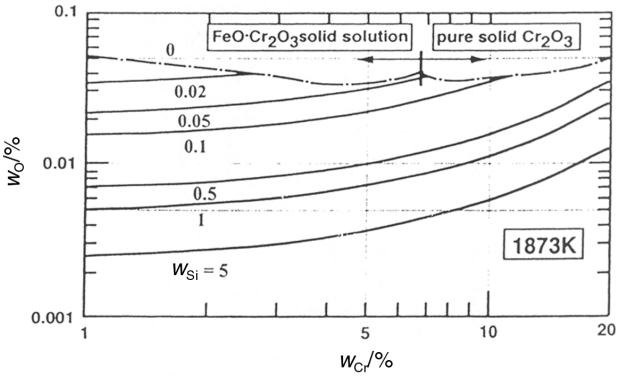

Figure 3: Equilibrium between the contents of chromium and oxygen in the steel bath at 1873 K for different contents of silicon[5]

Slika 3: Ravnotežje med vsebnostjo kroma in kisika v tekočem železu v odvisnosti od vsebnosti silicija pri 1873 K [5]

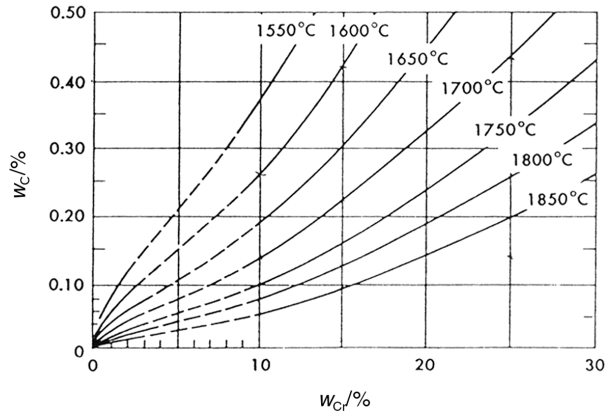

Figure 4: Thermodynamic equilibrium between carbon and chromium for different temperatures and a pressure of p_{co} = 1 bar [2]

Slika 4: Termodinamično ravnotežje med ogljikom in kromom v odvisnosti od temperature pri tlaku p_{co} = 1 bar [2]

The deoxidation power of silicon is lower with a higher content of chromium, e.g., by the addition of 1 % of silicon, the content of oxygen in the Fe + 5 % Cr bath is lowered from 350 μg/g to approximately 73 μg/g and for Fe + 18 % Cr it is lowered from 450 μg/g to 110 μg/g. For this reason, a low content of oxygen cannot be achieved with the addition of silicon alone. The oxidation-reduction equation for silicon and chromium is:

$$2Cr_2O_3 + 3[Si] = 4[Cr] + 3SiO_2 \quad (11)$$

The thermodynamics indicates that the content of silicon in the melt is proportional to the activity of SiO_2 in the slag; thus, the content of silicon in the melt is higher with a higher content of SiO_2 in the slag. The thermodynamics of the relations content of Cr_2O_3 in the slag, the content of chromium and silicon in the melt, the melt temperature and the activity of SiO_2 in the slag were investigated by McCoy and Langerberg[6]. The results of these investigations show that the loss of chromium is higher with a low content of silicon in the melt and with a higher bath temperature[6].

Furthermore, carbon, with an over critical content, delays the oxidation of chromium[2]. The equilibrium between chromium and carbon was, for the pressure of p_{co} = 1 bar and the different temperatures in **Figure 4**, determined by applying the following relations and considering the coefficient of interaction of the first order:

$$Cr_2O_3 + 4C = 3Cr + 4\,CO \quad (12)$$

$$\lg[(Cr)^{3/4} \cdot p_{CO}/a_C] = -11520/T + 7.64 \quad (13)$$

2.1 Stainless slags

The behaviour of chromium oxides (CrO_x) in metallurgical slags is complex because of the existence of ions with several valences and of the high melting temperature of the slags containing chromium[7]. In slags the non-stoichiometric quantity of CrO_x depends on the temperature, on the slag's alkalinity and on the content of chromium oxides in equilibrium with the metallic chromium. For the mixture of Cr_2O_3 with the other components of the slag in contact with metallic chromium at high temperature, the equilibrium of the oxides is:

$$2CrO_{1,5} + Cr = 3CrO \quad (14)$$

Chromium is found in the slag as two- and three-valence ions. The activity of CrO and $CrO_{1.5}$ increases with the increase of the total content of CrO_x and the basicity. In **Figure 5** the activity of CrO and $CrO_{1.5}$ in the system $CaO–SiO_2–CrO_x$ at 1873 K is shown. At higher temperature, the activity is lower and the content of the bivalent chromium in the slag is increased. In contrast, with increased basicity the activity of chromium oxides is increased and the content of bivalent chromium in the slag is diminished (**Figure 6**). A greater activity of chromium oxides in the slag is found with greater alkalinity, a higher ratio of CaO/MgO and a lower temperature. The lower content of MgO in the slag increases the activity of the chromium oxides in the slag up to a limit; however, it does not affect the oxidation state and, as a result, the content of Cr^{2+} and Cr^{3+}. Small additions of Al_2O_3 affect the activity of CrO_x, while larger amounts have little effect. Slag with greater

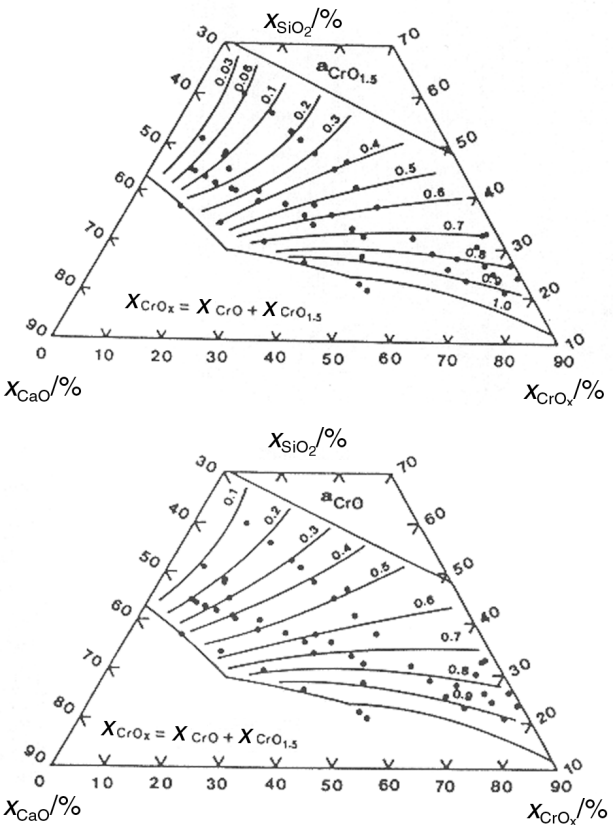

Figure 5: Iso-activity diagrams for $CrO_{1.5}$ and CrO in the $CaO-SiO_2-CrO_x$ quasi-ternary system at 1873 K [7]

Slika 5: Izoaktivnostni diagram molskih deležev (x/%) $CrO_{1,5}$ in CrO v $CaO-SiO_2-CrO_x$ v kvasiternarnem sistemu pri temperaturi 1873 K [7]

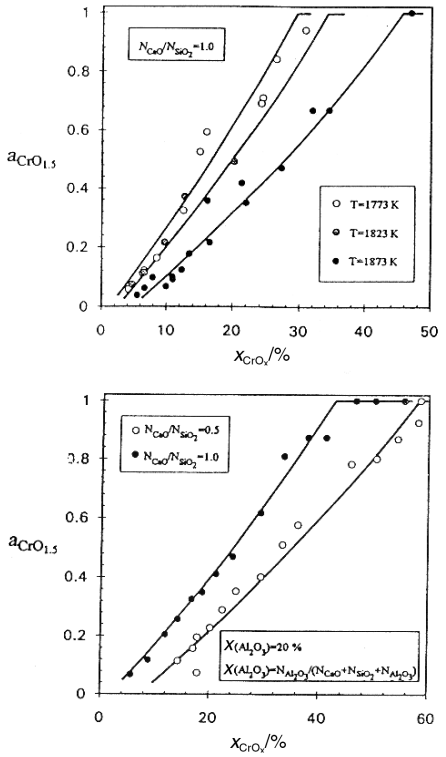

Figure 6: Effect of temperature on the activity of $CrO_{1.5}$ in the system $CaO-SiO_2-CrO_x$ and the effect of slag basicity on the activity of $CrO_{1.5}$ in the system $CaO-SiO_2-Al_2O_3-CrO_x$ at 1873 K [7]

Slika 6: Vpliv temperature na aktivnost $CrO_{1,5}$ v sistemu $CaO-SiO_2-CrO_x$ in vpliv bazičnosti žlindre na aktivnost $CrO_{1,5}$ v sistemu $CaO-SiO_2-Al_2O_3-CrO_x$ pri temperaturi 1873 K [7]

activity improves the reduction of chromium from the slag and increases the yield of chromium during the elaboration of stainless steels.

The stainless slag in the EAF consists mostly of CaO, MgO, Al_2O_3 and SiO_2[8]. The optimal composition in the system, $CaO–MgO–SiO_2$, shown in **Figure 7**, is the saturation with CaO and MgO[9], which is the necessary condition for a minimal content of Cr_2O_3 in the liquid slag and it is acceptable for the resistance of the refractory lining, also. The solubility of CrO_x in these slags is small. During the blowing of oxygen in the bath, the elements are oxidised according to their affinity to oxygen and their activity in the melt. Al and Si have a greater affinity for oxygen; however, chromium is also oxidised due to its greater activity. If CrO_x is absorbed in the molten slag, the equilibrium conditions change after the blowing of oxygen and the chromium is returned in the bath on the condition that there is a sufficient content of silicon. In the presence of chromium in the solid phase ($MgCrO_4$, $CaCrO_4$), the slag is rigid and the return of chromium in the bath is lower, also in the case of a higher content of silicon in the bath.

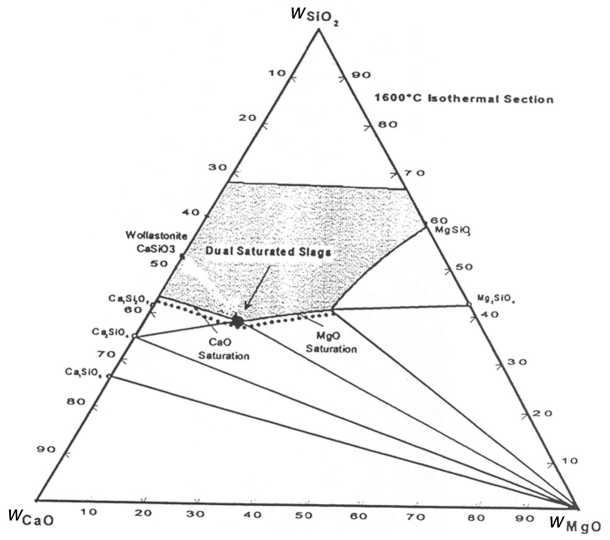

Figure 7: Isothermal section of the system $CaO-MgO-SiO_2$ at 1600 °C [9]

Slika 7: Izotermični prerez sistema $CaO-MgO-SiO_2$ pri 1600 °C [9]

3 REDUCTION OF CHROMIUM FROM THE SLAG

Several procedures were developed for the reduction of chromium from the slag during the elaboration of the steel in the furnace and during the discharge in the ladle using silicon and aluminium. It is, however, very important that the loss of chromium is minimised during the oxidation melting and blowing of different reductants. In **Figure 8 and 9** the equilibrium curves are shown for the oxidation of chromium with respect to the reactivity of silicon, carbon, aluminium and manganese

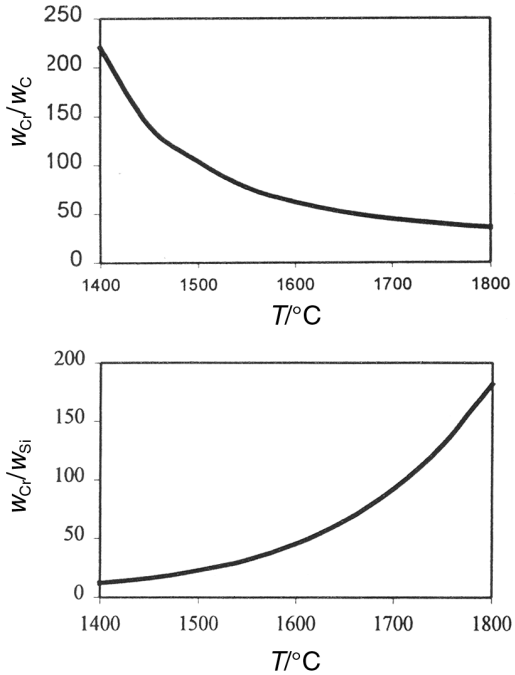

Figure 8: Effect of temperature on the ratio w_{Cr}/w_{Si} and w_{Cr}/w_C in the steel bath with 18 % Cr [10]

Slika 8: Vpliv temperature na razmerji masnih deležev w_{Cr}/w_{Si} in w_{Cr}/w_C v talinah jekel z 18 % Cr [10]

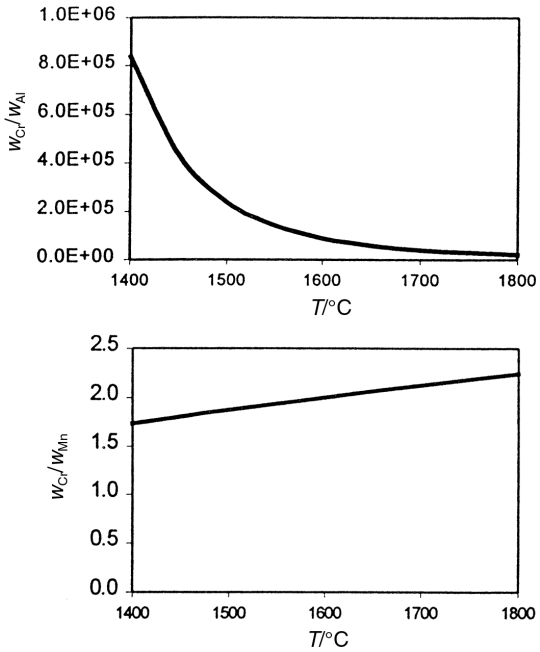

Figure 9: Effect of temperature on the ratio w_{Cr}/w_{Al} and w_{Cr}/w_{Mn} in the steel melt with 18 % Cr [10]
Slika 9: Vpliv temperature na razmerji masnih deležev w_{Cr}/w_{Al} in w_{Cr}/w_{Mn} v talinah jekel z 18 % Cr [10]

at the temperature of the elaboration of the steel T304L[10].

The thermodynamics of the relation w_{Cr}/w_{Si} in the melt with 18 % Cr shows that with a temperature of approximately 1500 °C the oxidation of silicon starts at 0.2 % Si and at 1700 °C at 0.4 % Si. Thus, at 1500 °C a content of 0.2 % Si in the melt already arrests the oxidation of chromium, while at higher temperatures a greater content of silicon is required. The ratio of w_{Cr}/w_C for 18 % Cr in the melt shows that the reactivity of the chromium increases with the temperature. For this reason, at higher temperatures a lower equilibrium content of carbon impairs the oxidation of chromium. **Figure 9** shows that the affinity of aluminium for oxygen is very high and that its activity decreases with increasing temperature. The activity of manganese is not affected by the temperature and in stainless steels with 2 % Mn the behaviour of manganese is different from that of chromium, carbon, aluminium and silicon.

Silicon impairs the oxidation of chromium at low temperatures, thus, during the melting of the charge, while carbon is efficient in this role and with sufficient concentration, at higher temperatures. The blowing in of the oxygen at high temperature (>1550 °C) increases the oxidation of carbon and strongly decreases the oxidation of chromium.

The slag basicity ((CaO+MgO)/(SiO_2+Al_2O_3)) has a strong effect on the reduction of chromium oxides, and with a higher basicity the content of chromium oxide in the slag is lower. The activity of SiO_2 and Al_2O_3 is also

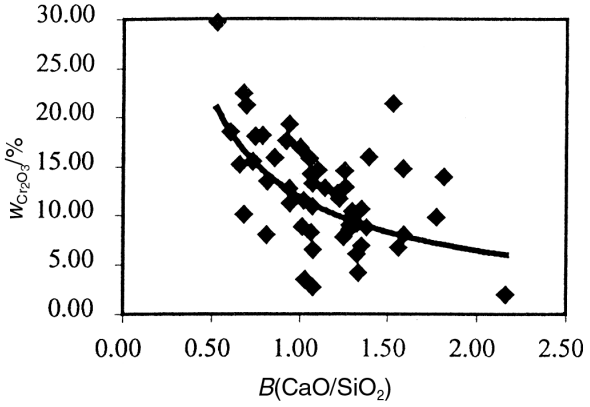

Figure 10: Effect of slag basicity on the content of Cr_2O_3 in the slag[11]
Slika 10: Učinek bazičnosti žlindre na vsebnost Cr_2O_3 v žlindri[11]

lower, while the activity of CrO_x is higher. All these levels of activity increase the rate of reduction of chromium oxide from the slag (**Figure 10**)[11]. According to this figure, the basicity should be approximately at the level of B = 1.8.

The efficient reduction of the furnace slag depends on the selection of a suitable reductant, dependent on the used procedure and the control of the furnace slag, which should ensure a high level of reduction of chromium oxide from the slag and should not contaminate the melt. The selection of the reductant depends on the furnace and the raffination practice.

However, of special importance is the decrease of the chromium losses during the oxidative melting with the blowing in of the different reductants. The first measure for the control of the content of Cr_2O_3 is the use of a charge and alloys (FeSi) with a high content of silicon, ensuring a content of 0.3 % Si after the melting of the charge. During the discharge, the reduction of chromium oxides is continued with silicon in solution.

For a decrease of the chromium oxidation, the injection of carbon is widely used because it is economically more suited than the reduction with Si and Al. These two elements are bound to form oxides, thereby decreasing the slag basicity, which requires the further addition of lime, resulting in the increase of the slag volume. With slag reduction as a result of the blowing in of carbon, carbon monoxide is formed, which is necessary for the formation of the foaming slag. However, for an efficient reduction of Cr_2O_3 with the blowing in of carbon, a high slag temperature is also necessary. For this reason, the blowing in of carbon is carried out with the parallel blowing in of oxygen. The reduction of chromium oxide with Si and C occurs by the reactions:

$$(Cr_2O_3) + 1{,}5\ [Si] = 2\ [Cr] + 1{,}5\ (SiO_2) \qquad (15)$$

$$(Cr_2O_3) + 3C_{(S)} = 2[Cr] + 3CO_{(g)} \qquad (16)$$

The reduction of chromium oxide is more efficient with conditions of:

- a high activity of Cr_2O_3 with increased alkalinity,
- a high activity of carbon, $a_c = 1$ during the blowing in of carbon,
- a low partial pressure,
- a low activity of chromium in the metallic phase,
- a high temperature.

Besides the used technology for the reduction with silicon and aluminium and the blowing in of carbon, the use of the blowing in of calcium carbide was reported also[12]. When this carbide reacts with oxides in the slag, the products of the reaction are chromium, lime and carbon monoxide. CaO has the function of a non-metallic addition for the formation of the slag, while carbon monoxide improves the slag foaming in comparison to the blowing in of carbon powder. The reduction of chromium oxide with calcium carbide (CaC_2) proceeds according to the reaction:

$$Cr_2O_3 + CaC_2 = 2Cr + 2CO_{(g)} + CaO \quad (17)$$

The change of Gibbs free energy with temperature for the reactions of chromium oxide with silicon, carbon and calcium carbide are shown in **Figure 11**. It is clear that the reduction of chromium with carbon is more efficient at high temperature; therefore, in practice it is performed with the parallel blowing in of oxygen. The reaction between silicon and chromium oxide is not strongly temperature dependent and occurs, for this reason, also at lower temperatures. The suitability of calcium carbide as a reductant is shown by the reaction between this carbide and chromium oxide, which has a lower Gibbs energy in the temperature range of 1550 °C to 1700 °C.

It is characteristic for slags containing iron and chromium oxides, that on the boundary between the slag

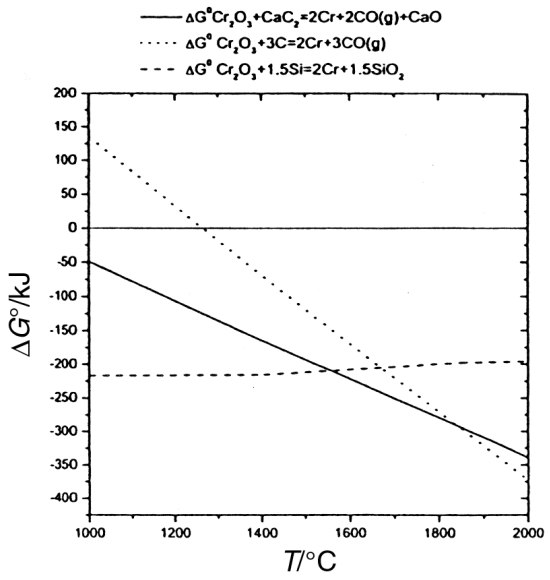

Figure 11: Temperature dependence of Gibbs free energy for the reduction of chromium with calcium carbide, silicon and carbon[12]

Slika 11: Temperaturna odvisnost Gibbsove proste energije za redukcijo kroma s kalcijevim karbidom, z ogljikom in s silicijem[12]

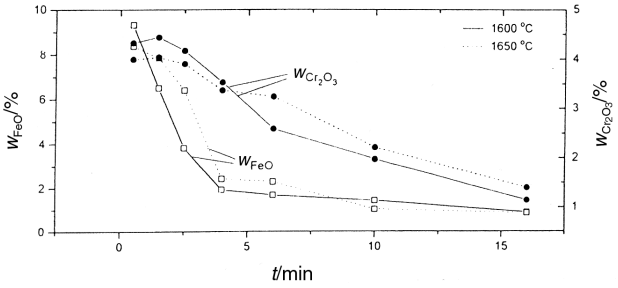

Figure 12: Content of FeO and Cr_2O_3 with respect to time at 1600 °C and 1650 °C [13]

Slika 12: Vsebnosti FeO in Cr_2O_3 v žlindri v odvisnosti od časa pri temperaturi 1600 °C in 1650 °C [13]

and the carbon the reduction starts immediately and without any incubation period, while the reduction of Cr_2O_3 has an incubation period and is slower than the reduction of FeO[13]. The reduction of Cr_2O_3 begins only after the reduction of a considerable amount of FeO (**Figure 12**).

In **Figure 13** the ratio $\ln(w_{Cr}/w_{Cro})$ with respect to time is shown for a slag with a different content of FeO with (%Cr) as the total content of chromium in the slag and with (Cr_o) as the reduced chromium in the slag at the time t[13]. The slope of the curves for the content of 5 % or 10 % of FeO shows that the reduced part of Cr_2O_3 is greater with a higher content of FeO in the slag. For a content of FeO = 0.5 % the incubation for the reduction becomes longer and the Cr_2O_3 reduction time is lengthened.

3.1 Foaming slag

The formation of foaming slag is a process dependent on a sufficient evolution of gases in a slag with a proper viscosity, which should not be too small, as a determined time of presence of gas bubbles in the slag is necessary

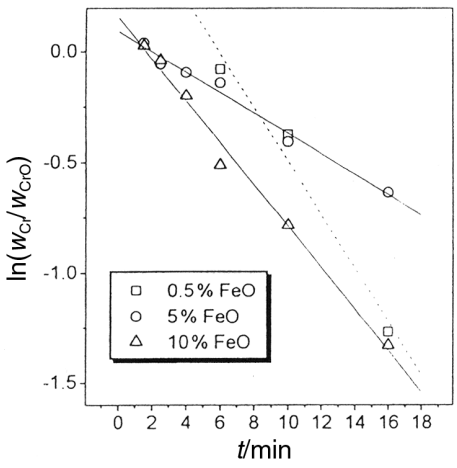

Figure 13: The kinetics of the reduction of chromium oxides for a different content of FeO in the slag and the slag alkalinity of $CaO/SiO_2 = 1.15$ [13]

Slika 13: Redukcija kromovega oksida v odvisnosti od vsebnosti FeO pri bazičnosti žlindre $CaO/SiO_2 = 1{,}15$ [13]

to maintain sufficient foaming. If the viscosity is too great, the foaming cannot occur, or occurs with insufficient intensity.

The foaming characteristics are improved with the lowering of the surface tension (σ) and density (ρ) and with the increase in the slag viscosity (η)[14]. The foaming stability and the foaming index (Σ) are determined from the average size of the bubbles (D_b).

$$\Sigma = 115\ \eta\ /(\ \sigma \cdot \rho)^{0,5} \quad (18)$$

$$\Sigma = \eta^{1,2}/(\ \sigma^{0,2} \cdot \rho \cdot D_b^{0,9}) \quad (19)$$

D_b is the increase of volume due to the arising CO bubbles in the slag. Small bubbles are of special importance for the slag stability. The presence in the slag of a suspension of different solid phases has a stronger effect on the foaming than the slag surface tension or the viscosity. An optimised slag is not entirely liquid; however, it is saturated with CaO (Ca_2SiO_4) and MgO. The particles in suspension act as nuclei for gas bubbles and enable the formation of a large number of small bubbles.

For the effect of particles in suspension on the slag viscosity, the following relation was developed:

$$\eta_e = \eta(1–1{,}35\theta)^{–5/2} \quad (20)$$

With: η_e – the effective slag viscosity

η – the viscosity of the liquid gas without particles in suspension

θ – the volume share of the solid phase in the slag

In **Figure 14** the dependence between the foaming index and the relative effective slag viscosity is shown[15]. If the relative effective slag viscosity is increased, the time of the presence of bubbles in the slag is lengthened, the foaming stability is increased and the foaming time is lengthened, also. As shown in **Figure 15**, the optimal quantity of solid particles is at the point G. Away from this point the slag becomes too crusty and the index of foaming is decreased.

The foaming slag has a positive effect in the EAF, since it decreases the electrodes radiation loss, decreases

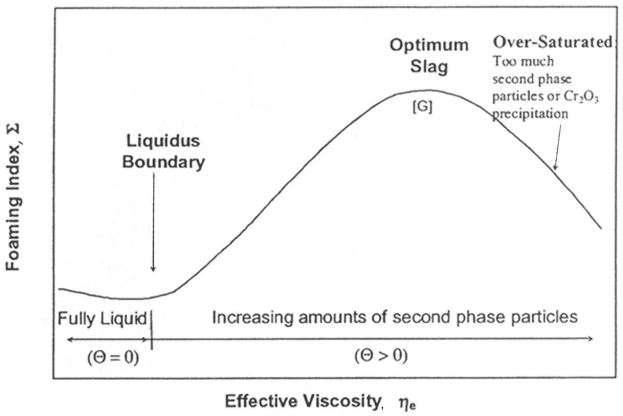

Figure 14: Foaming index versus the effective slag viscosity[15]
Slika 14: Indeks penjenja v odvisnosti od efektivne viskoznosti žlinder[15]

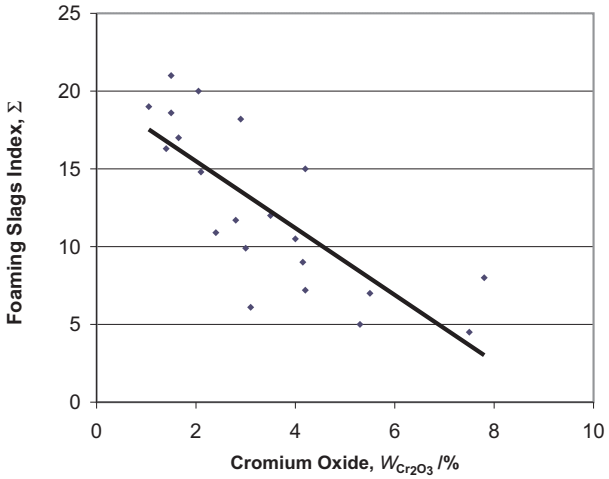

Figure 15: Content of chromium oxide in the slag after discharge of the furnace in dependence of the slag foaming index[16].
Slika 15: Vsebnost kromovega oksida v žlindri po prebodu na peči v odvisnosti od indeksa penjenja žlindre[16]

the spraying of the slag on the lining and on the water panels, decreases the loss of electrodes and lowers the effect of variation of electrical tension with a longer electric arc[16]. It was found, also, that the foaming slag increases the return of chromium from the slag in the metallic bath (**Figure 15**).

By the elaboration of the carbon steels with FeO as major oxidation product (> 20 % of FeO in the slag), the propensity of the slag to foam is achieved simply with the blowing in of carbon in the slag. The base reaction for the formation of gas bubbles in the slag is:

$$FeO_{(s,\ l)} + C_{(s)} = Fe_{(l)} + CO_{(g)} \quad (21)$$

The foaming of stainless slag is different from that during the elaboration of carbon steels. The foaming capacity of stainless slags is decreased by a low content of iron oxide and a high content of chromium oxide in the slag. Solid particles of chromium oxide in the slag with a high melting point increase the slag viscosity and impair the foaming. With a low FeO content and with slow kinetics of reduction of chromium oxide, the addition of carbon, which increases the quantity of CO, does not fulfil the condition for an efficient foaming[17].

The controlled formation of gas bubbles is very important for the formation of the foaming slag. During the elaboration of stainless steels, CO is produced, mainly with the carbon reduction of CrO_x and FeO_x. In stainless slags the Cr-O buffer appears at a much lower oxygen potential than the Fe-O buffer and, for this reason, chromium is oxidised before iron[18]. During the blowing in of oxygen in the melt CrO_x is formed as an oxidation product in place of FeO and for this reaction it is characteristic that:

- the solubility of CrO_x in the slag is low and it depends upon the ratio CaO/SiO_2 and the temperature,

- the share of reduction of CrO_x with carbon is small in comparison to the reduction of FeO. Consequently, the rate of formation of CO is small, since it forms mostly with the reduction of FeO.

In presence of FeO_x a greater quantity of CO is formed, and it can also be achieved with a greater degree of oxidation of the melt or the addition of FeO to the slag.

The second condition for the formation of the foaming slag is the proper slag fluidity. During the elaboration of stainless steels in the EAF the SiO_2 and Cr_2O_3 are the main oxidation products. SiO_2 is a flux component, while Cr_2O_3 is a component of the lining and it increases the rigidity of the slag. For this reason, the control of the Cr/Cr_2O_3 equilibrium in the melt is very important for achieving a foaming slag. The solubility of CrO_x in these slags is small (< 5 % CrO_x), and once the solubility is reached, the oxide CrO_x is precipitated.

If a moderate amount of secondary particles is available in the slag, the viscosity and thus the foaming index increases. However, at higher chromium contents, large solid particles destroy the bubble network and become detrimental to the slag's foamability. The data from the investigation shows that the Cr_2O_3 content should be kept lower than 16 % for the slag composition, temperature and oxygen potential used in the research[15].

The next parameter affecting the slag foaming is the temporal addition of additives during the elaboration of the steel in the furnace, since the composition of the slag is very important for the control of chromium and the achieving of the optimal degree of foaming. The formation of a fluid slag during the melting depends on the oxidation-reduction kinetics in the steel bath. An early fluid slag is achieved with the addition of wollastonite ($CaSiO_3$). The addition of MgO in the system $CaO\text{-}SiO_2$ increases the fluidity and decreases the melting point of the slags up to a content of 15 % MgO, above this level periclase or spinel are precipitated.

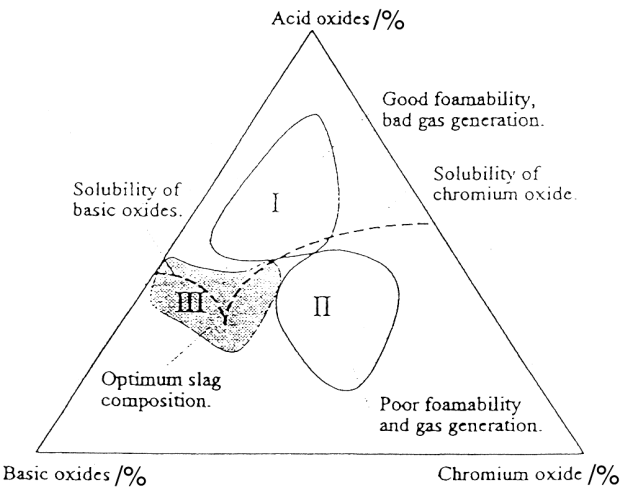

Figure 16: Areas of the tri-phase diagram with different activities of foaming/reduction[17]

Slika 16: Področja trifaznega diagrama s prikazom različnih lastnosti penjenja/redukcije[17]

Considering the above analysis, it is understandable that achieving foaming in EAF slags rich in Cr_2O_3 is a difficult task, especially with regard to the formation of a sufficient quantity of gas bubbles. The investigation of the foaming and the reduction confirm that the area of stable foaming for EAF stainless slags is small[19]. This area and the area of the formation of gases are schematically shown in **Figure 16**.

Area I: A low basicity slag with a high viscosity gives a good foamability, according to Equation (18). Unfortunately, the gas generation is very small. The overall result of this is a poor foaming without any industrial interest.

Area II: This area shows the composition of the slag after a poorly controlled oxidation. The slag has a high viscosity and it has a large content of Cr_2O_3 solid particles. The great viscosity and the share of the solid phase in the slag decrease the kinetics of the formation of gases.

Area III: This part of the slag system is optimal. The basicity is high and the conditions for the formation of the CO gas are optimal. With particles of solid CaO and Cr_2O_3 the viscosity is increased and the index of foaming is increased, also.

The reduction of chromium oxide in the foaming occurs according to the following reactions[18]:

$$(CrO_{1,5}) + \tfrac{3}{4}\,[Si] = [Cr] + \tfrac{3}{4}\,(SiO_2) \qquad (22)$$

$$(CrO) + \tfrac{1}{2}\,[Si] = [Cr] + 1/2\,(SiO_2) \qquad (23)$$

$$(CrO) + x\mathrm{C} = x\mathrm{CO} + [Cr] \qquad (24)$$

4 CONCLUDING REMARKS

During the elaboration of stainless steels in an EAF the loss of chromium is reduced with a decrease of the oxidation during the melting of the charge, the control of the blowing in of the oxygen by partial oxidation of the melt, with the slag composition and with efficient slag reduction.

The share of the oxidation of chromium depends on the composition of the charge, which may contain chromium oxides. During the melting, chromium is oxidised with other oxides present and with oxygen in the air. The dependence of the oxidation enthalpy on temperature shows that silicon and aluminium prevent the oxidation of chromium and that the sequence of oxidation depends on the activity of the element.

The 0.3 % content of silicon and the addition of silicon decrease significantly the oxidation of chromium during the melting because silicon is oxidised first and, in this way, the content of chromium in the slag is reduced. The oxidation of silicon is efficient during the melting and the heating of the charge and during the discharge of steel and slag from the furnace. The decrease of the oxidation of chromium with the addition

of FeSi requires the addition of lime to maintain the right slag basicity (CaO/SiO_2). These additions increase the volume of the slag.

During the refining period the reducing conditions must be secured by controlling the C/O_{tot} injection ratio and the temperature of the blowing of oxygen. For this reason it is recommended that the blowing in of oxygen is carried out at a high temperature > 1600 °C, when the oxidation of carbon is strong and the oxidation of chromium is minimised.

After the charge was melted and the blowing in of oxygen stopped, a significant content of chromium oxides in the slag is obtained. The chromium is returned in the bath with the reduction of slag during the heating up and the raffination of the bath and during the discharge from the EAF. The selection of the reductant and the procedure of reduction are significant for achieving a maximal return of chromium and a minimal content of reductant in the melt.

Suitable reductants are ferrosilicon, aluminium, calcium carbide and carbon. However, silicon and carbon are used the most. A second possibility is the addition of ferrosilicon with parallel blowing in of carbon powder in the slag when CO and gas bubbles are formed. Both are necessary to obtain a foaming slag. However, the blowing in of carbon is efficient at a high bath temperature. The alternative is the injection of calcium carbide into the slag, when CO and CaO are obtained as products. The advantage of calcium carbide is that it is an efficient reductant for chromium oxide even at lower bath temperatures.

Good mixing between the steel and the slag during tapping provides excellent conditions for dissolving the silicon to reduce the Cr_2O_3 in the slag. The chemical composition and the basicity of the slags affect strongly the reduction of chromium oxides. For furnace slag, the lowering of chromium oxide depends also on the lowering of the activity of SiO_2 and Al_2O_3. For a higher slag basicity the activity of SiO_2 and Al_2O_3 is lower and the reduction of chromium oxide greater. An basicity of 1.4 to 1.8 is the optimum range.

For the formation of the foaming slag an early presence of a sufficient volume of fluid slag is necessary. The final slag should be saturated with CaO and MgO (5–10 %) and have a viscosity suitable for the formation of the foaming process. The appropriate content of Si in the steel bath is necessary for the control of the ratio Cr/Cr_2O_3, since the solid chromium oxide increases the viscosity of the slag and impairs the foaming. Furthermore, the reactions should ensure the formation of small gas bubbles. The injection of carbon into the slag with a high potential of oxygen in the bath and a high content of FeO generates the formation of CO bubbles. For the stable foaming of stainless slags with a low content of FeO it is necessary to maintain the generation of gas bubbles with the injection of carbon and iron oxide in the slag.

5 REFERENCES

[1] J. Elliott: Physical Chemistry of Liquid Steel in Electric furnace Steelmaking, The Iron and Steel Society (Ed. By C. R. Taylor), 1985, 291

[2] J. Elliott, M. Gleiser: Thermochemistry for Steelmaking, The American iron and steel Institute, U.S.A., 1960

[3] F. Tehovnik, B. Arh, D. Kmetič, B. Arzenšek, M. Klinar, A. Kosmač, E. Šubelj, A. Lagoja, F. Perko: Optimization of continuous casting conditions by the elaboration of steels Acroni 19 and Acroni 19Si, Final Report, Institute of Metals and Technology, Ljubljana, Slovenia, 2001

[4] M. Kimoto, T. Itoh, T. Nagasaka, M. Hino: Thermodynamics of oxygen in liquid Fe-Cr alloy saturated with $FeO.Cr_2O_3$ solid solution, ISJ Int. 42 (**2002**), 1, 23–32

[5] T. Itoh, T. Nagasaka, M. Hino: Phase Equlibria between SiO_2 and Iron-Chromite Spinel Structure Solid Solution, and Deoxidation of liquid Fe-Cr alloy with Silicon, ISJ Int. 42 (**2002**) 1, 33–37

[6] C. W. McCoy, Langenberg: Journal of Metals, May 1964, 421–424

[7] Yanping Xiao, Lauri Holappa; Determination of Activities in Slag containing Chromium Oxides, ISIJ International, 33 (**1993**) 1, 66–74

[8] Mihael Tolar: Elektrojeklarstvo, Interner publication, SIJ-Acroni, d.o.o., Jesenice, 2005

[9] A. Maun and E. F. Osborn: Phase equilibria among oxides in steelmaking, Addison Wesly publishing company, 1965

[10] S. Sun, P. Uguccioni, M. Bryant, M. Ackroyd: Chromium control in the EAF during Stainless Steelmaking, Electric furnace conference proceedings 1997, 297–30

[11] D.C. Hilty and T.F. Kaveney: Stainless Steel Melting in Electric Furnace Steelmaking, The Iron and Steel Society, 1985, 143

[12] J. Björkvall, S. Angström, L. Kallin: Reduction of chromium oxide containing slags using CaC_2 injection, 7 International conference on Molten slag fluxes and salts, 2004

[13] M. Görnerup: Studies of Slag Metallurgy in Stainless Steelmaking, Doctoral thesis, Stockholm 1997

[14] Y. Zhang and R.J. Fruehan; Effect of the bubble Size and Chemical Reaction on Slag Foaming, Met.Trans. B (26B), 1995, 803–812

[15] K. Ito: Slag Foaming in New Iron and Steelmaking Processes, Met. Trans. B (20B), 1989, 515–521

[16] R. Krump, M. Willingshofer, W. Meyer, F. Rubenzucker: Quantitative detection of foaming slag in EAF, and its benefit for the production of high Cr-steels, 8th European Electric Steelmaking conference, 2005

[17] M. Juhart, M. Peter, K. Koch, J. Lamut, A. Rozman: Schäumverhalten von Schlaken aus der Produktion chromhaltiger Stähle im Elektrolicht-bogenofen, Stahl und Eisen 121 (2001) 9

[18] Eugene B. Pretorius, Robert C. Nunnington: Stainless Steel Slag Fundamental-From Furnace to Tundisch, Sixth internal Conference on Molten Slags, Fluxes and Salts, Stockholm, June 2000

[19] M. Görnerup and H. Jacobsson: Foaming slag-practice in Eletric stainless steelmaking, Electric furnace conference proceedings, 1997

UDK 621.74.047:519.68
Original scientific article/Izvirni znanstveni članek

ISSN 1580-2949
MTAEC9, 41(5)213(2007)

A NEW TOPOLOGY FOR THE TRAJECTORIES OF THE MENISCUS DURING CONTINUOUS STEEL CASTING

NOVA TOPOLOGIJA TRAJEKTORIJ MENISKUSA PRI NEPREKINJENEM LITJU JEKLA

Ice B. Risteski

2 Milepost Place # 606, Toronto, Ontario, Canada M4H 1C7
ice@scientist.com

Prejem rokopisa – received: 2007-04-13; sprejem za objavo – accepted for publication: 2007-07-10

The theoretical basis for a new computational method is given for the topology of the meniscus trajectories during continuous steel casting. The method is based on the solution of the meniscus equation in $\Re^3$. Here the topology is treated only in the sense of the categorization of trajectories in an orientation space. This suggests a new type of efficient self-adaptive scheme suitable for the solution of the shape of the meniscus. In the present work a new approach is used to overcome previously unknown pathological, non-physical predictions in various constitutive models derived using closure approximations. The generalized meniscus equation as well as its stability is solved. Here it is shown, for the first time, that the cyclic change of the shape of the meniscus depends on the coordinates, while up to now the cyclic change of the meniscus was presented only as a function of the time over the expression of the mould velocity.

Key words and phrases: topology of trajectories, shape of the meniscus, meniscus equation, generalized meniscus equation, meniscus stability.

Dana je teoretična podlaga za nov izračun topologije trajektorij meniskusa pri neprekinjenem litju jekla. Podlaga metode je rešitev enačbe meniskusa $\Re^3$. Topologija je obravnavana le v smislu kategorizacije trajektorij v nekem orientacijskem prostoru. To navaja na novo shemo, ki se sama primerno prilagaja za rešitev oblike meniskusa. V tem delu je uporabljen nov način, da bi se obvladalo preje neznane patološke, nefizikalne napovedi v različnih konstitutivnih modelih, ki so bili razviti z uporabo končnih aproksimacij. Rešeni sta splošna enačba meniskusa in njena stabilnost. Prvič je prikazano, da je ciklična sprememba oblike meniskusa odvisna od koordinat, medtem ko se je dosedaj ciklične spremembe meniskusa prikazalo samo kot funkcijo razmerja čas proti hitrosti kokile.

Ključne besede in stavki: topologija trajektorij, oblika meniskusa, enačba meniskusa, splošna enačba meniskusa, stabilnost meniskusa

1 INTRODUCTION

The study of the changes of the meniscus during continuous steel casting is neither an easy nor a simple task. It is, in fact, very complicated and requires a serious approach and hard work, because the meniscus's appearance depends on many factors of the continuous steel casting process. Generally speaking, this type of multidisciplinary research looks for a sufficient knowledge of steel metallurgy as well as the highest level of mathematics.

Many efforts have been spent to describe the shape of the meniscus during continuous steel casting. For instance, in [1] and [26] the authors considered the shape of the meniscus as a linear function and developed a model based on the Navier-Stokes equation for a hydrodynamic fluid. In [12], by virtue of complex functions, the movement of molten powder between the strand and mould wall is presented as a Newtonian fluid flowing between two parallel plates by neglecting the thermal contact resistance between the solidifying metal and the mould [11]. Particular cases of this complex model appear in the results given in [13,18]. In later research works [14,16] the meniscus is shaped with an exponential function by virtue of the meniscus's dimensions [17].

In [24,25] the authors developed a dimensionless model for the meniscus, introducing Reynolds' lubrication theory. A model closely related to the *free coating problem* [27], is solved numerically and is compared with the published data.

On other hand, in the simulation model [2] a fixed shape of the meniscus is used to calculate the fluid flow and heat transfer. The authors in [5] account for the interdependence of the shape of the flux gape and the fluid flow therein, but still require some parameters to be selected rather arbitrarily, if impossible, to determine the experimental measurements.

Research in [6,7] showed that the movement of molten powder in the flux space may be determined by a *pseudo-transient analytical solution* of the Navier-Stokes equation. The validity of this solution is verified using an explicit finite-difference discretization method and the MATLAB software package. The simulation and behavior of interfacial mould slag layers in the continuous casting of steel are investigated in [8].

In [28,29,30] the authors modified the model for lubrication on the meniscus, given in [14,16], with the difference between steel and flux density and extended it with the heat-transfer phenomena. They do not use the natural logarithm with base *e* for the description of the expo-

nential shape of the meniscus, and use instead the decade logarithm with base 10, without considering the correlation $\ln x \approx 2.303 \lg x$.

The newest research [4,10] is directed to cold model experiment on the infiltration of mould flux during the continuous casting of steel, neglecting the mould oscillations and the infiltration phenomena of molten powder derived from an analysis using the Reynolds equation.

Generally speaking, up to now in the literature the meniscus changes during continuous steel casting were approximately treated with one-dimensional mathematical models by virtue of some real function as a *fixed* shape. The treatment was adopted because the meniscus equation as a function of several variables was not known. In the present work, the introduced meniscus equation as a quasicyclic real function equation, *i.e.*, its solution, can be used for all the possible cases of meniscus changes occurring cyclically during the mould cycle. In this way the mathematical description of the shape of the meniscus is much better, because the shape of the meniscus is closer to its own real shape.

Up to now in relevant references the form of the meniscus was presented as a cyclical change independent of time over the mould speed only, while, in this article, it is shown that the change of the form of the meniscus depends on other coordinates too.

The present work gives a new approach to meniscus vicinity in a sufficiently sophisticated way, which is more complete than previous treatments. With the goal to shed new light on this topic, with this article a new shape of the meniscus is introduced by virtue of the solution of the meniscus equation. With the intention to better understand this approach, emphasis is given to the engineering experience and the theoretical knowledge of mathematical modeling of the continuous steel casting process.

2 PRELIMINARIES

Let $A = [a_{ij}]_{n\times n}$ be a real matrix. Suppose that by elementary transformations the matrix A is transformed into $A = P_1DP_2$, where P_1 and P_2 are regular matrices and D is a diagonal matrix with diagonal entries 0 and 1, such that the number of units is equal to the rank of the matrix A. The matrix $B = P_2^{-1}DP_1^{-1}$ satisfies the equality $ABA = A$. This means that the matrix equation $AXA = A$ has at least one solution for X.

If A satisfies the identity

$$A^r + k_1A^{r-1} + \cdots + k_{r-1}A = O$$

where $k_{r-1} \neq 0$ and O is the zero $n\times n$ matrix, then the matrix

$$X = -(A^{r-2} + k_1A^{r-3} + \cdots + k_{r-2}I)/k_{r-1}$$

where I is the unit $n\times n$ matrix, is also a solution of the equation $AXA = A$.

Now we recall the following theorem proven in [20].

Theorem 2.1. *If B satisfies the condition ABA = A, then*

1° $AX = O \Leftrightarrow X = (I - BA)Q$
(X and Q are $n \times m$ matrices),

2° $XA = O \Leftrightarrow X = Q(I - AB)$
(X and Q are $m \times n$ matrices),

3° $AXA = A \Leftrightarrow X = B + Q - BAQAB$
(X *and* Q are $n \times n$ matrices),

4° $AX = A \Leftrightarrow X = I + (I - BA)Q$,

5° $XA = A \Leftrightarrow X = I + Q(I - AB)$.

Throughout this paper, $\Re$ is a finite-dimensional real vector space. Vectors from $\Re$ will be denoted by $\boldsymbol{X}_i = (x_{1i},x_{2i},\ldots,x_{ni})^{\mathrm{T}}$, and also we denote with $\mathbf{O} = (0,0,\ldots,0)^{\mathrm{T}}$ the zero vector in $\Re$. Let $\otimes$ denote the exterior product in $\Re$ and let k ($1 \le k \le n$) be an integer. With respect to the canonical basis in the k-th exterior product space $\otimes^k \Re$, the k-th additive compound matrix $A^{[k]}$ of A is a linear operator on $\otimes^k \Re$ whose definition on a decomposable element $x_1 \otimes \cdots \otimes x_k$ is

$$A^{[k]}(x_1\otimes \cdots \otimes x_k) = \sum_{i=1}^{k} x_1 \otimes \cdots \otimes Ax_i \otimes \cdots \otimes x_k. \quad (2.1)$$

For any integer $i = 1, 2,\ldots, n!/k!(n - k)!$, let $(i) = (i_1,\ldots,i_k)$ be the i-th member in the lexicographic ordering of integer k-tuples such that $1 \le i_1 < \cdots < i_k \le n$. Then the (i, j)-th entry of the matrix $A^{[k]} = [q_{ij}]$ is

$$q_{ij} = a_{i1,i1} + \cdots + a_{ik,ik} \text{ if } (i) = (j)$$
$$q_{ij} = (-1)^{m+s}a_{jm,is} \quad (2.2)$$

if exactly one entry i_s of (i) does not occur in (j) and j_m does not occur in (i),

$$q_{ij} = 0$$

if (i) differs from (j) in two or more entries.

As special cases, we have $A^{[1]} = A$ and $A^{[n]} = \mathrm{tr}A$ [9].

Let $\sigma(A) = \{\lambda_i, 1 \le i \le n\}$ be the spectrum of A. Then the spectrum of $A^{[k]}$ is $\sigma(A^{[k]}) = \{\lambda_{i1} + \cdots + \lambda_{ik}, 1 \le i_1 < \cdots < i_k \le n\}$.

Let $|\cdot|$ denote a vector norm in $\Re^n$. The Lozinskiĭ measure μ on $\Re^n$ with respect to $|\cdot|$ is defined by

$$\mu(A) = \lim_{\rho\to 0+}(|I + \rho A| - 1)/\rho \quad (2.3)$$

The Lozinskiĭ measures of $A = [a_{ij}]_{n\times n}$ with respect to the three common norms

$$|x|_\infty = \sup_i |x_i|$$
$$|x|_1 = \Sigma_i |x_i|$$
$$|x|_2 = (\Sigma_i |x_i|^2)^{1/2}$$

are

$$\mu_\infty(A) = \sup_i (a_{ii} + \Sigma_{k,k\neq i} |a_{ik}|)$$
$$\mu_1(A) = \sup_k (a_{kk} + \Sigma_{i,i\neq k} |a_{ik}|) \quad (2.4)$$
$$\mu_2(A) = \mathrm{stab}[(A + A^{\mathrm{T}})/2]$$

where

$$\mathrm{stab}(A) = \max\{\lambda, \lambda\in\sigma(A)\}$$

is the stability modulus of the matrix A, and A^T denotes the transpose of A [3, p.41].

Definition 2. 2. A stable system is that system in which after the transitive action appearance a constant position is achieved [15, p.38].

3 TOPOLOGY OF THE SOLUTIONS OF THE MENISCUS EQUATION

In this section we will give a complete analysis of the meniscus equation represented by a quasicyclic real functional equation for all possible cases. For that purpose we will use techniques for the solution given in [19,21,23].

Let us consider now the equation

$$a_1f(x_1,x_2,x_3) + a_2f(x_2,x_3,x_1) + a_3f(x_3,x_1,x_2) = \\ = \alpha_1f(x_1,x_1,x_2) + \alpha_2f(x_2,x_2,x_3) + \alpha_3f(x_3,x_3,x_1) \quad (3.1)$$

f: $\Re^3 \to \Re$, where a_i, α_i $(1 \le i \le 3)$ are real constants. For equation (3.1) we suppose that $|a_1| + |a_2| + |a_3| > 0$.

If we permute cyclically the variables in the equations (3.1), we obtain

$$a_1f(x_2,x_3,x_1) + a_2f(x_3,x_1,x_2) + a_3f(x_1,x_2,x_3) = \\ = \alpha_1f(x_2,x_2,x_3) + \alpha_2f(x_3,x_3,x_1) + \alpha_3f(x_1,x_1,x_2) \quad (3.2)$$

$$a_1f(x_3,x_1,x_2) + a_2f(x_1,x_2,x_3) + a_3f(x_2,x_3,x_1) = \\ = \alpha_1f(x_3,x_3,x_1) + \alpha_2f(x_1,x_1,x_2) + \alpha_3f(x_2,x_2,x_3) \quad (3.3)$$

The determinant for the system of the equations (3.1), (3.2) and (3.3) is

$$\Delta_1 = \begin{vmatrix} a_1 & a_2 & a_3 \\ a_3 & a_1 & a_2 \\ a_2 & a_3 & a_1 \end{vmatrix}$$

Let us note the identity

$$\Delta = (a_1 + a_2 + a_3)[(a_1 - a_2)^2 + (a_2 - a_3)^2 + \\ + (a_3 - a_1)^2]/2 \quad (3.4)$$

First we consider the case

1° Let $\alpha_1 = \alpha_2 = \alpha_3 = 0$. Now the system (3.1), (3.2) and (3.3) takes the form

$$a_1f(x_1,x_2,x_3) + a_2f(x_2,x_3,x_1) + a_3f(x_3,x_1,x_2) = 0 \\ a_3f(x_1,x_2,x_3) + a_1f(x_2,x_3,x_1) + a_2f(x_3,x_1,x_2) = 0 \quad (3.5) \\ a_2f(x_1,x_2,x_3) + a_3f(x_2,x_3,x_1) + a_1f(x_3,x_1,x_2) = 0$$

If $\Delta \ne 0$, then the system (3.5) implies $f(x_1,x_2,x_3) = 0$.

Now let $\Delta = 0$. According to (3.4), this is possible if the real constants a_1, a_2, a_3 satisfy either $a_1 = a_2 = a_3$ or $a_1 + a_2 + a_3 = 0$.

First, let us suppose that $a_1 = a_2 = a_3$ $(\ne 0)$. Then system (3.5) is equivalent to the equation

$$f(x_1,x_2,x_3) + f(x_2,x_3,x_1) + f(x_3,x_1,x_2) = 0 \quad (3.6)$$

whose general solution according to [22] is

$$f(x_1,x_2,x_3) = F(x_1,x_2,x_3) - F(x_2,x_3,x_1) \quad (3.7)$$

where F: $\Re^3 \to \Re$, is an arbitrary function.

Now let us suppose that $\Delta = 0$, although the real constants are not all equal. Then necessarily $a_1 + a_2 + a_3 = 0$ and we can suppose, without any loss of generality, that $a_1 \ne a_2$. In this case we set $a_3 = -a_1 - a_2$ and system (3.5) can be written in the form

$$a_1[f(x_1,x_2,x_3) - f(x_2,x_3,x_1)] = a_2[f(x_3,x_1,x_2) - f(x_1,x_2,x_3)] \\ a_1[f(x_2,x_3,x_1) - f(x_3,x_1,x_2)] = a_2[f(x_1,x_2,x_3) - f(x_2,x_3,x_1)] \\ a_1[f(x_3,x_1,x_2) - f(x_1,x_2,x_3)] = a_2[f(x_2,x_3,x_1) - f(x_3,x_1,x_2)]$$

From this we derive easily

$$(a_1^3 - a_2^3)[f(x_1,x_2,x_3) - f(x_2,x_3,x_1)] = 0$$

With the assumption that $a_1 \ne a_2$ and they have real values, equation (3.4) reduces to

$$f(x_1,x_2,x_3) - f(x_2,x_3,x_1) = 0 \quad (3.8)$$

According to [20], the general solution of the above functional equation is

$$f(x_1,x_2,x_3) = F(x_1,x_2,x_3) + F(x_2,x_3,x_1) + F(x_3,x_1,x_2) \quad (3.9)$$

where F: $\Re^3 \to \Re$, is an arbitrary function.

The above results concerning the cyclic functional equation

$$a_1f(x_1,x_2,x_3) + a_2f(x_2,x_3,x_1) + a_3f(x_3,x_1,x_2) = 0$$

can be derived from those in [20], where a_1, a_2, a_3 are real constants.

From now we suppose that $|\alpha_1| + |\alpha_2| + |\alpha_3| > 0$. We can distinguish the following two cases:

2° Let $\Delta \ne 0$, from (3.1), (3.2) and (3.3) we obtain

$$f(x_1,x_2,x_3) = \begin{vmatrix} \alpha_1F(x_1,x_2) + \alpha_2F(x_2,x_3) + \alpha_3F(x_3,x_1) & a_2 & a_3 \\ \alpha_1F(x_2,x_3) + \alpha_2F(x_3,x_1) + \alpha_3F(x_1,x_2) & a_1 & a_2 \\ \alpha_1F(x_3,x_1) + \alpha_2F(x_1,x_2) + \alpha_3F(x_2,x_3) & a_3 & a_1 \end{vmatrix}$$

where F: $\Re^2 \to \Re$ is defined by $F(u,v) = f(u,u,v)/\Delta$.

If we introduce the notations

$$\Delta_1 = \begin{vmatrix} \alpha_1 & \alpha_2 & \alpha_3 \\ a_3 & a_1 & a_2 \\ a_2 & a_3 & a_1 \end{vmatrix} \quad \Delta_2 = \begin{vmatrix} \alpha_1 & \alpha_2 & \alpha_3 \\ a_2 & a_3 & a_1 \\ a_1 & a_2 & a_3 \end{vmatrix} \quad \Delta_3 = \begin{vmatrix} \alpha_1 & \alpha_2 & \alpha_3 \\ a_1 & a_2 & a_3 \\ a_3 & a_1 & a_2 \end{vmatrix}$$

then we can write

$$f(x_1,x_2,x_3) = \Delta_1F(x_1,x_2) + \Delta_2F(x_2,x_3) + \Delta_3F(x_3,x_1) \quad (3.10)$$

For (3.10) to be a solution of the functional equation (3.1), the following condition must be satisfied:

$$\alpha_1[(\Delta - \Delta_2)F(x_1,x_2) - \Delta_3F(x_2,x_1) - \Delta_1F(x_1,x_1)] + \\ + \alpha_2[(\Delta - \Delta_2)F(x_2,x_3) - \Delta_3F(x_3,x_2) - \Delta_1F(x_2,x_2)] + \\ + \alpha_3[(\Delta - \Delta_2)F(x_3,x_1) - \Delta_3F(x_1,x_3) - \Delta_1F(x_3,x_3)] = 0 \quad (3.11)$$

By a cyclic permutation of the variables x_1, x_2, x_3 in (3.11) we obtain two new equations. The system of these three equations has a nontrivial solution with respect to $(\Delta - \Delta_2)F(x_i,x_{i+1}) - \Delta_3F(x_{i+1},x_i) - \Delta_1F(x_i,x_i)$, $i = 1, 2, 3$ (with the convention $x_4 \equiv x_1$) if the following condition is satisfied

$$\begin{vmatrix} \alpha_1 & \alpha_2 & \alpha_3 \\ \alpha_2 & \alpha_3 & \alpha_1 \\ \alpha_3 & \alpha_1 & \alpha_2 \end{vmatrix} = 0 \quad (3.12)$$

By virtue of an equality of the type of (3.4) this is true if

$$\alpha_1 + \alpha_2 + \alpha_3 = 0 \text{ or } \alpha_1 = \alpha_2 = \alpha_3$$

First, we will consider the case

$$\alpha_1 + \alpha_2 + \alpha_3 = 0 \tag{3.13}$$

Since $a_1 + a_2 + a_3 \neq 0$ (because of the assumption $\Delta \neq 0$ and (3.4)), by putting into equation (3.1) $x_1 = x_2 = x_3$ we derive $F(x_1,x_2) = 0$. By using the last equality, the equation (3.11) for $x_3 = x_1$ becomes

$$[\alpha_1(\Delta - \Delta_2) - \alpha_2\Delta_3]F(x_1,x_2) - [\alpha_1\Delta_3 - \alpha_2(\Delta - \Delta_2)]F(x_2,x_1) = 0 \tag{3.14}$$

If we change the places of x_1 and x_2, the equation (3.14) is transformed into

$$-[\alpha_1\Delta_3 - \alpha_2(\Delta - \Delta_2)]F(x_1,x_2) + [\alpha_1(\Delta - \Delta_2) - \alpha_2\Delta_3]F(x_2,x_1) = 0 \tag{3.15}$$

Let

$$(\alpha_1^2 - \alpha_2^2)[(\Delta - \Delta_2)^2 - \Delta_3^2] \neq 0$$

then from (3.14) and (3.15) it follows that $F(x_1,x_2) = 0$ and then from (3.10) $f(x_1,x_2,x_3) = 0$.

The condition

$$(\alpha_1^2 - \alpha_2^2)[(\Delta - \Delta_2)^2 - \Delta_3^2] = 0 \tag{3.16}$$

implies $(\Delta - \Delta_2)^2 - \Delta_3^2 = 0$. Let us suppose that the last equality is not true. Now, if we set $x_3 = x_2$ into (3.11), we obtain

$$(\alpha_1^2 - \alpha_3^2)[(\Delta - \Delta_2)^2 - \Delta_3^2] = 0$$

The last equality, with (3.16), gives $\alpha_1^2 = \alpha_2^2 = \alpha_3^2$ which, by virtue of the assumption (3.13), yields $\alpha_1 = \alpha_2 = \alpha_3 = 0$, and this contradicts the hypothesis $|\alpha_1| + |\alpha_2| + |\alpha_3| > 0$.

Thus, we have $\Delta - \Delta_2 = \pm \Delta_3$. For the case $\Delta - \Delta_2 = \Delta_3 (\neq 0)$, equation (3.14) yields

$$(\alpha_1 - \alpha_2)\Delta_3[F(x_1,x_2) - \Delta_3 F(x_2,x_1)] = 0$$

so that, for $\alpha_1 \neq \alpha_2$, we have

$$F(x_1,x_2) = G(x_1,x_2) + G(x_2,x_1) \tag{3.17}$$

where G is an arbitrary function $\Re^2 \to \Re$ such that $G(x_1,x_1) \equiv 0$

If $\alpha_1 = \alpha_2$, then necessarily we must have $\alpha_1 \neq \alpha_3$, (because otherwise we would have $\alpha_1 = \alpha_2 = \alpha_3 = 0$) and by a procedure analogous to the one above we obtain (3.17).

Let $\Delta - \Delta_2 = -\Delta_3 (\neq 0)$, from (3.14) we obtain

$$(\alpha_1 + \alpha_2)\Delta_3[F(x_1,x_2) + F(x_2,x_1)] = 0 \tag{3.18}$$

For $\alpha_1 + \alpha_2 \neq 0$, the general solution of equation (3.18) is given by

$$F(x_1,x_2) = G(x_2,x_1) - G(x_2,x_1),\ G: \Re^2 \to \Re \tag{3.19}$$

If $\alpha_1 + \alpha_2 = 0$, then from (3.13) we deduce $\alpha_3 = 0$, and then $\alpha_1 + \alpha_3 = \alpha_1 \neq 0$ and we obtain (3.19) by an analogous procedure.

The condition (3.11), for the case $\Delta_3 = \Delta - \Delta_2 = 0$, is satisfied for every function $F(x_1,x_2)$ with the property $F(x_1,x_1) \equiv 0$.

If $(\Delta - \Delta_2)^2 \neq \Delta_3^2$, then, as was mentioned above, equations (3.14) and (3.15) have a trivial solution as a general solution. According to (3.10) we obtain

$$f(x_1,x_2,x_3) \equiv 0$$

Now we suppose that (3.12) is satisfied but (3.13) is not. This means that

$$\alpha_1 = \alpha_2 = \alpha_3 \neq 0 \tag{3.20}$$

It immediately follows that

$$\Delta_1 = \Delta_2 = \Delta_3 (\neq 0)$$

The quasicyclic equation (3.11) implies

$$(\Delta - \Delta_1)F(x_1,x_2) - \Delta_1 F(x_2,x_1) - \Delta_1 F(x_1,x_1) = = \Delta_1 P(x_1) - \Delta_1 P(x_2) \tag{3.21}$$

where P is an arbitrary function $\Re \to \Re$

For $\alpha_1 = \alpha_2 = \alpha_3$ and $x_1 = x_2 = x_3$ equation (3.1) becomes

$$(a_1 + a_2 + a_3 - 3\alpha_1)F(x_1,x_1) = 0$$

Let $a_1 + a_2 + a_3 = 3\alpha_1$, then $3\Delta_1 = \Delta$ and the equality (3.21) takes the form

$$2F(x_1,x_2) - F(x_2,x_1) = P(x_1) - P(x_2) + R(x_1)$$

where $R(x_1) = F(x_1,x_1)$.

By a permutation of the variables x_1 and x_2 it follows that

$$-F(x_1,x_2) + F(x_2,x_1) = P(x_2) - P(x_1) + R(x_2)$$

From the last two equalities we obtain

$$F(x_1,x_2) = [P(x_1) - P(x_2) + 2R(x_1) + R(x_2)]/3$$

By using the last equality, from (3.10) it follows that

$$f(x_1,x_2,x_3) = Q(x_1) + Q(x_2) + Q(x_3) \tag{3.22}$$

where $Q(x_1) = \Delta_1 R(x_1)$.

Let $a_1 + a_2 + a_3 \neq 3\alpha_1$, then $F(x_1,x_1) \equiv 0$ and the formula (2.21) yields

$$(\Delta - \Delta_1)F(x_1,x_2) - \Delta_1 F(x_2,x_1) = \Delta_1 P(x_1) - \Delta_1 P(x_2) \tag{3.23}$$

From the last equality, with a permutation of the variables we obtain

$$-\Delta_1 F(x_1,x_2) + (\Delta - \Delta_1)F(x_2,x_1) = \Delta_1 P(x_2) - \Delta_1 P(x_1)$$

The determinant of the system consisting of the last two equations is $\Delta(\Delta - 2\Delta_1)$. If $\Delta \neq 2\Delta_1$, the solution of the last two equations is

$$F(x_1,x_2) = \Delta_1[P(x_1) - P(x_2)]/\Delta$$

Then the equality (3.10) gives

$$f(x_1,x_2,x_3) \equiv 0$$

Let $\Delta = 2\Delta_1$, then from (3.23) we obtain

$$F(x_1,x_2) - P(x_1) = F(x_2,x_1) - P(x_2)$$

The general solution for the last equation is

$$F(x_1,x_2) = P(x_1) + G(x_1,x_2) + G(x_2,x_1) \tag{3.24}$$

where P: $\Re \to \Re$ and G: $\Re^2 \to \Re$ are arbitrary functions such that

$$G(x_1,x_2) = -P(x_1)/2$$

According to the last relation, the equality (3.24) takes the form

$$F(x_1,x_2) = G(x_1,x_2) + G(x_2,x_1) - 2G(x_1,x_1)$$

and the equality (3.10) becomes

$$f(x_1,x_2,x_3) = G(x_1,x_2) + G(x_2,x_1) - 2G(x_1,x_2) + G(x_2,x_3) + G(x_3,x_2) - 2G(x_2,x_2) + G(x_3,x_1) + G(x_1,x_3) - 2G(x_3,x_3) \quad (3.25)$$

where we have replaced $G(x_1,x_2)\Delta_1$ by $G(x_1,x_2)$.

For

$$\begin{vmatrix} \alpha_1 & \alpha_2 & \alpha_3 \\ \alpha_2 & \alpha_3 & \alpha_1 \\ \alpha_3 & \alpha_1 & \alpha_2 \end{vmatrix} \neq 0$$

from (3.10) we obtain

$$(\Delta - \Delta_2)F(x_1,x_2) - \Delta_3 F(x_2,x_1) - \Delta_1 F(x_1,x_1) = 0 \quad (3.26)$$

First we suppose that $\Delta - \Delta_1 - \Delta_2 - \Delta_3 \neq 0$. In this case, with the substitution $x_2 = x_1$, equation (3.26) reduces to $F(x_1,x_1) \equiv 0$. On the basis of the last equality, the equation (3.26) becomes

$$(\Delta - \Delta_2)F(x_1,x_2) - \Delta_3 F(x_2,x_1) = 0$$

From the permutation of the variables x_1 and x_2, from the above equation it follows that

$$-\Delta_3 F(x_1,x_2) + (\Delta - \Delta_2)F(x_2,x_1) = 0$$

The system of the last two equations has a nontrivial solution if and only if the following condition $(\Delta - \Delta_2)^2 = \Delta_3^2$ is satisfied.

Let $\Delta - \Delta_2 = \Delta_3$ ($\neq 0$), then we obtain

$$F(x_1,x_2) = G(x_1,x_2) + G(x_2,x_1)$$

where G satisfies $G(x_1,x_1) \equiv 0$.

For the case $\Delta - \Delta_2 = -\Delta_3$ ($\neq 0$) the general solution is

$$F(x_1,x_2) = G(x_1,x_2) - G(x_2,x_1)$$

For $\Delta - \Delta_2 = \Delta_3 = 0$, the unique condition that must be satisfied by the function F is $F(x_1,x_1) \equiv 0$.

The condition $(\Delta - \Delta_2)^2 \neq \Delta_3^2$ gives $F(x_1,x_2) \equiv 0$

Next we will pass on to the case $\Delta - \Delta_1 - \Delta_2 - \Delta_3 = 0$. Now equation (3.26) can be written as

$$(\Delta_1 + \Delta_3)F(x_1,x_2) - \Delta_3 F(x_2,x_1) = \Delta_1 R(x_1)$$

where $R(x_1) = F(x_1,x_1)$. By a permutation of the variables x_1 and x_2 we obtain

$$-\Delta_3 F(x_1,x_2) + (\Delta_1 + \Delta_3)F(x_2,x_1) = \Delta_1 R(x_2)$$

The determinant of this system is $(\Delta_1 + 2\Delta_3)\Delta_1$. If it is not zero, then

$$F(x_1,x_2) = [(\Delta_1 + \Delta_3)R(x_1) + \Delta_3 R(x_2)]/(\Delta_1 + 2\Delta_3)$$

From (3.10) it follows that

$$f(x_1,x_2,x_3) = (\Delta_1^2 + \Delta_1\Delta_3 + \Delta_3^2)Q(x_1) + (\Delta_1\Delta_2 + \Delta_1\Delta_3 + \Delta_2\Delta_3)Q(x_2) + \Delta_3\Delta Q(x_3)$$

where

$$Q(x_1) = R(x_1)/(\Delta_1 + 2\Delta_3)$$

Let $\Delta_1 = 0$, $\Delta_3 \neq 0$. Then

$$F(x_1,x_2) = F(x_2,x_1)$$

Thus

$$F(x_1,x_2) = G(x_1,x_2) + G(x_2,x_1)$$

where G is an arbitrary function $\Re^2 \to \Re$, and $f(x_1,x_2,x_3)$ is given by the formula (3.10).

Now we suppose that $\Delta_1 = -2\Delta_3 \neq 0$. Then

$$F(x_1,x_2) + F(x_2,x_1) = 2R(x_1) \quad (3.27)$$

By a permutation of the variables x_1 and x_2 we obtain

$$F(x_2,x_1) + F(x_1,x_2) = 2R(x_2) \quad (3.28)$$

From (3.27) and (3.28) we get

$$R(x_1) = R(x_2) = c$$

Thus (3.27) takes on the form

$$[F(x_1,x_2) - c] + [F(x_2,x_1) - c] = 0$$

which implies that

$$F(x_1,x_2) = G(x_1,x_2) - G(x_2,x_1) + c$$

where G: $\Re^2 \to \Re$ is an arbitrary function and c is an arbitrary real constant.

Now from (2.10) we find

$$f(x_1,x_2,x_3) = -2\Delta_3[G(x_1,x_2) - G(x_2,x_1)] + (\Delta + \Delta_3)[G(x_2,x_3) - G(x_3,x_2)] + \Delta_3[G(x_3,x_1) - G(x_1,x_3)] + c$$

where c is (another) arbitrary real constant.

In the case $\Delta_1 = \Delta_3 = 0$ equation (3.26) is satisfied for every function F: $\Re^2 \to \Re$.

Now we will use the following result.

Lemma 3. 1. Let $\Delta \neq 0$. Then the system

$$\Delta_1 = 0,\ \Delta_2 - \Delta = 0,\ \Delta_3 = 0 \quad (3.29)$$

implies $\alpha_1 = a_3$, $\alpha_2 = a_1$, $\alpha_3 = a_2$.

Proof. The system (3.29) can be written in the form

$$\begin{aligned} A_{11}(\alpha_1 - a_3) + A_{12}(\alpha_2 - a_1) + A_{13}(\alpha_3 - a_2) &= 0 \\ A_{21}(\alpha_1 - a_3) + A_{22}(\alpha_2 - a_1) + A_{23}(\alpha_3 - a_2) &= 0 \quad (3.30) \\ A_{31}(\alpha_1 - a_3) + A_{32}(\alpha_2 - a_1) + A_{33}(\alpha_3 - a_2) &= 0 \end{aligned}$$

where A_{ij} is the cofactor of the element a_{ij} ($1 \le i, j \le 3$) of the determinant Δ. The system (3.30) is a homogeneous linear system with respect to $\alpha_1 - a_3$, $\alpha_2 - a_1$, $\alpha_3 - a_2$. Its determinant is $\Delta^2 \neq 0$, so that it has only the zero solution.

Thus, the equation

$$a_1 f(x_1,x_2,x_3) + a_2 f(x_2,x_3,x_1) + a_3 f(x_3,x_1,x_2) = a_3 f(x_1,x_1,x_2) + a_1 f(x_2,x_2,x_3) + a_2 f(x_3,x_3,x_1)$$

has the general solution $f(x_1,x_2,x_3) = F(x_2,x_3)$.

3° Let $\Delta = 0$. Then from (3.4) it follows that

$$a_1 + a_2 + a_3 = 0 \text{ or } a_1 = a_2 = a_3 \neq 0.$$

First we will consider the case $a_1 = a_2 = a_3$. From (3.1) and (3.2) we obtain

$$(\alpha_1 - \alpha_3)F(x_1,x_2) + (\alpha_2 - \alpha_1)F(x_2,x_3) + \\ + (\alpha_3 - \alpha_2)F(x_3,x_1) = 0 \quad (3.31)$$

with the notation $f(x_1,x_1,x_2) = F(x_1,x_2)$. If $\alpha_1 = \alpha_2 = \alpha_3$, then the condition (3.31) is satisfied for every function F. For the case $\alpha_1 = \alpha_2 = \alpha_3$ ($\neq 0$), equation (3.1) takes the form

$$a_1 f(x_1,x_2,x_3) - \alpha_1 f(x_1,x_1,x_2) + a_1 f(x_2,x_3,x_1) - \\ - \alpha_1 f(x_2,x_2,x_3) + a_1 f(x_3,x_1,x_2) - \alpha_1 f(x_3,x_3,x_1) = 0 \quad (3.32)$$

This quasicyclic equation has the general solution

$$f(x_1,x_2,x_3) = (\alpha_1/a_1)F(x_1,x_2) + U(x_1,x_2,x_3) - U(x_2,x_3,x_1) \quad (3.33)$$

with the notation $f(x_1,x_1,x_2) = F(x_1,x_2)$.

By substitution of (3.33) into (3.32) we obtain

$$F(x_1,x_2) - (\alpha_1/a_1)F(x_1,x_1) - U(x_1,x_2,x_3) + U(x_1,x_2,x_1) \\ + F(x_2,x_3) - (\alpha_1/a_1)F(x_2,x_2) - U(x_2,x_2,x_3) + U(x_2,x_3,x_2) \\ + F(x_3,x_1) - (\alpha_1/a_1)F(x_3,x_3) - U(x_3,x_3,x_1) + U(x_3,x_1,x_3) = 0$$

This quasicyclic equation has the general solution

$$F(x_1,x_2) = (\alpha_1/a_1)F(x_1,x_1) + U(x_1,x_1,x_2) - U(x_1,x_2,x_1) + \\ + R(x_1) - R(x_2)$$

where R is an arbitrary function $\Re \to \Re$.

By using the last equality, for $\alpha_1 = a_1$, the equality (3.33) becomes

$$f(x_1,x_1,x_2) = U(x_1,x_2,x_3) - U(x_2,x_3,x_1) + U(x_1,x_1,x_2) - \\ - U(x_1,x_2,x_1) + S(x_1) - R(x_2) \quad (3.34)$$

where S: $\Re \to \Re$ is such that $F(x_1,x_1) = S(x_1) - R(x_1)$.

For $\alpha_1 \neq a_1$ it follows from (3.1) that $F(x_1,x_1) = 0$. According to the last identity, the equality (3.33) is transformed into

$$f(x_1,x_2,x_3) = U(x_1,x_2,x_3) - U(x_2,x_3,x_1) + \\ + (\alpha_1/a_1)[U(x_1,x_1,x_2) - U(x_1,x_2,x_1)] + R(x_1) - R(x_2)$$

Now we will suppose that the parameters α_i ($1 \leq i \leq 3$) are not all equal. Let $\alpha_1 \neq \alpha_3$. According to the equality (3.31) for $x_3 = a$ (a real constant) we obtain

$$F(x_1,x_2) = K(x_1) + H(x_1) \quad (3.35)$$

where we used the notations

$$K(x_1) = [(\alpha_2 - \alpha_3)/(\alpha_1 - \alpha_3)]F(a,x_1),\ H(x_2) = \\ = [(\alpha_1 - \alpha_2)/(\alpha_1 - \alpha_3)]F(x_2,a)$$

If we substitute $F(x_1,x_2)$ given by the expression (3.35) into (3.31), and if we set $x_1 = u$, $x_2 = x_3 = b$ (a real constant) and if, on the other hand, we set $x_1 = x_3 = b$, $x_2 = u$, we obtain respectively

$$(\alpha_1 - \alpha_3)[K(u) - K(b)] + (\alpha_3 - \alpha_2)[H(u) - H(b)] = 0 \quad (3.36)$$

$$(\alpha_2 - \alpha_1)[K(u) - K(b)] + (\alpha_1 - \alpha_3)[H(u) - H(b)] = 0 \quad (3.37)$$

The determinant of this system is

$$\begin{vmatrix} \alpha_1 - \alpha_3 & \alpha_3 - \alpha_2 \\ \alpha_2 - \alpha_1 & \alpha_1 - \alpha_3 \end{vmatrix} = [(\alpha_1 - \alpha_2)^2 + (\alpha_2 - \alpha_3)^2 + (\alpha_3 - \alpha_1)^2]/2$$

According to our assumption its value is not 0, then from (3.36) and (3.37) we find $K(u) = K(b)$ and $H(u) = H(b)$, hence

$$F(x_1,x_2) = m \text{ (a real constant)} \quad (3.38)$$

Now the equation (3. 1) becomes

$$f(x_1,x_2,x_3) - n + f(x_2,x_3,x_1) - n + f(x_3,x_1,x_2) - n = 0 \quad (3.39)$$

where

$$n = (\alpha_1 + \alpha_2 + \alpha_3)m/3a_1$$

The general solution of the cyclic functional equation (3.39) is

$$f(x_1,x_2,x_3) = p(x_1,x_2,x_3) - p(x_2,x_3,x_1) + n \quad (3.40)$$

From (3.38) and (3.40) we find

$$m = F(x_1,x_2) = p(x_1,x_1,x_2) - p(x_1,x_2,x_1) + n$$

If we put into the last equality $x_2 = x_1$, then $m = n$. This is possible if

$$\alpha_1 + \alpha_2 + \alpha_3 = 3a_1 \text{ or } n = 0$$

Moreover,

$$p(x_1,x_1,x_2) - p(x_1,x_2,x_1) = 0 \quad (3.41)$$

Now we will use the following result.

Lemma 3. 2. Let $f(x_1,x_2,x_3)$ be a function of the form

$$f(x_1,x_2,x_3) = p(x_1,x_2,x_3) - p(x_2,x_3,x_1)$$

such that $p(x_1,x_1,x_2) = 0$. Then

$$f(x_1,x_2,x_3) = U(x_1,x_2,x_3) - U(x_2,x_1,x_3) - U(x_2,x_3,x_1) - \\ - U(x_1,x_3,x_2) \quad (3.42)$$

where U: $\Re^3 \to \Re$ is an arbitrary function.

Proof. Let $p(x_1,x_2,x_3)$ satisfies equation (3.41). We are looking for $p(x_1,x_2,x_3)$ in the form

$$p(x_1,x_2,x_3) = k_1 q(x_1,x_2,x_3) + k_2 q(x_1,x_3,x_2) + k_3 q(x_2,x_1,x_3) + \\ + k_4 q(x_2,x_3,x_1) + k_5 q(x_3,x_1,x_2) + k_6 q(x_3,x_2,x_1)$$

where q: $\Re^3 \to \Re$ and k_i ($1 \leq i \leq 6$) are real constants.

By a substitution into (3.41) we find

$$k_5 = k_1 - k_2 + k_3,\ k_6 = k_4 - k_1 + k_2$$

Thus

$$f(x_1,x_2,x_3) = k[q(x_2,x_1,x_3) - q(x_1,x_2,x_3)] - \ell[q(x_1,x_3,x_2) - \\ - q(x_2,x_3,x_1)] + (\ell - k)[q(x_3,x_2,x_1) - q(x_3,x_1,x_2)]$$

where k, ℓ are real constants such that $k = k_3 - k_2$, $\ell = k_4 - k_1$

If we denote

$$U(x_1,x_2,x_3) = \ell q(x_2,x_3,x_1) + k q(x_3,x_1,x_2)$$

we obtain (3.42). Conversely, each function of the form (2.42) satisfies $f(x_1,x_1,x_2) = 0$ for arbitrary U: $\Re^3 \to \Re$. Moreover, $f(x_1,x_2,x_3)$ satisfies

$$f(x_1,x_2,x_3) + f(x_2,x_3,x_1) + f(x_3,x_1,x_2) = 0$$

We note that the representation (3.42) can be obtained just by putting

$$p(x_1,x_2,x_3) = U(x_1,x_2,x_3) - U(x_2,x_1,x_3)$$

Thus the general solution of the equation (3.1) is in this case given by

$$f(x_1,x_2,x_3) = U(x_1,x_2,x_3) - U(x_2,x_1,x_3) - \\ - U(x_2,x_3,x_1) + U(x_1,x_3,x_2) + n \qquad (3.43)$$

where U is an arbitrary function $\Re^3 \to \Re$ and n is an arbitrary real constant, $n = 0$ if $\alpha_1 + \alpha_2 + \alpha_3 \neq 3a_1$.

Now we will consider the case that a_1, a_2, a_3 are not all equal. Thus we have

$$a_1 + a_2 + a_3 = 0 \qquad (3.44)$$

Without any loss of generality, we can assume that $a_1 \neq a_2$. Equation (3.1) can be written as

$$a_1[f(x_1,x_2,x_3) - f(x_3,x_1,x_2)] - a_2[f(x_3,x_1,x_2) - f(x_2,x_3,x_1)] = \\ = \alpha_1 F(x_1,x_2) + \alpha_2 F(x_2,x_3) + \alpha_3 F(x_3,x_1) \qquad (3.45)$$

where $f(x_1,x_1,x_2) = F(x_1,x_2)$. Also from (3.2) and (3.3) it follows that

$$a_1[f(x_2,x_3,x_1) - f(x_1,x_2,x_3)] - a_2[f(x_1,x_2,x_3) - f(x_1,x_3,x_2)] = \\ = \alpha_1 F(x_2,x_3) + \alpha_2 F(x_3,x_1) + \alpha_3 F(x_1,x_2) \qquad (3.46)$$

$$a_1[f(x_3,x_1,x_2) - f(x_2,x_3,x_1)] - a_2[f(x_2,x_3,x_1) - f(x_1,x_2,x_3)] = \\ = \alpha_1 F(x_3,x_1) + \alpha_2 F(x_1,x_2) + \alpha_3 F(x_2,x_3) \qquad (3.47)$$

By adding (3.45), (3.46) and (3.47) we obtain

$$(\alpha_1 + \alpha_2 + \alpha_3)[F(x_1,x_2) + F(x_2,x_3) + F(x_3,x_1)] = 0$$

For $\alpha_1 + \alpha_2 + \alpha_3 \neq 0$, the following condition must be satisfied

$$F(x_1,x_2) + F(x_2,x_3) + F(x_3,x_1) = 0$$

This cyclic functional equation has the general solution

$$F(x_1,x_2) = P(x_1) - P(x_2) \qquad (3.48)$$

where P is an arbitrary function $\Re \to \Re$.

From the equation (3.45), (3.46) and (3.47), if we take into account (3.48), we get

$$f(x_1,x_2,x_3) + [1/(a_1^3 - a_2^3)]\{a_1^2[\alpha_1 P(x_1) + \alpha_2 P(x_2) + \\ + \alpha_3 P(x_3)] + a_2^2[\alpha_3 P(x_1) + \alpha_1 P(x_2) + \alpha_2 P(x_3)] + \\ + a_1 a_2[\alpha_2 P(x_1) + \alpha_3 P(x_2) + \alpha_1 P(x_3)]\} = \\ = f(x_1,x_2,x_3) + [1/(a_1^3 - a_2^3)]\{a_1^2[\alpha_1 P(x_2) + \alpha_2 P(x_3) + \\ + \alpha_3 P(x_1)] + a_2^2[\alpha_3 P(x_2) + \alpha_1 P(x_3) + \alpha_2 P(x_1)] + \\ + a_1 a_2[\alpha_2 P(x_2) + \alpha_3 P(x_3) + \alpha_1 P(x_1)]\}$$

The last equation has the general solution

$$f(x_1,x_2,x_3) + [1/(a_1^3 - a_2^3)]\{a_1^2[\alpha_1 P(x_2) + \alpha_2 P(x_3) + \\ + \alpha_3 P(x_1)] + a_2^2[\alpha_3 P(x_2) + \alpha_1 P(x_3) + \alpha_2 P(x_1)] + \\ + a_1 a_2[\alpha_2 P(x_2) + \alpha_3 P(x_3) + \alpha_1 P(x_1)]\} = \\ = p(x_1,x_2,x_3) + p(x_2,x_3,x_1) + p(x_3,x_1,x_2) \qquad (3.49)$$

where p is an arbitrary function $\Re^3 \to \Re$.

By virtue of (3.48) $f(x_1,x_2,x_3) = P(x_1) - P(x_2)$, then from (3.49) it follows that

$$P(x_1) - P(x_2) + [1/(a_1^3 - a_2^3)]\{a_1^2[(\alpha_1 + \alpha_3)P(x_1) + \\ + \alpha_2 P(x_2)] + a_2^2[(\alpha_2 + \alpha_3)P(x_1) + \alpha_1 P(x_2)] + a_1 a_2[(\alpha_1 + \\ \alpha_2)P(x_1) + \alpha_3 P(x_2)]\} = \\ = p(x_1,x_1,x_3) + p(x_1,x_2,x_1) + p(x_2,x_1,x_1) \qquad (3.50)$$

For $x_2 = x_1$ this equality takes the form

$$[(\alpha_1 + \alpha_2 + \alpha_3)(a_1^2 + a_2^2 + a_1 a_2)/(a_1^3 - a_2^3)]P(x_1) = \\ = 3p(x_1,x_1,x_1)$$

which implies

$$P(x_1) = [3(a_1 - a_2)/(\alpha_1 + \alpha_2 + \alpha_3)]p(x_1,x_1,x_1)$$

Now from (3.49) we find the general solution in the form

$$f(x_1,x_2,x_3) = p(x_1,x_2,x_3) + p(x_2,x_3,x_1) + p(x_3,x_1,x_2) - \\ - [3/(a_1^2 + a_2^3 + a_1 a_2)(\alpha_1 + \alpha_2 + \alpha_3)]\{a_1^2[\alpha_1 p(x_2,x_2,x_2) + \\ + \alpha_2 p(x_3,x_3,x_3) + \alpha_3 p(x_1,x_1,x_1)] + a_2^2[\alpha_1 p(x_3,x_3,x_3) + \\ + \alpha_2 p(x_1,x_1,x_1) + \alpha_3 p(x_2,x_2,x_2)] + a_1 a_2[\alpha_1 p(x_1,x_1,x_1) + \\ + \alpha_2 p(x_2,x_2,x_2) + \alpha_3 p(x_3,x_3,x_3)]\} \qquad (3.51)$$

where p: $\Re^3 \to \Re$ must satisfy the following condition derived from (3.50)

$$[3(a_1 - a_2)/(\alpha_1 + \alpha_2 + \alpha_3)][p(x_1,x_1,x_1) - p(x_2,x_2,x_2)] + \\ + [3/(a_1^2 + a_2^3 + a_1 a_2)(\alpha_1 + \alpha_2 + \alpha_3)]\{a_1^2[(\alpha_1 + \\ + \alpha_2)p(x_1,x_1,x_1) + \alpha_2 p(x_2,x_2,x_2)] + a_2^2[(\alpha_2 + \alpha_3)p(x_1,x_1,x_1) + \\ + \alpha_1 p(x_2,x_2,x_2)] + a_1 a_2[(\alpha_1 + \alpha_2)p(x_1,x_1,x_1) + \\ + \alpha_3 p(x_2,x_2,x_2)]\} = p(x_1,x_1,x_2) + p(x_1,x_2,x_1) + p(x_2,x_1,x_1) \qquad (3.52)$$

It is easy to see that (3.52) is an equation of the form

$$p(x_1,x_1,x_2) + p(x_1,x_2,x_1) + p(x_2,x_1,x_1) = \\ = (3 - \gamma)p(x_1,x_1,x_1) + \gamma p(x_2,x_2,x_2) \qquad (3.53)$$

where the real constant γ is given by

$$\gamma = -3(a_1 - a_2)/(\alpha_1 + \alpha_2 + \alpha_3) + 3(a_1^2\alpha_2 + a_2^2\alpha_1 + \\ + a_1 a_2 \alpha_3)/[(a_1^2 + a_2^2 + a_1 a_2)(\alpha_1 + \alpha_2 + \alpha_3)].$$

Lemma 3. 3. Let $f(x_1,x_2,x_3)$ be a function of the form

$$f(x_1,x_2,x_3) = p(x_1,x_2,x_3) + p(x_2,x_3,x_1) + p(x_3,x_1,x_2) \qquad (3.54)$$

such that $f(x_1,x_2,x_3) = 0$. Then

$$f(x_1,x_2,x_3) = U(x_1,x_2,x_3) + U(x_2,x_3,x_1) + U(x_3,x_1,x_2) - \\ - U(x_2,x_1,x_3) - U(x_1,x_3,x_2) - U(x_3,x_2,x_1) \qquad (3.55)$$

where U: $\Re^3 \to \Re$ is an arbitrary function.

Proof. We are looking for a function of the form

$$p(x_1,x_2,x_3) = k_1 q(x_1,x_2,x_3) + k_2 q(x_2,x_3,x_1) + k_3 q(x_3,x_1,x_3) + \\ + k_4 q(x_2,x_1,x_3) + k_5 q(x_1,x_3,x_2) + k_6 q(x_3,x_2,x_1)$$

where k_i $(1 \leq i \leq 6)$ are real constants, satisfying

$$p(x_1,x_1,x_2) + p(x_1,x_2,x_1) + p(x_2,x_1,x_1) = 0 \qquad (3.56)$$

for any function q: $\Re^3 \to \Re$. By a substitution into (3.56) we find

$$k_1 + k_2 + k_3 = k_4 + k_5 + k_6$$

Thus

$$f(x_1,x_2,x_3) = (k_1 + k_2 + k_3)[q(x_1,x_2,x_3) + q(x_2,x_3,x_1) + \\ + q(x_3,x_1,x_2)] - (k_1 + k_2 + k_3)[q(x_2,x_1,x_3) + q(x_1,x_3,x_2) + \\ + q(x_3,x_2,x_1)]$$

If we put

$$U(x_1,x_2,x_3) = (k_1 + k_2 + k_3)\, q(x_1,x_2,x_3)$$

we obtain the representation (3.55).

We note that the representation (3.55) can be obtained from (3.54) by putting

$$p(x_1,x_2,x_3) = U(x_1,x_2,x_3) - U(x_2,x_1,x_3)$$

Let us suppose that $p(x_1,x_2,x_3) = S(x_1) \neq 0$. The equation

$$p(x_1,x_1,x_2) + p(x_1,x_2,x_1) + p(x_2,x_1,x_1) = (3-\gamma)S(x_1) + \gamma S(x_2)$$

has a no constant solution of the form

$$p(x_1,x_1,x_2) = S(x_1)$$

or, more generally,

$$p(x_1,x_2,x_3) = m_1S(x_1) + m_2S(x_2) + (1 - m_1 - m_2)S(x_3)$$

only if $\gamma = 1$. Indeed, we have

$$(\gamma - 1)[S(x_1) - S(x_2)] = 0$$

On the other hand, any $S(x_1) \equiv a$, where a is a real constant, satisfies the last equality.

Let us put

$$p(x_1,x_2,x_3) = \tilde{U}(x_1,x_2,x_3) + S(x_1)$$

Then $\tilde{U}(x_1,x_2,x_3)$ satisfies an equation of the form (3.56) and we have proved this result.

Corollary 3. 4. Let $f(x_1,x_2,x_3)$ be a function of form (3.54) such that $p(x_1,x_2,x_3)$ satisfies (3.53). Then

$$\begin{aligned} f(x_1,x_2,x_3) = {} & U(x_1,x_2,x_3) + U(x_2,x_3,x_1) + U(x_3,x_1,x_2) - \\ & - U(x_2,x_1,x_3) - U(x_1,x_3,x_2) - U(x_3,x_1,x_2) + \\ & + S(x_1) + S(x_2) + S(x_3) \end{aligned}$$

where U: $\Re^3 \to \Re$ is an arbitrary function and S is an arbitrary function $\Re \to \Re$ for $\gamma = 1$, S is equal to a constant $a \in \Re$ otherwise.

Thus from (3.51) we find that $f(x_1,x_2,x_3)$ is given by (3.55) if $\gamma \neq 1$

$$\begin{aligned} f(x_1,x_2,x_3) = {} & S(x_1) + S(x_2) + S(x_3) - [3/(a_1^2 + a_2^2 + \\ & + a_1a_2)(\alpha_1 + \alpha_2 + \alpha_3)]\{a_1^2[\alpha_3S(x_1) + \alpha_1S(x_2) + \\ & + \alpha_2S(x_3)] + a_2^2[\alpha_2S(x_1) + \alpha_3S(x_2) + \alpha_1S(x_3)] + \\ & + a_1a_2[\alpha_1S(x_1) + \alpha_2S(x_2) + \alpha_3S(x_3)]\} + U(x_1,x_2,x_3) + \\ & + U(x_2,x_3,x_1) + U(x_3,x_1,x_2) - U(x_2,x_1,x_3) - \\ & - U(x_1,x_3,x_2) - U(x_3,x_2,x_1). \end{aligned}$$

Now we pass on the case $\alpha_1 + \alpha_2 + \alpha_3 = 0$. Then from (3.45), (3.46) and (3.47) we obtain

$$\begin{aligned} & f(x_3,x_1,x_2) - [1/(a_1^3 - a_2^3)]\{a_1^2[\alpha_1F(x_3,x_1) - \alpha_2F(x_2,x_3)] + \\ & + a_2^2[\alpha_1F(x_1,x_2) - \alpha_2F(x_3,x_1)] + a_1a_2[\alpha_1F(x_2,x_3) - \\ & - \alpha_2F(x_1,x_2)]\} = \\ & = f(x_1,x_2,x_3) - [1/(a_1^3 - a_2^3)]\{a_1^2[\alpha_1F(x_1,x_2) - \\ & - \alpha_2F(x_3,x_1)] + a_2^2[\alpha_1F(x_2,x_3) - \alpha_2F(x_1,x_2)] + \\ & + a_1a_2[\alpha_1F(x_3,x_1) - \alpha_2F(x_2,x_3)]\} \end{aligned} \tag{3.57}$$

The general solution of equation (3.57) is given as

$$\begin{aligned} f(x_1,x_2,x_3) = {} & [1/(a_1^3 - a_2^3)]\{a_1^2[\alpha_1F(x_1,x_2) - \alpha_2F(x_3,x_1)] + \\ & + a_2^2[\alpha_1F(x_2,x_3) - \alpha_2F(x_1,x_2)] + a_1a_2[\alpha_1F(x_3,x_1) - \\ & - \alpha_2F(x_2,x_3)]\} + q(x_1,x_2,x_3) + q(x_2,x_3,x_1) + q(x_3,x_1,x_2) \end{aligned} \tag{3.58}$$

where q: $\Re^3 \to \Re$ is an arbitrary function.

From the equality (3.58) we obtain

$$\begin{aligned} F(x_1,x_2) = {} & [1/(a_1^3 - a_2^3)]\{a_1^2[\alpha_1F(x_1,x_1) - \alpha_2F(x_2,x_1)] - \\ & + a_2^2[\alpha_1F(x_1,x_2) - \alpha_2F(x_1,x_1)] + a_1a_2[\alpha_1F(x_2,x_1) - \\ & - \alpha_2F(x_1,x_2)]\} + q(x_1,x_1,x_2) + q(x_1,x_2,x_1) + q(x_2,x_1,x_1) \end{aligned} \tag{3.59}$$

For $x_2 = x_1$ (3.59) yields

$$F(x_1,x_2) = [(\alpha_1 - \alpha_2)/(a_1 - a_2)]F(x_1,x_1) + 3q(x_1,x_1,x_1) \tag{3.60}$$

If $\alpha_1 - \alpha_2 = a_1 - a_2$, then $q(x_1,x_1,x_1) = 0$ and $F(x_1,x_1) = P(x_1)$, where P is an arbitrary function $\Re \to \Re$. Now we have

$$\begin{aligned} & [1 + a_2(\alpha_1 - a_1)/(a_1^2 + a_2^2 + a_1a_2)]F(x_1,x_2) + \\ & + [a_1(\alpha_1 - a_1)/(a_1^2 + a_2^2 + a_1a_2)]F(x_2,x_1) = \\ & = [\alpha_1(a_1 + a_2) + a_2^2]P(x_1)/(a_1^2 + a_2^2 + a_1a_2) + \\ & + q(x_1,x_1,x_2) + q(x_1,x_2,x_1) + q(x_2,x_1,x_1) \end{aligned} \tag{3.61}$$

First we consider the particular case, $\alpha_1 = a_1$ (then $\alpha_2 = a_2$, $\alpha_3 = a_3 = -(a_1 + a_2)$)

Now

$$F(x_1,x_2) = P(x_1) + q(x_1,x_1,x_2) + q(x_1,x_2,x_1) + q(x_2,x_1,x_1)$$

Thus, we find that the functional equation

$$\begin{aligned} & a_1f(x_1,x_2,x_3) + a_2f(x_2,x_3,x_1) - (a_1 + a_2)f(x_3,x_1,x_2) = \\ & = a_1f(x_1,x_1,x_2) + a_2f(x_2,x_2,x_3) - (a_1 + a_2)f(x_3,x_3,x_1) \end{aligned}$$

has the general solution

$$\begin{aligned} f(x_1,x_2,x_3) = {} & P(x_1) + q(x_1,x_1,x_2) + q(x_1,x_2,x_1) + q(x_2,x_1,x_1) + \\ & + q(x_1,x_2,x_3) + q(x_2,x_3,x_1) + q(x_3,x_1,x_2) \end{aligned}$$

where P: $\Re \to \Re$ is an arbitrary function and q: $\Re^3 \to \Re$ is an arbitrary function satisfying $q(x_1,x_1,x_1) \equiv 0$.

Now we consider equation (3.61) in the general case. With a permutation of the variables x_1 and x_2 we derive the equation

$$\begin{aligned} & [a_1(\alpha_1 - a_1)/(a_1^2 + a_2^2 + a_1a_2)]F(x_1,x_2) + \\ & + [1 + a_2(\alpha_1 - a_1)/(a_1^2 + a_2^2 + a_1a_2)]F(x_2,x_1) = \\ & = [\alpha_1(a_1 + a_2) + a_2^2]P(x_2)/(a_1^2 + a_2^2 + a_1a_2) + \\ & + q(x_2,x_2,x_1) + q(x_2,x_1,x_2) + q(x_1,x_2,x_2) \end{aligned} \tag{3.62}$$

The determinant of the system (3.61), (3.62) is

$$\begin{aligned} & (a_2^2 + a_1\alpha_1 + a_2\alpha_1)(2a_1^2 + a_2^2 - a_1\alpha_1 + a_2\alpha_1)/ \\ & /(a_1^2 + a_2^2 + a_1a_2)^2 \end{aligned} \tag{3.63}$$

If this expression is not 0, then the solution of this system is

$$\begin{aligned} F(x_1,x_2) = {} & [(a_1^2 + a_2^2 + a_2\alpha_1)P(x_1) - a_1(\alpha_1 - a_1)P(x_2)]/ \\ & /(2a_1^2 + a_2^2 - a_1\alpha_1 + a_2\alpha_1) + [(a_1^2 + a_2^2 + a_1a_2)/ \\ & /(a_2^2 + a_1\alpha_1 + a_2\alpha_1)(2a_1^2 + a_2^2 - a_1\alpha_1 + a_2\alpha_1)] \times \\ & \times\{(a_1^2 + a_2^2 + a_2\alpha_1)[q(x_1,x_1,x_2) + q(x_1,x_2,x_1) + \\ & + q(x_2,x_1,x_1)] - a_1(\alpha_1 - a_1)[q(x_2,x_2,x_1) + \\ & + q(x_2,x_1,x_2) + q(x_1,x_2,x_2)]\} \end{aligned}$$

Now let us suppose that the expression (3.63) is 0. First let

$$a_2^2 + \alpha_1(a_1 + a_2) = 0$$

If $a_1 + a_2 = 0$, then $a_1 = a_2 = a_3 = 0$, which is contradiction. Thus

$$\alpha_1 = -a_2^2/(a_1 + a_2),\ \alpha_2 = -a_1^2/(a_1 + a_2)$$

Now (3.58) takes the form

$$f(x_1,x_2,x_3) = [a_1F(x_3,x_1) + a_2F(x_2,x_3)]/(a_1 + a_2) + \\ + q(x_1,x_2,x_3) + q(x_2,x_3,x_1) + q(x_3,x_1,x_2)$$

while (3.61) becomes

$$[a_1/(a_1 + a_2)][F(x_1,x_2) - F(x_2,x_1)] = \\ = q(x_1,x_1,x_2) + q(x_1,x_2,x_1) + q(x_2,x_1,x_1) \qquad (3.64)$$

Equation (3.64) implies

$$q(x_1,x_1,x_2) + q(x_1,x_2,x_1) + q(x_2,x_1,x_1) = 0$$

and

$$F(x_1,x_2) - F(x_2,x_1) = 0$$

i.e.,

$$q(x_1,x_2,x_3) + q(x_2,x_3,x_1) + q(x_3,x_1,x_2) = \\ = U(x_1,x_2,x_3) + U(x_2,x_3,x_1) + U(x_3,x_1,x_2) - U(x_2,x_1,x_3) - \\ - U(x_1,x_3,x_2) - U(x_3,x_2,x_1)$$

where U: $\Re^3 \to \Re$ is an arbitrary function, and

$$F(x_1,x_2) = G(x_1,x_2) + G(x_2,x_1)$$

where G: $\Re^2 \to \Re$ is an arbitrary function.

Thus the general solution of the functional equation

$$a_1f(x_1,x_2,x_3) + a_2f(x_2,x_3,x_1) - (a_1 + a_2)f(x_3,x_1,x_2) = \\ = -[a_2^2/(a_1 + a_2)]f(x_1,x_1,x_2) - [a_1^2/(a_1 + a_2)]f(x_2,x_2,x_3) - \\ - [(a_1^2 + a_2^2)/(a_1 + a_2)]f(x_3,x_3,x_1)$$

is given by the relation

$$f(x_1,x_2,x_3) = \{a_1[G(x_1,x_3) + G(x_3,x_1) + a_2[G(x_2,x_3) + \\ + G(x_3,x_2)]\}/(a_1 + a_2) + U(x_1,x_2,x_3) + U(x_2,x_3,x_1) + \\ + U(x_3,x_1,x_2) - U(x_2,x_1,x_3) - U(x_1,x_3,x_2) - U(x_3,x_2,x_1)$$

Next we suppose that

$$2a_1^2 + a_2^2 - (a_1 - a_2)\alpha_1 = 0$$

Since $a_1 \neq a_2$, we have

$$\alpha_1 = (2a_1^2 + a_2^2)/(a_1 - a_2),\ \alpha_2 = (a_1^2 + 2a_1a_2)/(a_1 - a_2)$$

Now (3.58) takes the form

$$f(x_1,x_2,x_3) = [2a_1F(x_1,x_2) - a_1F(x_3,x_{11}) - a_2F(x_2,x_3)]/ \\ /(a_1 - a_2) + q(x_1,x_2,x_3) + q(x_2,x_3,x_1) + q(x_3,x_1,x_2)$$

while (3.61) becomes

$$[a_1/(a_1 - a_2)][F(x_1,x_2) + F(x_2,x_1) - 2F(x_1,x_1)] = \\ = q(x_1,x_1,x_2) + q(x_1,x_2,x_1) + q(x_2,x_1,x_1) \qquad (3.65)$$

Equation (3.65) implies

$$q(x_1,x_1,x_2) + q(x_1,x_2,x_1) + q(x_2,x_1,x_1) = 0$$

and

$$F(x_1,x_2) + F(x_2,x_1) - 2F(x_1,x_1) = 0$$

i.e.,

$$q(x_1,x_1,x_2) + q(x_1,x_2,x_1) + q(x_2,x_1,x_1) = U(x_1,x_2,x_3) + \\ + U(x_2,x_3,x_1) + U(x_3,x_1,x_2) - U(x_2,x_1,x_3) - \\ - U(x_1,x_3,x_2) - U(x_3,x_2,x_1)$$

where U: $\Re^3 \to \Re$ is an arbitrary function, and

$$F(x_1,x_2) = G(x_1,x_2) - G(x_2,x_1) + c$$

where G: $\Re^2 \to \Re$ is an arbitrary function and $c \in \Re$ is an arbitrary constant.

Thus, the general solution of the functional equation

$$a_1f(x_1,x_2,x_3) + a_2f(x_2,x_3,x_1) - (a_1 + a_2)f(x_3,x_1,x_2) = \\ = [(2a_1^2 + a_2^2)/(a_1 - a_2)]\, f(x_1,x_1,x_2) + \\ + [(a_1^2 + 2a_1a_2)/(a_1 - a_2)]\, f(x_2,x_2,x_3) - \\ - [(3a_1^2 + 2a_1a_2 - a_2^2)/(a_1 - a_2)]\, f(x_3,x_3,x_1)$$

is given by the relation

$$f(x_1,x_2,x_3) = [1/(a_1 - a_2)]\{2a_1[G(x_1,x_2) - G(x_2,x_1)] + \\ + a_1[G(x_1,x_3) - G(x_3,x_1)] - a_2[G(x_2,x_3) - G(x_3,x_2)]\} + c + \\ + U(x_1,x_2,x_3) + U(x_2,x_3,x_1) + U(x_3,x_1,x_2) - U(x_2,x_1,x_3) - \\ - U(x_1,x_3,x_2) - U(x_3,x_2,x_1)$$

Now let $[(\alpha_1 - \alpha_2)/(a_1 - a_2)] = \gamma \neq 1$. Then from (2.60) we find

$$F(x_1,x_1) = [3/(1 - \gamma)]\, q(x_1,x_1,x_1) \qquad (3.66)$$

Now we have

$$[1 + a_2(\alpha_1 - a_1\gamma)/(a_1^2 + a_2^2 + a_1a_2)]F(x_1,x_2) + \\ + [a_1(\alpha_1 - a_1\gamma)/(a_1^2 + a_2^2 + a_1a_2)]F(x_2,x_1) = \\ = 3[\alpha_1(a_1 + a_2) + a_2^2\,\gamma]q(x_1,x_1,x_1)/(a_1^2 + a_2^2 + a_1a_2) \times \\ \times (1 - \gamma) + q(x_1,x_1,x_2) + q(x_1,x_2,x_1) + q(x_2,x_1,x_1) \qquad (3.67)$$

By a permutation of the variables x_1 and x_2 we derive the equation

$$[a_1(\alpha_1 - a_1\gamma)/(a_1^2 + a_2^2 + a_1a_2)]F(x_1,x_2) + \\ + [1 + a_2(\alpha_1 - a_1\gamma)/(a_1^2 + a_2^2 + a_1a_2)]F(x_2,x_1) = \\ = 3[\alpha_1(a_1 + a_2) + a_2^2\,\gamma]q(x_2,x_2,x_2)/(a_1^2 + a_2^2 + a_1a_2) \times \\ \times (1 - \gamma) + q(x_2,x_2,x_1) + q(x_2,x_1,x_2) + q(x_1,x_2,x_2) \qquad (3.68)$$

The determinant of the system (3.67) and (3.68) is

$$[(a_1^2 + a_1a_2)(1 - \gamma) + a_2^2 + (a_1 + a_2)\alpha_1] \times \\ \times [a_1^2(1 + \gamma) + a_1a_2(1 - \gamma) + a_2^2 - (a_1 - a_2)\alpha_1]/ \\ /(a_1^2 + a_2^2 + a_1a_2)^2 \qquad (3.69)$$

If the above expression is not 0, then

$$F(x_1,x_2) = 3[\alpha_1(a_1 + a_2) + a_2^2\,\gamma]/[(a_1^2 + a_1a_2)(1 - \gamma) + \\ + a_2^2 + (a_1 + a_2)\alpha_1]\ \{[a_1^2 + a_2^2 + a_1a_2(1 - \gamma) + a_2\alpha_1] \times \\ \times q(x_1,x_1,x_1) - a_1(\alpha_1 - a_1\gamma)q(x_2,x_2,x_2)\}/ \\ /[a_1^2(1 + \gamma) + a_1a_2(1 - \gamma) + a_2^2 - (a_1 - a_2)\alpha_1] + \\ + (a_1^2 + a_2^2 + a_1a_2)/[(a_1^2 + a_1a_2)(1 - \gamma) + a_2^2 + \\ + (a_1 + a_2)\alpha_1]\ \{[a_1^2 + a_2^2 + a_1a_2(1 - \gamma) + a_2\alpha_1] \times \\ \times [q(x_1,x_1,x_2) + q(x_1,x_2,x_1) + q(x_2,x_1,x_1)] - \\ - a_1(\alpha_1 - a_1\gamma)[q(x_2,x_2,x_1) + q(x_2,x_1,x_2) + q(x_1,x_2,x_2)]\}/ \\ /[a_1^2(1 + \gamma) + a_1a_2(1 - \gamma) + a_2^2 - (a_1 - a_2)\alpha_1]$$

Now let us suppose that the expression (3.69) is 0. First let

$$(a_1^2 + a_1a_2)(1 - \gamma) + a_2^2 + (a_1 + a_2)\alpha_1 = 0$$

Then

$$\alpha_1 = -[a_2^2 + (a_1^2 + a_1a_2)(1 - \gamma)]/(a_1 + a_2),\ \alpha_2 = \\ = -[a_1^2 + (a_2^2 + a_1a_2)(1 - \gamma)]/(a_1 + a_2)$$

Now (3.58) takes the form

$$f(x_1,x_2,x_3) = (1 - \gamma)F(x_1,x_2) + [a_1F(x_3,x_1) + a_2F(x_2,x_3)]/ \\ /(a_1 + a_2) + q(x_1,x_2,x_3) + q(x_2,x_3,x_1) + q(x_3,x_1,x_2),$$

while (3.67) becomes

$$a_1[F(x_1,x_2) - F(x_2,x_1)]/(a_1 + a_2) = q(x_1,x_1,x_2) + \\ + q(x_1,x_2,x_1) + q(x_2,x_1,x_1) - 3q(x_1,x_1,x_1)$$

The last equation implies

$$q(x_1,x_2,x_3) + q(x_2,x_3,x_1) + q(x_3,x_1,x_2) = U(x_1,x_2,x_3) + U(x_2,x_3,x_1) + U(x_3,x_1,x_2) - U(x_2,x_1,x_3) - U(x_1,x_3,x_2) - U(x_3,x_2,x_1) + P(x_1) + P(x_2) + P(x_3)$$

$$F(x_1,x_2) = G(x_1,x_2) + G(x_2,x_1) - (a_1 + a_2)P(x_1)/a_1$$

where U: $\Re^3 \to \Re$, G: $\Re^2 \to \Re$ and P: $\Re \to \Re$ are arbitrary functions. The condition (3.66) yields

$$2G(x_1,x_1) = [(a_1 + a_2)/a_1 + 3/(1 - \gamma)]P(x_1)$$

Next we suppose that

$$a_1^2(1 + \gamma) + a_1a_2(1 - \gamma) + a_2^2 - (a_1 - a_2)\alpha_1 = 0$$

In this case we have

$$\alpha_1 = [a_1^2 + a_1^2(1 + \gamma) + a_1a_2(1 - \gamma)]/(a_1 - a_2)$$
$$\alpha_2 = [a_1^2 + a_2^2(1 - \gamma) + a_1a_2(1 + \gamma)]/(a_1 - a_2)$$

Now (3.58) takes the form

$$f(x_1,x_2,x_3) = \{[a_1(1 + \gamma) + a_2(1 - \gamma)]F(x_1,x_2) - a_1F(x_3,x_1) - a_2F(x_2,x_3)\}/(a_1 - a_2) + q(x_1,x_2,x_3) + q(x_2,x_3,x_1) + q(x_3,x_1,x_2),$$

while (3.67) becomes

$$[a_1/(a_1 - a_2)][F(x_1,x_2) + F(x_2,x_1)] = [3/(a_1 - a_2)][(1 + \gamma)a_1/(1 - \gamma) + a_2]q(x_1,x_1,x_1) + q(x_1,x_1,x_2) + q(x_1,x_2,x_1) + q(x_2,x_1,x_1)$$

If

$$[3/(a_1 - a_2)][(1 + \gamma)a_1/(1 - \gamma) + a_2] \neq -1$$

i.e.,

$$(2 + \gamma)a_1 + (1 - \gamma)a_2 \neq 0,$$

as above we find that

$$q(x_1,x_2,x_3) + q(x_2,x_3,x_1) + q(x_3,x_1,x_2) = U(x_1,x_2,x_3) + U(x_2,x_3,x_1) + U(x_3,x_1,x_2) - U(x_2,x_1,x_3) - U(x_1,x_3,x_2) - U(x_3,x_2,x_1)$$

$$F(x_1,x_2) = G(x_1,x_2) - G(x_2,x_1)$$

and

$$f(x_1,x_2,x_3) = \{[a_1(1 + \gamma) + a_2(1 - \gamma)][G(x_1,x_2) - G(x_2,x_1)] + a_1[G(x_1,x_3) - G(x_3,x_1)] - a_2[G(x_2,x_3) - G(x_3,x_1)]\}/ /(a_1 - a_2) + U(x_1,x_2,x_3) + U(x_2,x_3,x_1) + U(x_3,x_1,x_2) - U(x_2,x_1,x_3) - U(x_1,x_3,x_2) - U(x_3,x_2,x_1)$$

where G: $\Re^2 \to \Re$ and U: $\Re^3 \to \Re$ are arbitrary functions.

If, however

$$(2 + \gamma)a_1 + (1 - \gamma)a_2 = 0$$

then

$$q(x_1,x_2,x_3) + q(x_2,x_3,x_1) + q(x_3,x_1,x_2) = U(x_1,x_2,x_3) + U(x_2,x_3,x_1) + U(x_3,x_1,x_2) - U(x_2,x_1,x_3) - U(x_1,x_3,x_2) - U(x_3,x_2,x_1) + a_1[P(x_1) + P(x_2) + P(x_3)]$$

$$F(x_1,x_2) = G(x_1,x_2) - G(x_2,x_1) + (a_1 - a_2)P(x_1)$$

where P: $\Re \to \Re$ and U: $\Re^3 \to \Re$ are arbitrary functions, and

$$f(x_1,x_2,x_3) = \{a_1[- G(x_1,x_2) + G(x_2,x_1) + G(x_1,x_3) - G(x_3,x_1)] - a_2[G(x_2,x_3) - G(x_3,x_2)]\}/(a_1 - a_2) + (a_1 - a_2)P(x_2) + U(x_1,x_2,x_3) + U(x_2,x_3,x_1) + U(x_3,x_1,x_2) - U(x_2,x_1,x_3) - U(x_1,x_3,x_2) - U(x_3,x_2,x_1)$$

Example 3. 5. Now we will assume as a meniscus the relation (3.6). Let assume further as arbitrary its general solution (3.7) is the function

$$F(x_1,x_2,x_3) \equiv (x_1/\zeta_1)^{2/3} + (x_2/\zeta_2)^{2/3} + (x_3/\zeta_3)^{2/3} = 1$$

where ζ_i $(1 \leq i \leq 3)$ are real constants, then the shape of the meniscus will be given by the expression

$$f(x_1,x_2,x_3) = (\zeta_1^{-2/3} - \zeta_3^{-2/3})x_1^{2/3} + (\zeta_2^{-2/3} - \zeta_1^{-2/3})x_2^{2/3} + (\zeta_3^{-2/3} - \zeta_2^{-2/3})x_3^{2/3}$$

This shows that the shape of the meniscus changes cyclically during the mould cycle.

Remark 3. 6. Also, the above results hold for the vector extension of equation (3.1) of the form

$$a_1f(\boldsymbol{X}_1,\boldsymbol{X}_2,\boldsymbol{X}_3) + a_2f(\boldsymbol{X}_2,\boldsymbol{X}_3,\boldsymbol{X}_1) + a_3f(\boldsymbol{X}_3,\boldsymbol{X}_1,\boldsymbol{X}_2) = \alpha_1f(\boldsymbol{X}_1,\boldsymbol{X}_1,\boldsymbol{X}_2) + \alpha_2f(\boldsymbol{X}_2,\boldsymbol{X}_2,\boldsymbol{X}_3) + \alpha_3f(\boldsymbol{X}_3,\boldsymbol{X}_3,\boldsymbol{X}_1)$$

f: $\Re^3 \to \Re$, where $\boldsymbol{X}_i = (x_{1i},x_{2i},x_{3i})^{\mathrm{T}}$ are real vectors and a_i, α_i $(1 \leq i \leq 3)$ are real constants.

4 GENERALIZED RESULTS

As a natural consequence of the previous considered meniscus equation, we will give the following more general result.

Theorem 4. 1. The generalized meniscus equation

$$\mathrm{E}(f) \equiv \sum_{i=1}^{n} a_i f(x_i,x_{i+1},\ldots,x_{i+n-1}) = \tag{4.1}$$

$$= \sum_{i=1}^{n} a_i f(x_i,x_i,x_{i+1},\ldots,x_{i+n-2}) \; (x_{n+i} \equiv x_i,\, n > 1)$$

where a_i, α_i $(1 \leq i \leq n)$ are real constants, has a solution if the right-hand side of (4.1) satisfies

$$(AC + I)\Lambda[g(x_1,x_2,\ldots,x_{n-1}), g(x_2,x_3,\ldots,x_n),\ldots,g(x_n,x_1,\ldots,x_{n-2})]^{\mathrm{T}} = \mathbf{O} \tag{4.2}$$

where $A = \mathrm{cycl}(a_1,a_2,\ldots,a_n)$, $\Lambda = \mathrm{cycl}(\alpha_1,\alpha_2,\ldots,\alpha_n)$, $g(x_1,x_2,\ldots,x_{n-1}) = f(x_1,x_1,x_2,\ldots,x_{n-1})$, C is any non-zero $n\times n$ cyclic matrix with constant real entries satisfying $ACA + A = O$, O is the $n\times n$ zero matrix and I is the $n\times n$ unit matrix.

If the equality (4.2) holds for some C, then the general solution of equation (4.1) is given by the following formula

$$[f(x_1,x_2,\ldots,x_n),f(x_2,x_3,\ldots,x_n,x_1),\ldots,f(x_n,x_1,\ldots,x_{n-1})]^{\mathrm{T}} = \mathrm{B}[h(x_1,x_2,\ldots,x_n),h(x_2,x_3,\ldots,x_n,x_1),\ldots,h(x_n,x_1,\ldots,x_{n-1})]^{\mathrm{T}} - \Lambda[g(x_1,x_2,\ldots,x_{n-1}),g(x_2,x_3,\ldots,x_n),\ldots,g(x_n,x_1,\ldots,x_{n-2})]^{\mathrm{T}} \tag{4.3}$$

where the non-zero $n\times n$ cyclic matrix B given by

$$B = \mathrm{cycl}(b_1,b_2,\ldots,b_n)$$

satisfies the condition

$$AB = \mathrm{O}$$

and h is an arbitrary real function $\Re^n \to \Re$.

Proof. By a cyclic permutation of the variables in (4.1) we get

$$a_1 f(x_1,x_2,\ldots,x_n) + a_2 f(x_2,x_3,\ldots,x_n,x_1) + \cdots + a_n f(x_n,x_1,\ldots,x_{n-1}) = \alpha_1 g(x_1,x_2,\ldots,x_{n-1}) + \alpha_2 g(x_2,x_3,\ldots,x_n) + \cdots + \alpha_n g(x_n,x_1,\ldots,x_{n-2})$$

$$a_n f(x_1,x_2,\ldots,x_n) + a_1 f(x_2,x_3,\ldots,x_n,x_1) + \cdots + a_{n-1} f(x_n,x_1,\ldots,x_{n-1}) = \alpha_n g(x_1,x_2,\ldots,x_{n-1}) + \alpha_1 g(x_2,x_3,\ldots,x_n) + \cdots + \alpha_{n-1} g(x_n,x_1,\ldots,x_{n-2})$$

$$\vdots$$

$$a_2 f(x_1,x_2,\ldots,x_n) + a_3 f(x_2,x_3,\ldots,x_n,x_1) + \cdots + a_1 f(x_n,x_1,\ldots,x_{n-1}) = \alpha_2 g(x_1,x_2,\ldots,x_{n-1}) + \alpha_3 g(x_2,x_3,\ldots,x_n) + \cdots + \alpha_1 g(x_n,x_1,\ldots,x_{n-2})$$

i.e., in matrix form

$$AF = \Lambda G \tag{4.4}$$

where

$$F = [f(x_1,x_2,\ldots,x_n), f(x_2,x_3,\ldots,x_n,x_1),\ldots,f(x_n,x_1,\ldots,x_{n-1})]^{\mathrm{T}}$$

and

$$G = [g(x_1,x_2,\ldots,x_{n-1}), g(x_2,x_3,\ldots,x_n),\ldots,g(x_n,x_1,\ldots,x_{n-2})]^{\mathrm{T}}$$

We suppose that equation (4.4) has a solution F and C satisfies $ACA + A = O$. Then

$$(AC + I)\Lambda G = (AC + I)AF = (ACA + A)F = \boldsymbol{O}$$

i.e., equation (4.2) must be satisfied. Conversely, let equation (4.2) hold for a cyclic matrix C. Then $- C\Lambda G$ is easily seen to be a solution of equation (4.4):

$$A(- C\Lambda G) = - (AC + I)\Lambda G + I\Lambda G = I\Lambda G = \Lambda G$$

Now let us prove that equality (4.3) gives the general solution of equation (4.1).

Let f be a solution of equation (4.1), which we will write in the form

$$E(f) = L(g) \tag{4.5}$$

We denote by f_h the general solution of the equation $E(f) = 0$, and by f_p we denote a particular solution of equation (4.5).

Then $f = f_h + f_p$ is the general solution of equation (4.5). Indeed

$$E(f_h + f_p) = E(f_h) + E(f_p) = E(g)$$

On the other hand, let f be an arbitrary solution of equation (4.5). Then

$$E(f - f_p) = E(f) - E(f_p) = L(g) - L(g) = 0$$

i.e., $f - f_p$ is a solution of the associated homogeneous equation. So there exists a specialization f_h^* of the expression f_h such that

$$f - f_p = f_h^*, \text{ i.e., } f = f_h^* + f_p$$

Thus $f_h + f_p$ includes all the solutions of equation (4.5).

The general solution of the homogeneous equation $E(f) = 0$ given in matrix form is BH, where

$$\mathrm{H} = [h(x_1,x_2,\ldots,x_n), h(x_2,x_3,\ldots,x_n,x_1),\ldots,h(x_n,x_1,\ldots,x_{n-1})]^{\mathrm{T}}$$

and a particular solution of the equation $E(f) = L(g)$ in matrix form is $- C\Lambda G$, then $F = BH - C\Lambda G$ includes all the solutions of the nonhomogeneous equation.

On the other hand, every function of the form (4.3) satisfies the functional equation (4.1).

Remark 4. 2. The same results hold for the vector extension of equation (4.1) of the form

$$E(f) \equiv \sum_{i=1}^{n} a_i f(\boldsymbol{X}_i,\boldsymbol{X}_{i+1},\ldots,\boldsymbol{X}_{i+n-1}) =$$

$$= \sum_{i=1}^{n} a_i f(\boldsymbol{X}_i,\boldsymbol{X}_i,\boldsymbol{X}_{i+1},\ldots,\boldsymbol{X}_{i+n-2}) \ (\boldsymbol{X}_{n+i} \equiv \boldsymbol{X}_i,\ n > 1)$$

f: $\Re^n \to \Re$, where $\boldsymbol{X}_i = (x_{1i},x_{2i},\ldots,x_{ni})^{\mathrm{T}}$ are real vectors and a_i, α_i $(1 \le i \le n)$ are real constants.

5 MENISCUS STABILITY

The meniscus stability was considered for the first time in [15,16], but only according to definition 2.2 for the solution of the Navier-Stokes equation, including the pressure gradient. Here, we will give a completely new matrix approach to the solution of the meniscus stability problem.

Now we will derive a necessary and sufficient condition for the stability of the meniscus given by the quasicyclic functional equation (4.1), *i.e.,* its matrix form (4.4) using a simple spectral property of compound matrices.

Let $\det A \neq 0$, then relation (4.4) takes the form

$$F = A^{-1}\Lambda G \equiv SG \tag{5.1}$$

where S is also a cyclic matrix.

Definition 5. 1. The quasicyclic functional equation (5.1) is stable if stab(S) < 0.

Proposition 5. 2. For any cyclic matrix $S \in \Re$ it holds

$$\mathrm{stab(S)} = \inf\{\mu(S),\ \mu \text{ is a Lozinskiĭ measure on } \Re^n\} \tag{5.2}$$

Proof. The relation (5.2) obviously holds for diagonizable matrices in view of

$$\mu_{\mathrm{T}}(S) = \mu(TST^{-1}) \ (T \text{ is an invertible matrix}) \tag{5.3}$$

and the first two relations in (2.4). Furthermore, the infimum in (5.2) can be achieved if S is diagonizable. The general case can be shown based on this observation, the fact that S can be approximated by diagonizable matrices in $\Re$ and the continuity of $\mu(\cdot)$, which is implied by the property

$$|\mu(A) - \mu(B)| \le |A - B|$$

Remark 5. 3. From the above proof it follows that

$$\mathrm{stab}(S) = \inf\{\mu_\infty(TST^{-1}),\ T \text{ is invertible}\}.$$

The same relation holds if μ_∞ is replaced by μ_1.

Corollary 5. 4. Let $S \in \Re$. Then $\mathrm{stab}(S) < 0 \Leftrightarrow \mu(S) < 0$ for some Lozinskiĭ measure μ on $\Re^n$.

Theorem 5. 5. For stab(S) < 0 it is sufficient and necessary that stab($S^{[2]}$) < 0 and $(-1)^n$ det(S) > 0.

Proof. Using the spectral property of $S^{[2]}$, the condition stab($S^{[2]}$) < 0 implies that at least one eigenvalue of S can be nonnegative. We may thus suppose that all eigenvalues are real. It is then simple to see that the existence of one and only one non-negative eigenvalue is precluded by the condition $(-1)^n$det(S) > 0.

Theorem 5.5 and Corollary 5.4 lead to the following result.

Theorem 5. 6. Suppose that $(-1)^n$det(S) > 0. Then S is stable if and only if $\mu(S^{[2]}) < 0$ for some Lozinskiĭ measure μ on $\Re^N$, $N = n!/2!(n-2)!$.

Theorem 5. 7. If stab($S^{[2]}(\beta)$) < 0 for $\beta \in (a, b)$, then (a, b) contains no Hopf bifurcation points of $S(\beta)$.

Proof. Let $\beta \rightarrow S(\beta) \in \Re$ be a function that is continuous for $\beta \in (a, b)$. A point $\beta_0 \in (a, b)$ is said to be a Hopf bifurcation point for $S(\beta)$ if $S(\beta)$ is stable for $\beta < \beta_0$, and there exists an eigenvalue $\lambda(\beta)$ of $S(\beta)$ such that $\lambda(\beta) > 0$, while the rest of the eigenvalues of $S(\beta)$ are non-zero for $\beta > \beta_0$. From the proof of Theorem 5.5 we see that stab($S^{[2]}$) $\leq$ 0 precludes the existence of a non-negative eigenvalue of S.

Let S and P be $n \times n$ real cyclic matrices. A subspace $\Omega \in \Re$ is invariant under S if $S(\Omega) \subset \Omega$. S is said to be stable with respect to an invariant subspace Ω if the restriction of S to Ω, $S|_\Omega$: $\Omega \rightarrow \Omega$ is stable. Let the matrix P be such that rank $P = r$ $(1 < r < n)$ and

$$PS = O \tag{5.4}$$

Then Ker$P$ = $\{x \in \Re, Px = 0\}$ satisfies $S(\Re) \subset$ Ker$P$. In particular, Ker$P$ is an $(n-r)$-dimensional invariant space of S. It is of interest to study the stability of S with respect to Ker$P$ when (5.4) holds.

Lemma 5. 8. Let $\Omega \subset \Re$ be a subspace such that $S(\Re) \subset \Omega$ and dimΩ = k < n. Then 0 is an eigenvalue of S, and there exist $n - k$ null eigenvectors that do not belong to Ω.

Proof. Let $\Im$ be the quotient space $\Re/\Omega$. Then $\Re \cong \Omega \oplus \Im$ and $S(\Im) = \{0\}$ since $S(\Re) \subset \Omega$. This establishes the lemma.

Theorem 5. 9. Suppose that P and S satisfy (5.4) and rank$P = r$ $(1 < r < n)$. Then for S to be stable with respect to Ker$P$, it is necessary and sufficient that

1° stab($S^{[r+2]}$) < 0

and

2° $$\limsup_{\varepsilon \to 0+} \text{sign } [\det(\varepsilon I + S)] = (-1)^{n-r}$$

Proof. Let λ_i $(1 \leq i \leq n-r)$ be eigenvalues of $S|_{\text{Ker}P}$. By Lemma 5.8, the eigenvalues of S can be written as

$$\lambda_1, \lambda_2, \ldots, \lambda_{n-r}, 0, \ldots, 0, (r \text{ zeros})$$

and thus $\{\lambda_i + \lambda_j, 1 \leq i < j \leq n - r\} \subset \sigma(S^{[r+2]})$ by the spectral property of additive compound matrices discussed in Section 2. It follows that stab($S^{[r+2]}$) < 0 precludes the possibility of more than one non-negative λ_i $(1 \leq i \leq n - r)$. For $\varepsilon > 0$ sufficiently small

$$\text{sign}[\det(\varepsilon I + S)] = \text{sign}(\varepsilon^r \lambda_1 \cdots \lambda_{n-r})$$

The theorem can be proved using the same arguments as in the proof of Theorem 5.5.

Remark 5. 10. If $r = n$ in (5.4), then P is of full rank and hence $S = O$. If $r = n - 1$, then Ker$P$ is of dimension 1 and thus the eigenvalues of S are λ_1 and 0 of multiplicity $n - 1$. From the above proof we know that Theorem 5.9 still holds in this case, if condition 1° is replaced by tr(S) < 0.

Corollary 5. 11. Suppose that S and P_1 satisfy

$$P_1 S = \beta P_1 \tag{5.5}$$

and rank$P_1 = r$ $(1 < r < n)$. Thus S is stable with respect to KerP_1 if and only if the following conditions hold:

1° stab($S^{[r+2]}$) < $(r + 2)\beta$

and

2° $(\text{sign } \beta)^r (-1)^{n-r} \det(S) > 0$

Proof. Let the matrix P_1 be such that rank$P_1 = r$ $(1 < r < n)$ and (5.5) holds for some scalar $\beta \neq 0$. Then KerP_1 is an invariant subspace of S. Noting that (5.5) is equivalent to $P_1(S - \beta I) = O$, one can apply Theorem 5.9 to $S - \beta I$ and obtain the proof.

6 DISCUSSION

The previous results may be extended in two different ways.

1° A first possible generalization of equation (3.1) is the following functional equation

$$a_1 f_1(x_1,x_2,x_3) + a_2 f_2(x_2,x_3,x_1) + a_3 f_3(x_3,x_1,x_2) = \alpha_1 f_1(x_1,x_1,x_2) + \alpha_2 f_2(x_2,x_2,x_3) + \alpha_3 f_3(x_3,x_3,x_1)$$

f_i: $\Re^3 \rightarrow \Re$, where a_i, α_i $(1 \leq i \leq 3)$ are real constants.

In other words, it means to extend the representation of the meniscus with three unknown functions f_i $(1 \leq i \leq 3)$ instead of by one unknown function f, as was shown in Section 3. This kind of meniscus representation is really much better, but this problem is very hard and it requires a new method of solvability.

If we continue in this way, it will hold for the generalization of equation (4.1) given by the formula

$$E(f) \equiv \sum_{i=1}^{n} a_i f_i(x_i,x_{i+1},\ldots,x_{i+n-1}) = \sum_{i=1}^{n} a_i f_i(x_i,x_i,x_{i+1},\ldots,x_{i+n-2}) \; (x_{n+i} \equiv x_i, n > 1)$$

f_i: $\Re^n \rightarrow \Re$, where a_i, α_i $(1 \leq i \leq n)$ are real constants. This equation is extremely hard and its solution is unknown up to now.

2° A second generalization of equation (3.1) is the vector equation

$$a_1 f_1(\boldsymbol{X}_1,\boldsymbol{X}_2,\boldsymbol{X}_3) + a_2 f_2(\boldsymbol{X}_2,\boldsymbol{X}_3,\boldsymbol{X}_1) + a_3 f_3(\boldsymbol{X}_3,\boldsymbol{X}_1,\boldsymbol{X}_2) =$$
$$= \alpha_1 f_1(\boldsymbol{X}_1,\boldsymbol{X}_1,\boldsymbol{X}_2) + \alpha_2 f_2(\boldsymbol{X}_2,\boldsymbol{X}_2,\boldsymbol{X}_3) + \alpha_3 f_3(\boldsymbol{X}_3,\boldsymbol{X}_3,\boldsymbol{X}_1)$$

f_i: $\Re^3 \to \Re$, where $\boldsymbol{X}_i = (x_{1i},x_{2i},x_{3i})^{\mathrm{T}}$ are real vectors and a_i, α_i $(1 \le i \le 3)$ are real constants.

For equation (4.1) its generalized form is given by the equation

$$E(f) \equiv \sum_{i=1}^{n} a_i f_i(\boldsymbol{X}_i,\boldsymbol{X}_{i+1},\ldots,\boldsymbol{X}_{i+n-1}) =$$
$$= \sum_{i=1}^{n} a_i f_i(\boldsymbol{X}_i,\boldsymbol{X}_i,\boldsymbol{X}_{i+1},\ldots,\boldsymbol{X}_{i+n-2}) \; (\boldsymbol{X}_{n+i} \equiv \boldsymbol{X}_i,\ n > 1)$$

f_i: $\Re^n \to \Re$, where $\boldsymbol{X}_i = (x_{1i},x_{2i},\ldots,x_{ni})^{\mathrm{T}}$ are real vectors and a_i, α_i $(1 \le i \le n)$ are real constants.

Really, in this section the considered equations are more sophisticated than the solved equations in previous sections, but their solutions are extremely difficult and up to now unknown to the author. In any case, their solutions will describe the meniscus form in a way that will be much closer to reality.

7 CONCLUSION

In this work the analyzed meniscus equation shows that it is possible to interpret the meniscus shape with a quasicyclic real functional equation. During continuous steel casting, the shape of the meniscus changes according to the mould cycle. The derived results are appropriate for use in a huge mathematical model for a description of all the appearances on the meniscus considering the technical characteristics of the process.

The mathematical results are summarized as follows:

1) The meniscus equation is completely solved in $\Re^3$, for all possible cases. The induced topology only categorizes the trajectories in an orientation space.
2) The extended form of the meniscus equation is derived too in $\Re^n$ by a compact matrix approach, different from the method used for the solution of the meniscus equation in $\Re^3$.
3) The meniscus stability problem is solved by using a simple spectral property of the compound matrices and Lozinskiĭ measure on $\Re^n$.

In this work the shape of the meniscus during continuous steel casting is considered for the first time as a non-fixed characteristic according to the cyclic operation of the mould. The analysis has shown that it is more appropriate to use this kind of meniscus modeling than some approximate form. It is also shown that the old one-dimensional interpretations of the meniscus may only be used as an approximation.

8 REFERENCES

[1] E. Anzai, T. Shigezumi, T. Nakano, T. Ando, M, Ikeda, *Hydrodynamic behavior of molten powder in meniscus zone of continuous casting mold,* Nippon Steel Tech. Rep. **34** (1987), 31–40

[2] D. R. Bland, *Flux and continuous casting of steel,* IMA J. Appl. Math. **32** (1984), 89–112

[3] W. A. Coppel, *Stability and Asymptotic Behaviour of Differential Equations*, Heath, Boston, 1965

[4] T. Kajitani, K. Okazawa, W. Yamada, H. Yamamura, *Cold model experiment on infiltration of mould flux in continuous casting of steel: Simple analysis neglecting mould oscillations*, ISIJ Int. **46** (2006), 250–256

[5] J. R. King, A. A. Lacey, C. P. Please, P. Wilmott, A. Zarik, *The formation of oscillation marks on continuously cast steel,* Math. Eng. Ind. **4** (1993) 2, 91–106

[6] Y. Meng, B. G. Thomas, *Modeling transient slag-layer phenomena in the shell/mold gap in continuous casting of steel*, Metall. & Mat. Trans. **34B** (2003), 707–725

[7] Y. Meng, Modeling Interfacial Slag Layer Phenomena in Shell/ Mold Gap in Continuous Casting of Steel, Ph. D. Thesis, Univ. Illinois at Urbana-Champaign, Urbana 2004

[8] Y. Meng, B. G. Thomas, *Simulation of microstructure and behavior of interfacial mold slag layers in continuous casting of steel*, ISIJ Int. **46** (2006), 660–669

[9] J. S. Muldowney, *Compound matrices and ordinary differential equations,* Rocky Mountain J. Math. **20** (1990), 857–872

[10] K. Okazawa, T. Kajitani, W. Yamada, H. Yamamura, *Infiltration phenomena of molten powder in continuous casting derived from analysis using Reynolds equation: Part 1, Study Analysis*, ISIJ Int. **46** (2006), 226–233

[11] I. B. Risteski, *Mathematical method for determination of thermal contact resistance between solidifying metal and mold*, Acta Tech. Acad. Sci. Hungary **99** (1986), 333–348

[12] I. B. Risteski, *Mathematical modeling of the casting powder movement in the mould during continuous steel casting*, Zborn. Rad. JUKEM, **13** (1988), 357–363

[13] I. B. Risteski, *Modeling of molten powder velocity in the contact zone between the slab and the mould*, Benelux Métall. **29** (1989), 55–61

[14] I. B. Risteski, *A mathematical model of the conduct of the molten powder in the gap between the mould and the slab in the vicinity of the meniscus*, Int. Steel & Metals Mag. **28** (1990), 661–665

[15] I. B. Risteski, *Modeling of the Appearances in the Meniscus Vicinity during Continuous Slabs Casting*, Inst. Min. & Metall., Skopje 1990

[16] I. B. Risteski, *Mathematical Modeling of the Appearances in the Meniscus Vicinity during Continuous Steel Casting*, Ph. D. Thesis, Univ. Zagreb, 1991

[17] I. B. Risteski, *Meniscus dimensioning during continuous steel casting,* Metals-Alloys-Technologies **26** (1992), 271–274

[18] I. B. Risteski, *A mathematical model of the movement of the molten powder in the vicinity of the meniscus during the continuous casting of steel*, Rev. Metal. Madrid **28** (1992), 288–296

[19] I. B. Risteski, *Solution of a class of complex vector linear functional equations*, Missouri J. Math. Sci. **13** (2001), 195–203

[20] I. B. Risteski, *Matrix method for solving linear complex vector functional equations*, Int. J. Math. & Math. Sci. **29** (2002), 217–238

[21] I. B. Risteski, *Some higher order complex vector functional equations,* Czechoslovak Math. J. **54** (2004), 1015–1034

[22] I. Risteski, V. Covachev, *Complex Vector Functional Equations,* World Scientific, New Jersey – London – Singapore – Hong Kong 2001

[23] I. B. Risteski, V. C. Covachev, *On some general classes of partial linear complex vector functional equations,* Sci. Univ. Tokyo J. Math. **36** (2002), 105–146

[24] Ch. Rudischer, *The Interaction Between Fluid Flow, Heat Transfer and Solidification in a Continuous Casting Mould*, Ph. D. Thesis, Univ. Technol., Vienna 2001

[25] H. Steinrück, Ch. Rudischer, *Numerical investigation of the entrainment of flux into the lubrication gap in continuous casting of steel,* Proc. 5-th World Congress Comp. Mechanics, July 7 – 12,

2002 Vienna, Eds. H. A. Mang, F. G. Rammerstorfer, J. Ebehardsteiner, Univ. Technol., Vienna 2002, 1–16

[26] E. Takeuchi, J. K. Brimacombe, *The formation of oscillation marks in the continuous casting of steel slabs*, Metall. Trans. B, **15B** (1984), 493–509

[27] S. D. R. Wilsson, *The drag-out problem in film coating theory,* J. Eng. Math. **16** (1982), 209–221

[28] A. Yamauchi, *Heat Transfer Phenomena and Mold Flux Lubrication in Continuous Casting of Steel*, Ph. D. Thesis, Royal Inst. Technol., Stockholm 2001

[29] A. Yamauchi, T. EMI, S. Seetharaman, *A mathematical model for prediction of thickness of mould flux film and friction in continuous casting mould*, Int. J. Cast Metals Res. **15** (2002), 345–353

[30] A. Yamauchi, T. Emi, S. Seetharaman, *A mathematical model for prediction of thickness of mould flux film and friction in continuous casting mould*, ISIJ Int. **42** (2002), 1084 – 1093.

UDK 539.42:548.4
Original scientific article/Izvirni znanstveni članek

ISSN 1580-2949
MTAEC9, 41(5)227(2007)

MULTISCALE MODELLING OF SHORT CRACKS IN RANDOM POLYCRYSTALLINE AGGREGATES

VEČNIVOJSKO MODELIRANJE KRATKIH RAZPOK V NAKLJUČNIH VEČKRISTALNIH SKUPKIH

Leon Cizelj, Igor Simonovski

"Jožef Stefan" Institute, Reactor Engineering Division, Jamova 39, 1000 Ljubljana, Slovenia
Leon.Cizelj@ijs.si, Igor.Simonovski@ijs.si

Prejem rokopisa – received: 2006-05-17; sprejem za objavo – accepted for publication: 2007-08-16

The identification and explanation of processes potentially responsible for the initiation and development of intergranular cracks are topics of wide concern. Especially the early phase of the development of cracks seems to be beyond the present state-of-the-art explanations. An effort was therefore made by the authors to construct a computational model of the crack growth kinetics at the grain-size scale. The main idea is to divide continuum (e.g., polycrystalline aggregate) into a set of subcontinua (grains). Random grain structure is modelled using Voronoi-Dirichlet tessellation. Each grain is assumed to be a monocrystal with random orientation of crystal lattice. Elastic behaviour of grains is assumed to be anisotropic. Crystal plasticity is used to describe (small to moderate) plastic deformation of monocrystal grains, caused mainly by the strains along the "incompatible" grain boundaries and at triple points. Finite element method is used to obtain numerical solutions of strain and stress fields. The analysis is currently limited to two-dimensional models. The paper focuses on the dependence of crack tip loading (J-integral) on the random orientation of neighbouring grains. The limited number of calculations indicate that the incompatibility strains, which develop along the boundaries of randomly oriented grains, influence the local stress fields (J-integrals) at crack tips significantly.

Key words: short cracks, random polycrystalline aggregates, multiscale modelling

Spoznavanju in pojasnjevanju procesov, ki bi lahko povzročili nastanek in razvoj medkristalnih razpok, namenjajo raziskovalci po svetu veliko pozornost. Še najmanj raziskane in pojasnjene so zgodnje faze razvoja razpok. Avtorja sta zato sestavila računalniški model napredovanja razpok na nivoju kristalnih zrn. Ključna ideja je razdelitev kontinuuma (večkristalni skupek) na množico med sabo povezanih manjših kontinuumov (kristalno zrno) z uporabo Voronojevega oz. Dirichletovega mozaika. Vsako izmed kristalnih zrn nato opišemo kot monokristal z naključno orientirano kristalno rešetko. Predpostavimo anizotropno elastično vedenje, zmerne plastične deformacije pa opišemo s kristalno plastičnostjo. Veliko plastičnih deformacij povzročijo že nekompatibilnosti specifičnih deformacij ob kristalnih mejah in v trojnih točkah. Deformacijska in napetostna polja računsko ocenimo z metodo končnih elementov. Analize so sedaj omejene na ravninske primere. V članku smo se osredinili na odvisnost vrednosti J-integrala od naključne orientacije okoliških kristalnih zrn. Omejeno število izračunov nakazuje močan vpliv nekompatibilnih deformacij vzdolž kristalnih mej na porazdelitev napetosti ter specifičnih deformacij v okolici razpoke, s tem pa tudi na vrednosti J-integrala.

Ključne besede: kratke razpoke, naključni večkristalni skupki, večnivojsko modeliranje

1 INTRODUCTION

The identification and explanation of processes potentially responsible for the initiation and development of intergranular cracks are topics of wide concern. Despite significant research performed in the past decades, the root mechanisms of intergranular (stress corrosion) cracking (IGC, IGSCC) are still not understood completely. Recent research shows that the intergranular cracking is strongly dominated by the microstructural features, especially those on the grain boundaries.

Computational algorithms aiming at modelling and visualization of the IGSCC initiation and growth on the grain-size scale have already been proposed [1]. Randomness of the grain structure and of the crack initiation and growth processes were assumed. The random crack growth was simulated with algorithms allowing for crack branching, coalescence and interference. The method yielded patterns of cracks with shapes and structure comparable to those observed in experiments. However, a number of potentially important microscopic features (e.g., random orientation and anisotropy of grains, grain boundary mismatch etc.) were not taken into account. A convenient approximation with isotropically elastic continuum was implemented instead, allowing for simplified but efficient estimation of stress intensity factors.

In this paper, the dependence of crack tip loading (J-integral) on the random orientation of neighbouring grains under anisotropic elasto-plastic material response is numerically investigated. The simulation framework [2] relies on explicit models of a random grain structure and finite element solution of the boundary value problem using standard crystal plasticity models. Similar approach has been followed by Simonovski et al [3] while analyzing a transgranular crack emanating from the surface of a polycrystal. A very detailed study of the crack tip opening displacements of short crack in mono- and bi-crystals modelled using standard crystal plasticity models is available in [4].

The results obtained are discussed and compared with solutions for homogeneous isotropic and anisotropic plates. The results obtained are important for the future developments of the already proposed modelling and visualization of the IGSCC initiation and growth at the grain-size scale [1].

2 MODEL

The essential features of the proposed multiscale simulation model are briefly described in this section. Further details are available in [2].

The random grain structure is modelled as a planar Voronoi tessellation representing a cell structure constructed from a Poisson point process by introducing planar cell walls perpendicular to lines connecting neighbouring points. This results in a set of convex polygons embedding the points and their domains of attraction, which completely fill up the underlying space. The concept of Voronoi tessellation has recently been extensively used in materials science, especially to model random microstructures like aggregates of grains in polycrystals, patterns of intergranular cracks and composites.

All tessellations used in this paper were generated using the code VorTESS [5]. Only a subset of Voronoi tessellations is considered suitable for the finite element meshing with quadrilaterals [6].

Constitutive modelling. Each grain (as formed randomly by the Voronoi tessellation) is assumed to be anisotropically elasto-plastic with randomly oriented crystallographic directions. The utilized crystal plasticity model assumes that plastic deformation takes place by simple shear on a specific set of slip planes. A further constitutive assumption is that the shear rate depends on the stress only through the Schmid resolved shear stress.

Detailed description of the constitutive models and algorithmic framework used is given in [7].

Homogenisation. Volume averaging of mesoscopic strain and stress tensors is used to estimate the effective macroscopic stress and strain tensors.

The crack tip loading. The loading of the crack tips is achieved through the prescribed remote macroscopic biaxial stress field. The J-integrals are then calculated for each crack tip using the built–in features of ABAQUS [8], which rely on the Virtual Crack Extension method combined with the divergence theorem, transforming the integration domain onto the area enclosed by the chosen contour.

The scatter caused by the randomly shaped isoparametric finite element meshes at crack tips randomly positioned within Voronoi tessellations has been studied in isotropic continuum and reported as reasonable (e.g., up to about 10 %) elsewhere [9,10]. The accuracy of the J-integral estimates in randomly oriented anisotropically elastic media has been found reasonable in [10].

3 NUMERICAL EXAMPLE

The planar structure with 101 grains is depicted in **Figure 1** with blue lines representing the intact grain boundaries. The red line between points A and B represents cracked grain boundary – a simple straight inclined crack.

The finite element mesh (isoparametric 8-noded quadrilaterals with reduced integration) used in subsequent calculations is depicted in **Figure 1**, too. The loading of the mesh is prescribed by tensile macrostress with magnitudes 600 MPa and 300 MPa in directions X and Y, respectively. The size of the model studied was significantly smaller than the size of a representative volume element (RVE), which has been estimated for a similar non-cracked case to be about 350 grains in elastic and 800 grains in plastic deformation modes [2]. Both essential types of macroscopic boundary conditions were therefore simulated: (1) prescribed macroscopic stress and (2) prescribed macroscopic strain.

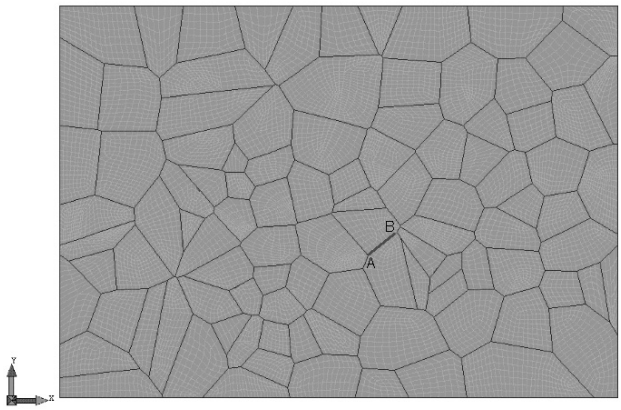

Figure 1: FE Model of a inclined crack in polycrystal
Slika 1: Mreža končnih elementov s poševno razpoko v večkristalnem skupku

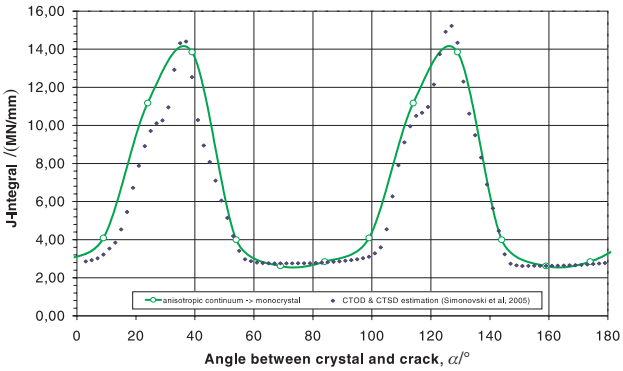

Figure 2: J-integrals and CTOD for an inclined crack in an anisotropic monocrystal (macroscopic equivalent strain of 0.2 %)
Slika 2: Vrednosti J-integrala in CTOD za poševno razpoko v anizotropnem monokristalu (makroskopska ekvivalentna specifična deformacija 0,2 %)

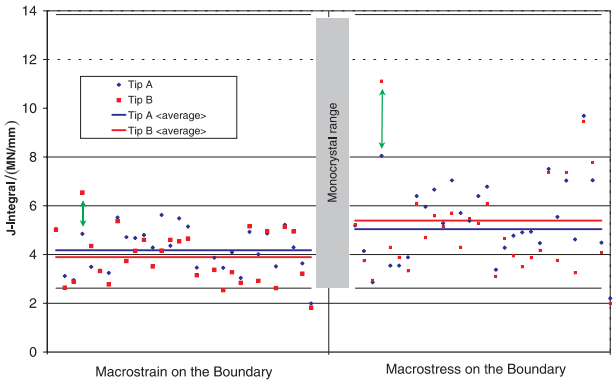

Figure 3: J-integrals and CTOD for an inclined crack in a polycrystal (macroscopic equivalent strain of 0.2 %)
Slika 3: Vrednosti J-integrala in CTOD za poševno razpoko v večkristalnem skupku (makroskopska ekvivalentna specifična deformacija 0,2 %)

Two distinct cases are studied: (1) anisotropic continuum representing a monocrystal and (2) polycrystalline aggregate with grains modelled as randomly oriented anisotropic continua. In both cases, the influence of grain orientations on the magnitude and orientation of the crack tip loading are sought under the assumption of plane strain and both macroscopic boundary conditions.

Reasonably constant estimates of J-Integral were obtained for three different contours. The average value of those three estimates is consistently used in subsequent discussion. The scatter of J-integral in plain strain is presumably governed by the random orientations of grains in the simulated system. It is therefore useful to compare such scatter by the variability of J-integral estimates obtained by assuming an inclined crack in a homogenous anisotropic plate. For this reason, all grains in **Figure 2** were identically oriented (= monocrystal), and material orientations were systematically varied in increments of 15 degrees. Results are given as a function of crack orientation. Additionally, the J integral estimates obtained from scaled Crack Tip Opening and Crack Tip Sliding Displacements (CTOD and CTSD, resp.) in a similar case [3] are also plotted for comparison. Qualitative agreement between J and CTOD&CTSD estimated is deemed reasonable. It should however be noted, that [3] analyzed a surface crack, which might well explain the quantitative differences in the response.

The scatter of J-integral in a polycrystal was studied using 30 realizations of random grain orientations within the fixed grain structure (**Figure 3**). The results are presented for macrostress and macrostrain boundary conditions. Two data points (Tip B and Tip A) are plotted for each realization of random grain orientations and each type of boundary conditions. A rather large difference between J integrals in both crack tips (extremes indicated by green arrows) is found in some cases. This significantly exceeds the finite element numerical error and therefore clearly indicates existence of a preferential crack growth direction as opposed to the well-known symmetric behaviour of such crack in isotopic conditions. The observed scatter seems to be generally consistent with the angular variations of J-integrals in monocrystal.

The total strain of about 0.2 % indicates that the calculations were performed in the neighbourhood of the macroscopic yield strength, with only a subset of grains experiencing plastic deformation. This particular choice is expected to maximize the scatter of J-integrals due to highly scattered microscopic stress and strain fields.

4 CONCLUSIONS

The influence of randomly oriented anisotropic elasto-plastic grains on the microscopic stress fields at crack tips is studied numerically in this paper using Voronoi tessellation and finite element method. The limited number of calculations indicates that the incompatibility strains, which develop along the boundaries of randomly oriented grains, influence the local stress fields (J-integrals) at crack tips significantly.

Results clearly indicate significant difference between the J-integrals at both crack tips. This supports existence of a preferential crack growth direction as opposed to the well-known symmetric behaviour of the same crack in isotopic conditions. It is also a clear indication that mode II represents a significant part of the total crack tip loading. Purely elastic estimates of J integral at the onset of global yielding (0.2% strain) may be more than one order of magnitude lower than those calculated with account for the incompatibility strains along the grain boundaries. The influence of the macroscopic boundary conditions seems to be pronounced at the onset of global plastification.

The results obtained are especially important for the future developments of the modelling and visualization of the initiation and growth of intergranular and transgranular cracks on the grain-size scale.

5 REFERENCES

[1] Cizelj, Leon, Riesch-Oppermann, Heinz. Modeling the early development of secondary side stress corrosion cracks in steam generator tubes using incomplete random tessellation. Nuclear Engineering and Design 212 (**2001**), 21–29
[2] Kovač, Marko. Influence of microstructure on development of large deformations in reactor pressure vessel steel. Dissertation. University of Ljubljana, Slovenia, 2004
[3] Simonovski, Igor, Nilsson, K.-F., Cizelj, L. Crack tip displacements of microstructurally small cracks in 316L steel and their dependance on crystallographic orientations of grains, Fatigue and Fracture of Eng. Materials and Structures 30 (**2007**), 463–478
[4] Potirniche, G.P. Finite element modeling of crack tip plastic anisotropy with application to small fatigue cracks and textured aluminum alloys. Dissertation. Mississippi State University, Mississippi, USA, 2003
[5] Riesch-Oppermann, Heinz. VorTess, Generation of 2-D random Poisson-Voronoi Mosaics as Framework for the Micromechanical

Modelling of Polycristalline Materials. Karlsruhe, Germany: Forschungszentrum Karlsruhe; Report FZKA 6325, 1999

[6] Weyer, Stefan; Fröhlich, Andreas; Riesch-Oppermann, Heinz; Cizelj, Leon, Kovač, Marko. Automatic Finite Element Meshing of Planar Voronoi Tessellations. Engineering Fracture Mechanics 69 (**2002**), 954–958

[7] Huang, Yonggang. A User-material Subroutine Incorporating Single Crystal Plasticity in the ABAQUS Finite Element Program. Cambridge, Massachussets: Harvard University; MECH-178, 1991

[8] Hibbit, Karlsson & Sorensen Inc. ABAQUS/Standard User's Manual, Version 5.8. Pawtucket, R.I., USA: Hibbit, Karlsson & Sorensen Inc., 1998

[9] Kovač, Marko and Cizelj, Leon. Numerical Analysis of Interacting Cracks in Biaxial Stress Field. Proc of Int Conf Nuclear Eergy in Central Europe; Portorož, Slovenia. 1999. 259–266

[10] Cizelj Leon, Kovše, Igor. Short intergranular cracks between randomly oriented anisotropically elastic grains. 4th CNS International Steam Generator Conference, May 5–8, 2002, Toronto, Ontario, Canada. Proceedings. Canadian Nuclear Society, 2002

UDK 539.42:669.14.018.252:621.785
Original scientific article/Izvirni znanstveni članek

ISSN 1580-2949
MTAEC9, 41(5)231(2007)

CHANGES TO THE FRACTURE BEHAVIOUR OF MEDIUM-ALLOYED LEDEBURITIC TOOL STEEL AFTER PLASMA NITRIDING

SPREMEMBE V NAČINU PRELOMA SREDNJE LEGIRANEGA LEDEBURITNEGA JEKLA ZARADI PLAZEMSKEGA NITRIRANJA

Jurči Peter[1], František Hnilica[2], Jiří Cejp[2]

[1]ECOSOND, s. r. o., Křížová 1018, 150 21 Prague 5, Czech Republic
[2]Czech Technical University, Faculty of Mechanical Engineering, Karlovo nám. 2, 121 35 Prague 2, Czech Republic
jurci@ecosond.cz

Prejem rokopisa – received: 2006-09-19; sprejem za objavo – accepted for publication: 2007-07-17

Three-point test specimens made from VANADIS 4 Extra cold-work steel were heat treated using two basic regimes and a different hardness was obtained in each case. The cross-section of the specimens was 10 mm × 10 mm. Plasma nitriding was carried out using various combinations of temperature, processing time and atmosphere. Fracture-toughness tests using the method of static three-point bending showed the dominant role of the presence of a nitrided layer on both the bending strength and the fracture mechanism. Only if the material was not plasma nitrided did the role of the austenitizing temperature become clear, and in this case the higher the temperature, the lower the bending strength. The initiation and the propagation of the fracture were low-energy ductile for the steel that was hardened and tempered. The presence of the plasma-nitrided region on the surface changed the initiation as well as the propagation mechanism to that of cleavage. The thickness of the cleavage region increased as the nitrided region became thicker, which additionally lowered the bending strength.

Key words: Vanadis 4 cold work steel, heat treatment, plasma nitriding, three-point bending strength, fracture surface

Tritočkovni preizkušanci iz jekla Vanadis 4 Ekstra za hladna orodja so bili toplotno obdelani na dva osnovna načina na različno trdoto. Prerez preizkušancev je bil 10 mm × 10 mm. Nitriranje v plazmi je bilo izvršeno z različno kombinacijo temperature, procesiranja in atmosfere. Preizkusi žilavosti loma po metodi tritočkovnega upogiba so pokazali dominantno vlogo nitrirane plasti na upogibno trdnost in na mehanizem preloma, le pri jeklu, ki ni bilo nitrirano, je prišel do izraza vpliv temperature: čim višja je bila temperatura, tem nižja je bila upogibna trdnost. Začetek in propagacija preloma sta bila duktilna-maloenergijska pri kaljenem in popuščenem jeklu. Zaradi nitrirane plasti sta se spremenila začetek in propagacija razpoke v cepljenje. Debelina cepilne plasti je bila večja pri večji debelini nitrirane plasti, kar je dodatno zmanjšalo upogibno trdnost.

Ključne besede: jeklo Vanadis za hladna orodja, toplotna obdelava, nitriranje, tritočkovni upogib, površina preloma

1 GENERAL REMARKS

The ledeburitic steels made via the powder metallurgy (P/M) technique have a considerably finer and much more isotropic microstructure than materials with the same chemical composition produced by the conventional ingot-fabrication route. The favourable structural parameters are reflected in the fracture toughness, which is several times greater than that of conventionally produced steels. To improve the surface hardness and to increase the wear resistance, the steels are nitrided, PVD- or CVD-layered or duplex-coated. The occurrence of surface layers formed by various diffusion processes affects the mechanical properties, markedly improving the wear resistance, hardness, and in many cases also the fatigue strength; however, these layers also lower the fracture toughness. Nevertheless, it is very important to determine exactly the extent of the lowering of the fracture toughness, since this property is a very important parameter for the end-user of the tools.

The powder metallurgy of rapidly solidified particles, which is a common name for the production of the group of materials with an excellent combination of microstructure and properties, is a rapidly expanding area in metallurgy. Many newly developed materials are introduced to industry every year. For these materials, the understanding of their behaviour under the condition of surface layering is of essential importance. In this paper, the results of an investigation of fracture behaviour for the newly developed cold-work steel Vanadis 4 Extra processed with plasma nitriding are presented and discussed.

2 EXPERIMENTAL

Specimens of the steel Vanadis 4 Extra (1.37 % C, 0.43 % Si, 0.38 % Mn, 4.66 % Cr, 3.47 % Mo, 3.65 % V, 0.08 % Cu, Fe bal.) were heat treated (hardened and tempered) in a vacuum furnace to different hardnesses, **Table 1**. Next, the specimens were plasma nitrided in a RUBIG – Micropuls plasma furnace using various combinations of temperature and dwell time (**Table 1**).

The fracture toughness was determined with a three-point bending test, with a distance between the supports of 80 mm. The specimens were loaded at the central point with a loading speed of 1 mm/min up to fracture.

The nitrided layers were investigated using light microscopy (the thickness of the diffusion layer), microhardness tests (depth profiles of the microhardness, Nht*), a WDX analyser (concentration depth profiles), X-ray diffraction (phase constitution of the surface). Scanning electron microscopy was used for the examination of the surface of the fractures.

Table 1: Nitriding of the specimens
Tabela 1: Nitriranje preizkušancev

Specimen set	Hardness HRC	Plasma nitriding
1–4	57	470 °C/30 min/N_2:H_2 = 1:3, 500 °C/60 min/N_2:H_2 = 1:3, 530 °C/120 min/N_2:H_2 = 1:3, 470 °C/30 min + 470 °C/75 min, N_2:H_2 = 1:10
5–8	60	470 °C/30 min/N_2:H_2 = 1:3, 500 °C/60 min/N_2:H_2 = 1:3, 530 °C/120 min/N_2:H_2 = 1:3, 470 °C/30 min + 470 °C/75 min, N_2:H_2 = 1:10

3 RESULTS AND THEIR DISCUSSION

The microstructure of the substrate steel after quenching and tempering to a hardness of *HRC* 57 is shown in **Figure 1**. It consists of a martensitic matrix and fine (several microns) globular carbide particles (Figure 1). The microstructure of the steel processed to a hardness of 60 HRC is similar to that with the hardness of *HRC* 57 (**Figure 2**).

The nitrided region differs from the substrate strongly in terms of etching sensitivity due to the nitride precipitates formed in the near-surface layer; this is typical for all nitrided ledeburitic steels. For the steel processed at a low temperature, the nitrided layer is free of a compound sub-layer (**Figure 3**). For the materials processed at a higher temperature and/or for a longer

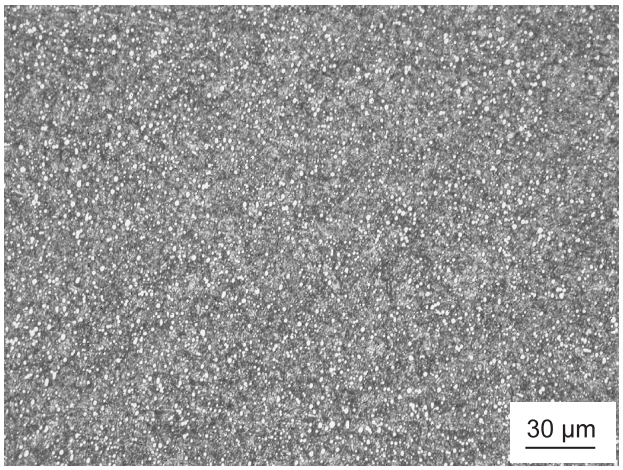

Figure 1: Microstructure of the steel heat treated to *HRC* 57
Slika 1: Mikrostruktura jekla, ki je bilo toplotno obdelano na trdoto *HRC* 57

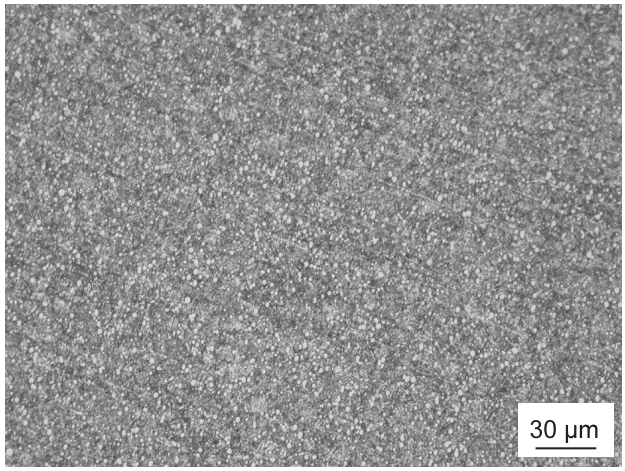

Figure 2: Microstructure of the steel heat treated to *HRC* 60
Slika 2: Mikrostruktura jekla, ki je bilo toplotno obdelano na trdoto *HRC* 60

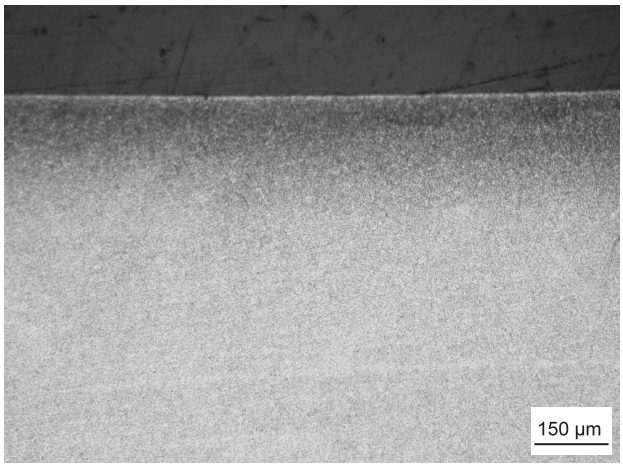

Figure 3: Microstructure of the steel heat treated to *HRC* 57 and nitrided at 470 °C for 30 min
Slika 3: Mikrostruktura jekla, ki je bilo toplotno obdelano na *HRC* 57 in nitrirano 30 min pri 470 °C

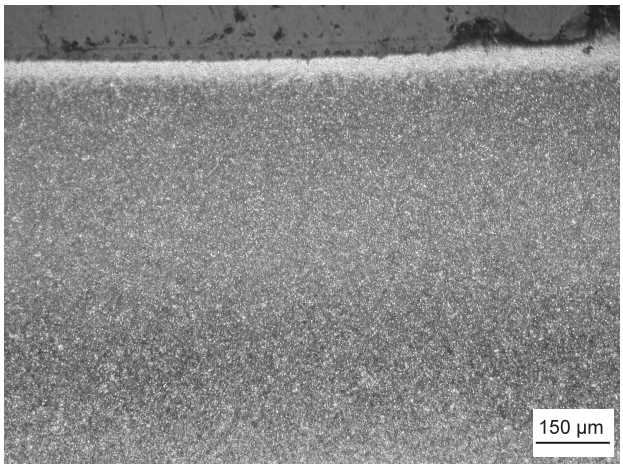

Figure 4: Microstructure of the steel heat treated to *HRC* 57 and nitrided at 530 °C for 120 min
Slika 4: Mikrostruktura jekla, ki je bilo toplotno obdelano na *HRC* 57 in nitrirano 120 min pri 530 °C

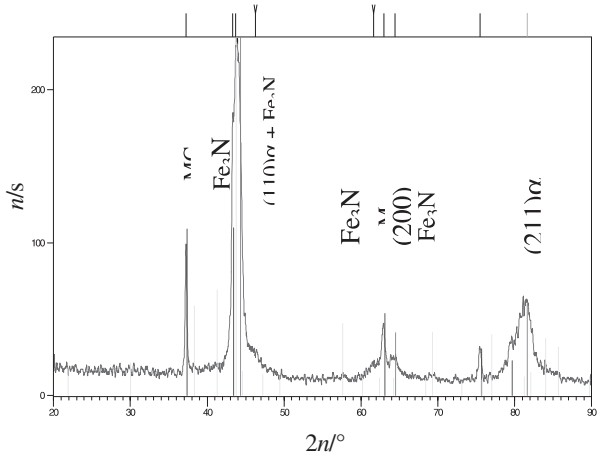

Figure 5: X-ray patterns of the steel, nitrided at 470 °C for 30 min
Slika 5: Rentgenski spekter jekla, ki je bilo nitrirano 30 min pri 470 °C

time, a compound "white" layer is also obtained (**Figure 4**).

The X-ray diffraction spectra show no presence of a compound layer on the surface of the specimens processed at 470 °C for 30 min. The surface microstructure consists of martensite and 13 % is the ε-nitride (**Figure 5**). On the other hand, up to 70 % of the ε-nitride was found in the case of the specimen processed at 530 °C for 120 min. This definitely indicates the presence of a compound layer with a thickness of several μm (**Figure 6**).

The input of nitrogen into the surface induces a considerable surface hardness increase. The hardness is also increased below the surface and the thickness of the region with elevated hardness is related to the diffusion depth of nitrogen. The initial hardness of the material does not have any substantial effect on the surface hardness, but influences slightly the depth of the nitrided region, according to the criterion: core hardness $HV_{0.05}$ = 50 (**Figures 7 and 8**).

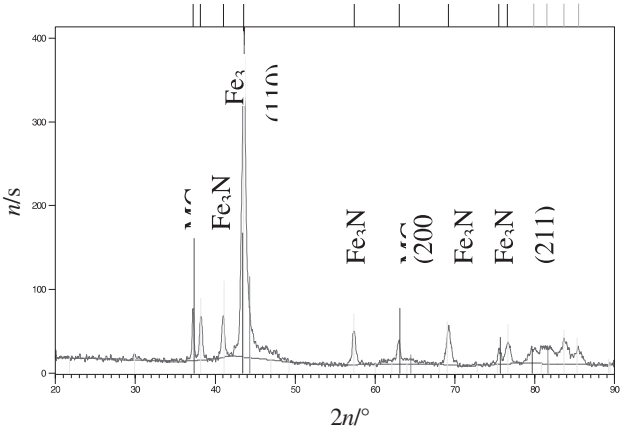

Figure 6: X-ray patterns of the steel, nitrided at 530 °C for 120 min
Slika 6: Rentgenski spekter jekla, ki je bilo nitrirano 120 min pri 530 °C

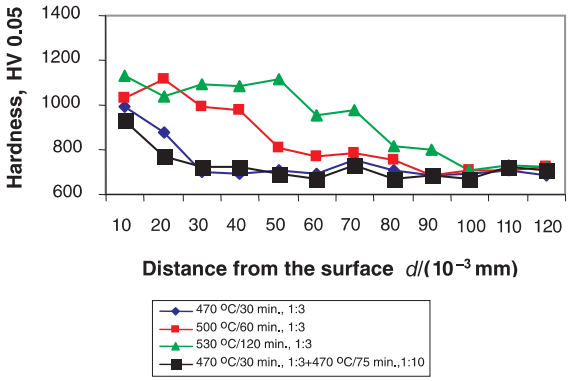

Figure 7: Hardness depth profiles of the nitrided steel with a core hardness of *HRC* 57
Slika 7: Globinski profil trdote nitriranega jekla s trdoto jekla *HRC* 57

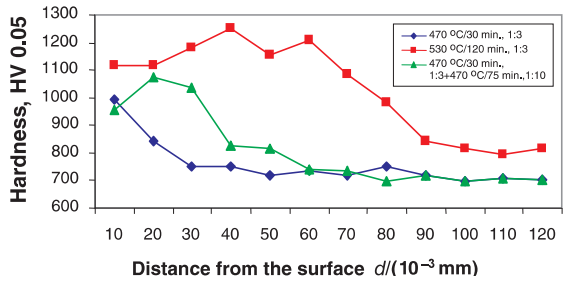

Figure 8: Hardness depth profiles of the nitrided steel with a core hardness of *HRC* 60
Slika 8: Globinski profil trdote nitriranega jekla s trdoto jekla *HRC* 60

Figure 9 shows how the bending strength changes when the core hardness, nitriding temperature and the processing dwell time are increased. It is evident that the austenitising temperature, resulting in a different core hardness, is a relevant factor influencing the three-point bending strength only when the steel is not nitrided. In the nitrided steel, the presence of the nitrided layer by itself lowers the bending strength considerably and the austenitizing temperature does not play a significant role. The bending strength is decreased if the thickness of the nitrided region is increased. It is also important that the diffusion annealing in a nitrogen-poor atmosphere (the

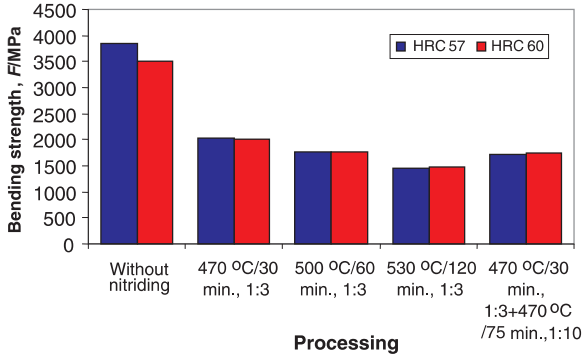

Figure 9: Bending strength as a function of nitriding parameters and core hardness
Slika 9: Upogibna trdnost pri različnih parametrih nitriranja in trdoti jekla

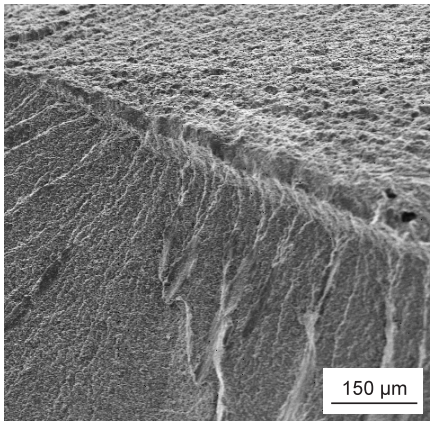

Figure 10: Fracture surface of un-nitrided specimen, processed to *HRC* 57
Slika 10: Prelomna površina preizkušanca s trdoto *HRC* 57, ki ni bil nitriran

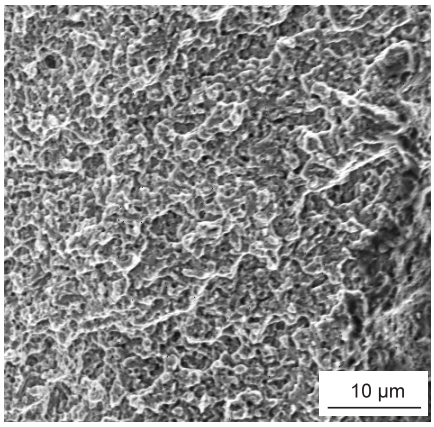

Figure 11: Fracture surface of the specimen in **Figure 10**
Slika 11: Prelomna površina preizkušanca s **slike 10**, detail

last two columns) does not lead to an improvement in the bending strength.

The bending strength of the non-nitrided Vanadis 4 Extra steel is higher than that of Vanadis 6 and comparable with that of M2-type steel [5]. The nature of the difference was not explained so far; however, it can be assumed that Vanadis 4 Extra differs from Vanadis 6 in the molybdenum content and that molybdenum nitride particles can affect the bending strength in an undesirable way. Nevertheless, the M2-type steel also contains molybdenum and the bending strength of the nitrided material remained much higher. Further and more detailed investigations are needed to make a more reliable conclusion about the cause of the change in the bending strength after nitriding.

The fractographical analysis was designed to investigate the fracture initiation and propagation for specimens with and without a nitrided region of different thickness.

In all of the specimens the fracture is initiated on the tensile strained side, in several centres, and propagated in the specimen (**Figure 10**). The crack propagation is different for the non-nitrided and nitrided samples. In the case of the non-nitrided material, the propagation of the crack occurs with the de-cohesion at the carbide-matrix interface and the fracture surface exhibits a shallow dimpled morphology (**Figure 11**). The crack propagation does not consume a large amount of energy, since the dimples are relatively flat and the plastically deformed volume of steel is not large. For this reason, this type of fracture is low-energy transcrystalline. Similarly, as for steel Vanadis 6, a lower austenitizing temperature did not change the mechanism of the failure and only some secondary cracks were observed at the surface [5].

The steel austenitized at a lower temperature had a higher fracture toughness because of its smaller grain size. The austenite grain size increased with the temperature and the products of the austenite decomposition (like martensite) were coarser, too. These phenomena are well known as the limiting ones for the fracture toughness and can explain the obtained results of the three-point bending strength.

The mechanism of fracture initiation in the case of the nitrided specimens differs a great deal from that of the non-nitrided specimens. The fracture clearly exhibits the characteristics of transcrystalline cleavage (**Figure 12**) with the thickness of the cleavage layer corresponding to that of the nitrided region. At higher magnification, small steps are visible on the cleavage facets, indicating the microcracks' propagation at different levels of the same lattice plane. The investigations on various ledeburitic steels showed that the microstructure of the nitrided steel consisted of martensitic platelets containing nitrogen, and ultra-fine nitride particles [6]. Coarser nitride particles are broken during the propagation of the crack and can act as nuclei for the crack re-initiation. In the SEM micrograph in **Figure 14**, the case of a brittle particle with spokewise cracks propagating in the surrounding area is shown. The steps on the cleavage facets can be related to the platelet shape of martensite. **Figure 15** shows that in the core

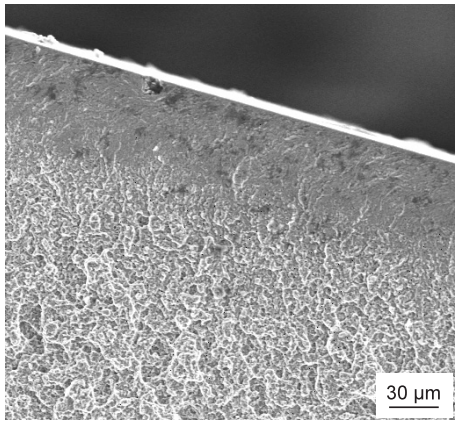

Figure 12: Fracture surface of specimen nitrided at 530 °C for 120 min
Slika 12: Prelomna površina preizkušanca, ki je bil nitriran 120 min pri 530 °C

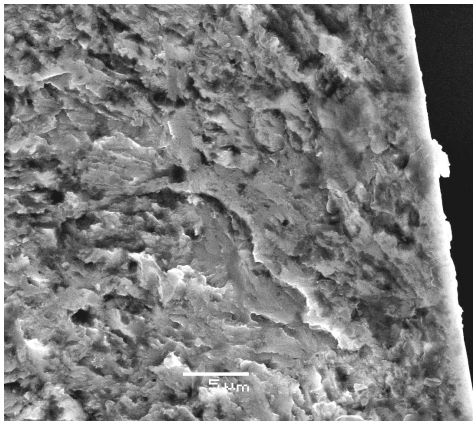

Figure 13: Fracture surface of the specimen in **Figure 12**
Slika 13: Prelomna površina preizkušanca s **slike 12**, detail

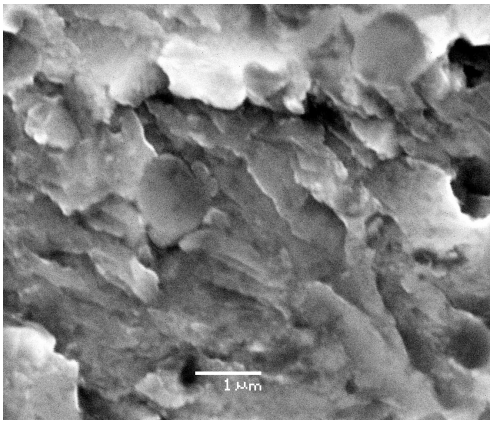

Figure 14: Fracture surface of the specimen in **Figure 12**, detail of cleavage facets
Slika 14: Prelomna površina preizkušanca s **slike 12**, detail s cepilnimi facetami

material, the fracture propagates again according to the trancrystalline low-energy ductile mechanism with de-cohesion at the carbide-matrix interface and a small plastic deformation.

The lowering of the bending strength after the plasma nitriding is due to the fact that cleavage crack propagation requires only a negligible plastic deformation. All of the energy input into the material is spent only for the formation of two new surfaces. This is a different, when compared to the non-nitrided material, where a low plastic deformation occurs throughout the specimens and, as a consequence, the three-point strength was considerably higher. The lowering of the fracture toughness at an increased nitriding temperature and/or time can be explained by the fact that the area of cleavage of the total cross-sectional area is greater due to the thickness of the nitrided layer.

Based on the results presented in this work as well as in the papers published previously [5,6] it seems that the lowering of the bending strength, and fracture toughness in general, due to the occurrence of a nitrided region of the surface, is a systematic phenomenon and cannot be

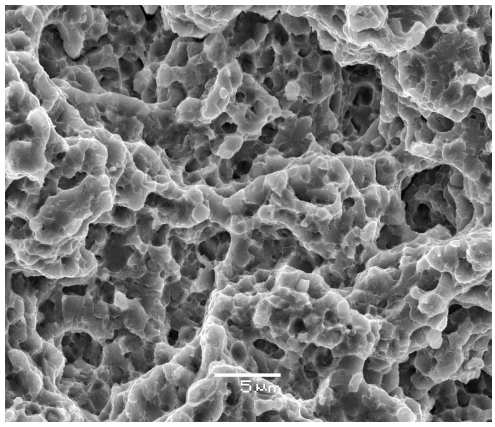

Figure 15: Fracture surface of the specimen in **Figure 12**, core steel
Slika 15: Prelomna površina preizkušanca s **slike 12**, jedro preizkušanca

avoided completely. On the other hand, the nitriding brings several beneficial effects to the materials and components, such as an increase in the fatigue lifetime of the specimens and tools, and an improvement in the wear resistance, corrosion resistance, adhesion of thin PVD layers, etc. Therefore, the nitriding will be required from industrial producers and/or users of tools. It is, therefore, necessary to minimize the lowering of the fracture toughness, through the optimization of the nitriding process.

4 CONCLUDING REMARKS

- In the case of the non-nitrided steel, the austenitizing temperature has an important influence on the fracture behaviour. The three-point bending strength decreases as the austenitizing temperature increases because of the grain coarsening at the higher austenitizing temperature.
- The main mechanism of the fracture initiation is the nucleation of dimples at the carbide-matrix interface in the case of non-nitrided specimens. The fracture propagation is ductile and low energy.
- The presence of the plasma-nitrided layer at the surface lowers significantly the bending strength. The thicker is the nitrided layer the lower is the fracture toughness, since the cleavage region, where a small amount of energy is spent for the crack propagation, in greater with a thicker nitrided region.
- The lowering of the bending strength for the steel Vanadis 4 Extra is more remarkable than that for the steels Vanadis 6 and M2, processed in the same nitriding conditions.
- Transcrystalline cleavage was found to be the main mechanism of crack propagation in the case of nitrided layers. The thickness of the cleavage regions corresponds well with the thickness of the nitrided regions determined by metallographic methods.

ACKNOWLEDGEMENTS

The authors wish to thank the Ministry of Education and Youth of the Czech Republic for the financial support for the solution of the Project Eureka E!3437 PROSURFMET.

5 LITERATURE

[1] Jurči, P., Suchánek, J., Stolař, P.: In.: Proceedings of the 5th ASM Heat Treatment and Surface Engineering Conference in Europe, 7–9 June 2000, Gothenburg, Sweden, 197

[2] Jurči, P., Suchánek, J., Stolař, P., Hnilica, F., Hrubý, V.: In.: Proceedings of the European PM 2001 Congress, October 22–24, 2001, Nice, France, 303–308

[3] Musilová, A., Jurči, P.: Acta Metallurgica Slovaca, 7 (**2001**), 1, Special Issue METALLOGRAPHY 01, Gabriel Janák, 25–27 April 2001, Stará Lesná, Slovak republic, 265–268

[4] Jurči, P., Hnilica, F.: Powder Metallurgy Progress, 3 (**2003**)1, 10–19

UDK 539.42:691.49:546.831
Original scientific article/Izvirni znanstveni članek

ISSN 1580-2949
MTAEC9, 41(5)237(2007)

THE FRACTURE AND FATIGUE OF SURFACE-TREATED TETRAGONAL ZIRCONIA (Y-TZP) DENTAL CERAMICS

PRELOM IN UTRUJENOST POVRŠINSKO OBDELANE TETRAGONALNE (Y-TZP) DENTALNE KERAMIKE

Tomaž Kosmač[1], Čedomir Oblak[2], Peter Jevnikar[2]

[1]Jožef Stefan Institute, Jamova 39, 1001 Ljubljana, Slovenia;
[2]Faculty of Medicine, University of Ljubljana, Vrazov trg 2, 1101 Ljubljana, Slovenija
tomaz.kosmac@ijs.si

Prejem rokopisa – received: 2006-05-17; sprejem za objavo – accepted for publication: 2007-06-26

The effects of dental grinding and sandblasting on the biaxial flexural strength of Y-TZP ceramics containing the mass fraction of 3 % yttria were evaluated. Dental grinding at high rotation speed lowers the mean strength under static loading and the survival rate under cyclic loading. Sandblasting, in contrast, may provide a powerful tool for surface strengthening also resulting in a substantially higher survival rate under cyclic loading. Fractographic examination of ground specimens revealed that failure originated from radial cracks extending up to 50 μm from the grinding groves into the bulk of the material. However, no evidence of grinding-induced surface cracks could be obtained by SEM analysis of the ground samples, prepared by a standard bonded-interface technique. Sandblasting, in contrast, introduces lateral cracks, which are not detrimental to the strength of Y-TZP ceramics. The "medical-grade" Y-TZP ceramics also containing 0.25 % of dispersed alumina used in this work exhibited full stability under hydrothermal conditions.

Key words: tetragonal zirconia; dental grinding; sandblasting; fracture origin; fatigue

Ocenjen je bil vpliv zobnih brušenj in peskanja na dvoosno upogibno trdnost keramike Y-TZP z molskim deležem itrijevega oksida 3 %. Zobno brušenje pri veliki hitrosti vrtenja zmanjša trdnost pri statični obremenitvi in trajnostno dobo pri ciklični obremenitvi. Nasprotno pa je peskanje lahko učinkovit način za utrditev površine, ki pomembno poveča tudi trajnostno dobo pri ciklični obremenitvi. Fraktografsko opazovanje brušenih preizkušancev je pokazalo, da se je prelom začel iz radialnih razpok v globino do 50 μm iz dna brusilnih žlebov v notranjost preizkušanca, čeprav pri SEM pregledu ni bila odkrita nobena površinska brusilna razpoka na brušenih preizkušancih, pripravljenih po standardni površinsko vezani tehniki. Peskanje nasprotno od brušenja ustvari lateralne razpoke, ki ne vplivajo na trdnost keramike Y-TZP. Tetragonalna (Y-TZP) keramika za medicinske namene, ki vsebuje tudi 0,25 % dispergiranega aluminijevega oksida in je bila uporabljena v tem delu, je bila popolnoma stabilna v hidrotermalnih razmerah.

Ključne besede: tetragonalni cirkonijev oksid, zobno brušenje, peskanje, začetek razpoke, utrujenost

1 INTRODUCTION

Yttria partially stabilized tetragonal zirconia (Y-TZP) has become increasingly popular as an alternative high-toughness core material in dental restorations because of its biocompatibility, acceptable aesthetics and attractive mechanical properties. Compared to other dental ceramics, the superior strength, fracture toughness and damage tolerance of Y-TZP are due to a stress-induced transformation toughening mechanism operating in this particular class of ceramics [1]. Y-TZP is currently used as a core material in full-ceramic crowns and bridges, implant superstructures, orthodontic brackets and root dental posts [2–5]. Like most technical ceramics, zirconia dental restorations are produced by dry- or wet-shaping of ceramic green bodies which are than sintered to high density. For the material's selection and microstructural design the following two criteria should be taken into consideration: the damage tolerance upon mechanical surface treatment and the aging behavior in an aqueous environment. Dental grinding is involved in reshaping and the final adjustment of the prosthetic work, whereas sandblasting is commonly used to improve the bond between the luting agent and the prosthetic work. Because Y-TZP ceramics exhibit a stress-induced transformation, the surface of the mechanically treated prosthetic work is expected to be transformed into the monoclinic form, i.e. constrained, and also damaged. Under clinical conditions, where dental restorations are exposed to thermal and mechanical cycling in a chemically active aqueous environment over long periods, these grinding- and impact-induced surface flaws may grow to become stress intensifiers, facilitating fracture at lower levels of applied stress. Furthermore, with prolonged time under clinical conditions the metastable tetragonal zirconia may start transforming spontaneously into the monoclinic structure [6]. This transformation is diffusion-controlled and is accompanied by extensive microcracking, which ultimately leads to strength degradation [7]. Therefore, extensive research work was undertaken to evaluate the effects of mechanical surface treatment and aging on the strength and reliability of various Y-TZP ceramics.

In our previous studies [8,9] we have shown that dental grinding using a coarse-grit diamond burr at a high rotation speed lowers the mean strength and reliability, whereas sandblasting improves the mean strength, at the expense of somewhat lower reliability. The fine-grained materials exhibited higher strength after sintering, but they were less damage tolerant upon grinding than tougher, coarse-grained materials. Standard grade 3Y-TZP ceramics were more susceptible to low-temperature degradation than a special, corrosion resistant 3Y-TZP grade also containing a small amount of dispersed alumina. Besides, no grain-size dependence of the diffusion-controlled transformation was observed with this material. Based on these results, coarse-grained zirconia containing a small amount of alumina was suggested for dental applications.

Here we report on the fracture and fatigue of surface-treated tetragonal zirconia (Y-TZP) dental ceramics. Fracture mechanics was used to calculate the effective length of mechanically induced surface flaws acting as the stress concentrators, relative to the depth of the stress-induced surface compressive layer which contributes to strengthening. The results were verified by a conventional fractographic examination as well as by SEM analysis of surface-treated samples, which were prepared by a standard bonded-interface technique.

2 EXPERIMENTAL WORK

Disc-shaped specimens ((15.5 ± 0.03) mm in diameter ad (1.5 ± 0.03) mm thick) were fabricated from a commercially available ready-to-press Y-TZP powder (TZ-3YSB-E, Tosoh, Japan) containing the mass fraction of yttria 3 % in the solid solution and a 0.25 % alumina addition to suppress the t-m transformation during aging, by uniaxial dry pressing and pressureless sintering in air for 4 h at 1450 °C and 1550 °C, respectively.

After firing, the top surface of the specimens was submitted to a different surface treatment. A coarse grit (150 μm) and a fine grit (50 μm) diamond burr were chosen for dry and wet surface grinding, in order to simulate clinical conditions. The grinding load of about 100 g was exerted by finger pressure, the grinding speed was 150,000 r/min. For sandblasting, discs were mounted in a sample holder at a distance of 30 mm from the tip of the sandblaster unit, equipped with a nozzle of 5 mm in diameter. Samples were sandblasted for 15 s with 110 μm fused alumina particles at 4 bar. Before and after each surface treatment the samples were analyzed by XRD, using CuKα radiation. The relative amount of transformed monoclinic zirconia on the specimens' surfaces was determined according to the method of Garvie and Nicholson [10]. The thickness of the transformed surface layer of surface-treated samples was calculated using the x-ray determination method [11]. Although this method yields conservative values, it can be used to compare the influence of various surface treatments on the thickness of the surface compressive layer.

Aging of pristine and mechanically treated materials in an aqueous environment was performed under isothermal conditions at 140 °C for 24 h. After aging, specimens were analysed by XRD for phase composition.

Biaxial flexural strength measurements were performed according to ISO 6872 at a loading rate of 1 mm/min. Surface-treated specimens were fractured with the surface treated side under tension. The load to failure was recorded for each disc and the flexural strength was calculated using the equations of Wachtman et al.[12]. The variability of the flexural strength values was analyzed using the two-parameter Weibull distribution function.

Cyclic loading experiments were performed using an Instron Ltd, Model 8871 machine. The load varied from 50 N to 850 N at a freqency of 15 Hz. After 10^6 cycles the specimens were "statically" loaded to fracture. For specimens which failed before one milion cycles The number of cycles to failure was registered.

After biaxial flexural strength measurements the fracture surfaces were examined by SEM. The existence of grinding- and sandblasting-induced sub-surface flows was evidenced by SEM analysis of polished interfaces perpendicular to the ground and sandblasted surface, respectively. For this examination, specimens were prepared using a standard bonded-interface technique, as described elsewhere [13].

3 RESULTS AND DISCUSSION

The main characteristics of the sintered materials are listed in **Table 1**. The relative density of sintered specimens exceeded 99 % of the theoretical value and they were 100 % tetragonal. An SEM micrograph of the sintered material, showing equiaxed grains with the mean size of 0.57 μm, is represented in **Figure 1**.

Table 1: Sintering conditions and main characteristics of sintered ceramics
Tabela 1: Pogoji sintranja in osnovne značilnosti sintrane keramike

Sintering conditions	Mean grain size d/μm	Flexural strength MPa (SD)	K_{Ic} MPa $m^{1/2}$ (SD)
1450 °C/4 h	0.51	1080 (75)	5.08 (0.10)
1550 °C/4 h	0.59	990 (111)	5.18 (0.12)

Tosoh, Tokyo, Japan

During dental grinding, tens of μm of material were removed by a single pass as the burr was moved back and forth across the surface and the process was always accompanied by extensive sparking. During sandblasting about 60 μm of material was uniformly removed but sparks were not observed during this operation. Microscopic examination of the ground and sandblasted samples revealed that in both cases the materials surface

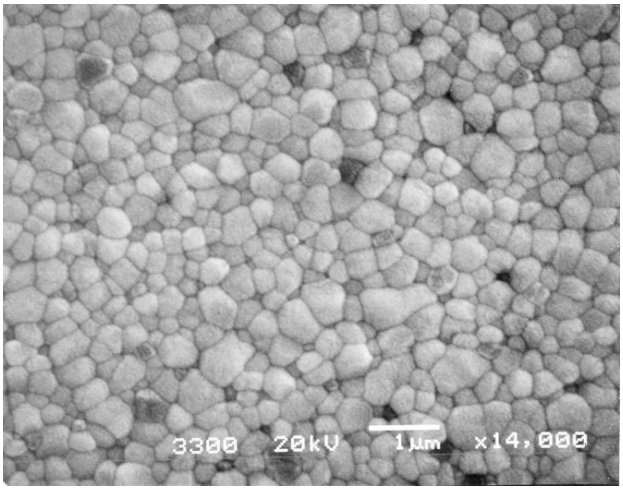

Figure 1: SEM micrograph showing the microstructure of sintered tetragonal zirconia

Slika 1: SEM-posnetek, ki prikazuje mikrostrukturo sintranega cirkonijevega oksida

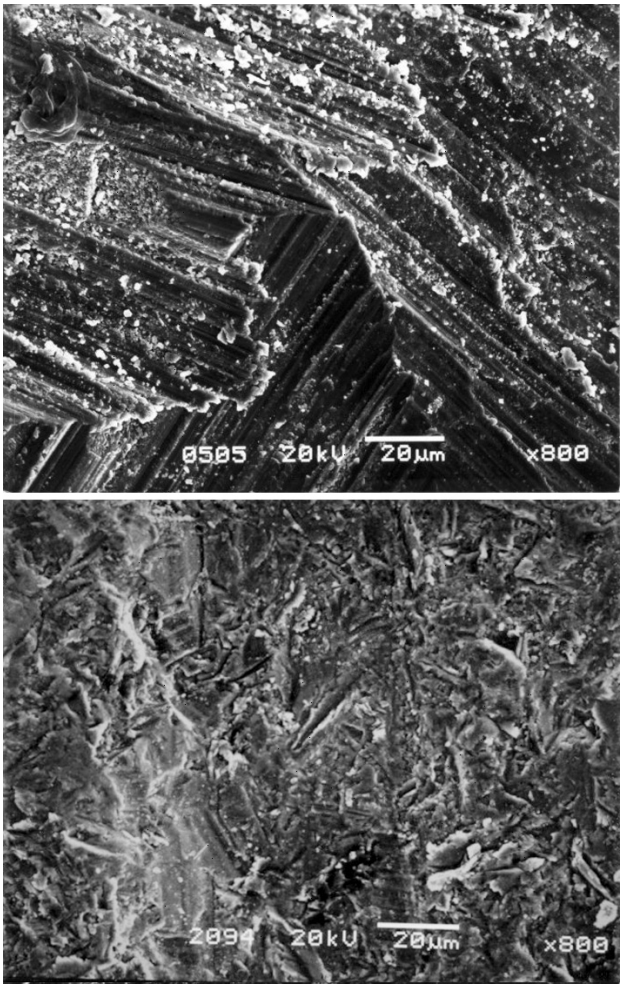

Figure 2: SEM micrographs showing Y-TZP surface morphology after: A) dry grinding using 150 µm diamond burr and B) sandblasting

Slika 2: SEM-posnetka, ki prikazujeta morfologijo površine keramike Y-TZP po: A) suhem brušenju z diamantnim brusom 150 µm in B) po peskanju

was in part plastically deformed (**Figure 2**). The depth of the intersecting grinding grooves and parallel grit scratches, representing the most characteristic feature of the ground surface morphology, varied with the diamond grit size. The eroded surface was wrinkled with sharp, randomly oriented scores, and surface pits were readily observed on an otherwise plain sandblasted surface. In spite of high stresses during grinding the amount of transformed zirconia on the ground surfaces was almost negligible, and so was the transformed zone depth, as calculated from the relative amounts of the monoclinic phase. It is assumed that during grinding the locally developed temperatures exceeded the m->t transformation temperature and the reverse transformation occurred. Higher amounts of the monoclinic zirconia, about 15–17%, were detected on sandblasted samples, which yielded the transformed-zone depth values ranging from 0,3 µm to 0,5 µm. It is interesting to note that these values roughly correspond to the mean grain size of the sintered ceramics.

The mean values of biaxial flexural strength and the respective standard deviations are graphically represented in **Figure 3**. Dental grinding evidently lowered the mean strength, whereas sandblasting provided a powerful tool for strengthening. The counteracting effect of dental grinding and sandblasting on flexural strength can be explained by considering two competing factors influencing the strength of surface treated Y-TZP ceramics: residual surface compressive stresses, which contribute to strengthening, and mechanically induced surface flaws, which cause strength degradation [8].

Since almost no monoclinic zirconia was detected on the ground specimens, the contribution of the grinding-induced strengthening must have been negligible, regardless of grinding conditions used and the material tested. The strength of ground materials is thus mainly

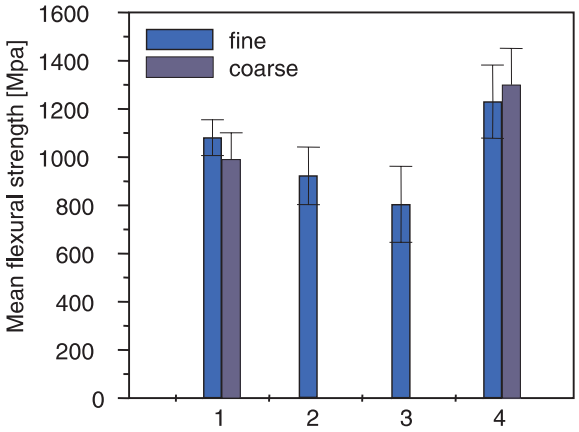

Figure 3: Mean biaxial flexural strength values for as-sintered and surface treated Y-TZP ceramics. 1 – As sintered, 2 – Dry ground (50 µm diamond burr), 3 – Dry ground (150 µm diamond burr), 4 – Sandblasted. Error bars represent one SD from the mean.

Slika 3: Povprečna dvoosna upogibna trdnost sintrane in površinsko obdelave keramike Y-TZP. 1 – sintrano, 2 – suho brušeno (diamantni brus 50 µm), 3 – suho brušeno (diamantni brus 150 µm), 4 – peskano. Območje raztrosa prikazuje eno SD od povprečja.

determined by the critical defect size to initiate failure, which can be estimated using the Griffith strength relation [14]

$$\delta_f = \frac{1}{\varphi} \cdot \frac{K_{IC}}{\sqrt{c_{cr}}} \quad (1)$$

where δ_f is the fracture stress, φ is a geometric constant (= $2/\pi^{1/2}$ for surface line cracks), K_{IC} is the fracture toughness and c_{cr} is the critical defect size to initiate failure. Calculated c_{cr} values for sintered coarse-grained specimens before and after dry grinding using 150 μm and 50 μm grit burr were 17.3, 31.0 μm and 24.1 μm, respectively. Since Eq. (1) does not take into account any of the residual surface stresses that may exist in the material, the calculated c_{cr} values should be regarded as the effective length of strength-controlling defects, which would result in an equivalent strength of the material without any residual surface stresses. Surface grinding increases the effective critical defect size, presumably by generating radial surface cracks. A fractographic examination of the ground specimens indeed revealed that failure originated from radial cracks extending several tens of μm (up to 50 μm) from the grinding grooves into the bulk of the material (**Figure 4**). However, no evidence of grinding-induced surface cracking could be obtained by SEM examination of a polished interface perpendicular to the ground surface (**Figure 5**). This observation is in agreement with recently published results by Xu et al [15], who reported on a noticeable grit size dependence of strength degradation upon machining of Y-TZP, but they could not find any evidence of grinding-induced surface cracking. Since radial cracks, which are readily seen in fracture surfaces, were not formed during grinding, they must have been initiated and extended from a grinding groove during loading until they reached the critical length for failure initiation.

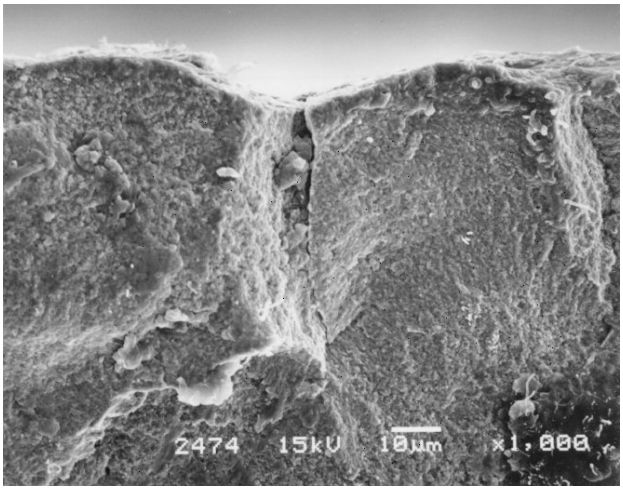

Figure 4: SEM micrograph of the fracture surface of fine grained dry ground Y-TZP
Slika 4: SEM-posnetek prelomne površine fino suho brušene Y-TZP

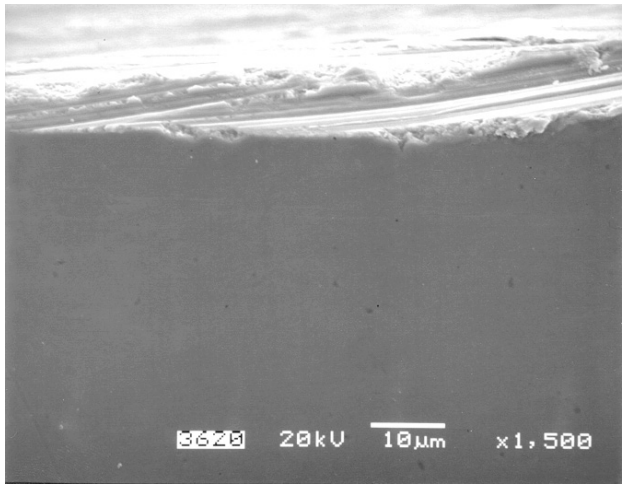

Figure 5: SEM micrograph of a polished interphase perpendicular to the ground (150 μm grit) of a fine grained Y-TZP
Slika 5: SEM-posnetek polirane površine, pravokotne na brušeno (zrno 150 μm) fino zrnato Y-TZP

Subcritical crack growth from a grinding groove during cyclic loading resulted in the lowest survival rate during fatigue experiments, whereas the strength of "survived" specimens was nearly the same as that of the material which was not subjected to cyclic loading.

In contrast to grinding, sandblasting is capable of transforming a larger amount of zirconia in the surface of Y-TZP ceramics indicating lower temperatures during this operation. Surface flaws, which are introduced by sandblasting, do not seem to be strength determining, otherwise the strength of the material would have been reduced instead of being increased. Since lateral crack chipping is the most prevalent mechanism involved in the erosive wear of ceramics, lateral cracks could be expected in these samples, which was later confirmed by

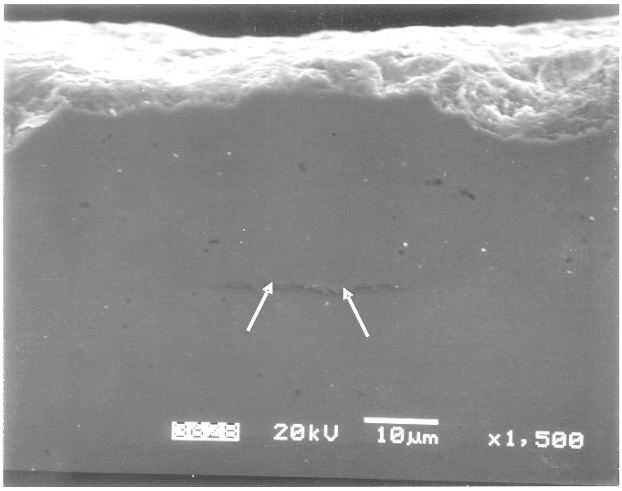

Figure 6: SEM micrograph of a polished interphase perpendicular to the sandblasted surface of a fine-grained Y-TZP, showing lateral crack chipping
Slika 6: SEM-posnetek polirane površine, pravokotne na peskano ploskev fino zrnate Y-TZP, ki prikazuje lateralno luščilno razpoko

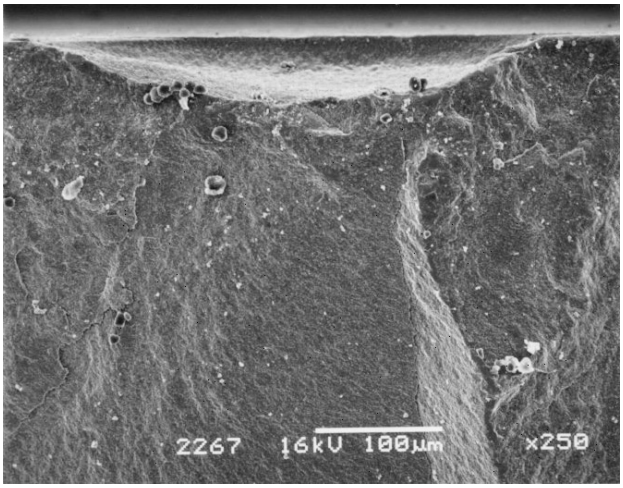

Figure 7: SEM micrograph of a fracture surface of fine-grained dry ground and sandblasted Y-TZP. Failure originated from a 50 µm deep surface pit

Slika 7: SEM-posnetek prelomne površine finozrnate suho brušene in peskane Y-TZP. Začetek preloma je v 50 µm globoki površinski zajedi.

microscopic examination using a bonded-interface technique (**Figure 6**). Fractographic examination of sandblasted samples confirmed that the failure of these samples was initiated from a lateral crack linked to subsurface cracks (**Figure 7**). It seems that sandblasting introduces surface flaws, which are not detrimental to the strength of Y-TZP ceramics statically loaded to fracture. However, under clinical conditions these impact flaws may grow to become stress intensifiers, causing accidental failure at lower levels of applied stress.

After autoclaving at 140 °C for 24 h, traces of the monoclinic zirconia were identified on the surface of sintered specimens, but the strength degradation has not yet occurred. The same observation was made with the ground and sandblasted specimens.

4 CONCLUSIONS

The surface grinding using a coarse-grit diamond burr at a high rotation speed lowers the mean strength of tetragonal zirconia Y-TZP ceramics, whereas sandblasting provides a powerful method for surface strengthening. The counteracting effect of dental grinding and sandblasting was explained in terms of two competing factors influencing the strength of surface treated 3Y-TZP ceramics: residual surface compressive stresses, which contribute to strengthening, and mechanically induced surface flaws, which cause strength degradation.

5 REFERENCES

[1] E. C. Subbarao: Adv. Ceram., 3 (**1981**), 1–24
[2] O. Keith, R. P. Kusy, J. Q. Whitley: Am. J. Orthod. Dentofacial. Orthop., 106 (**1994**), 605–614
[3] K. H. Meyenberg, H. Lüthy, P. Schärer: J. Esthet. Dent. 7 (**1995**), 73–80
[4] A. Wohlwend, S. Studer, P. Schärer: Quintessence. Dent. Technol., 1 (**1997**), 63–74
[5] R. Luthardt, V. Herold, O. Sandkuhl, B. Reitz, J. P. Knaak, E. Lenz: Dtsch. Zahnarztl. Z., 53 (**1998**), 280–285
[6] T. Sato., M. Shimada: J. Am. Ceram. Soc. 68 (**1985**) 68, 356–359
[7] D. J. Kim: J. Euro. Ceram. Soc., 17 (**1997**) 17, 897–903
[8] T. Kosmač, Č. Oblak, P. Jevnikar, N. Funduk, L. Marion: Dent. Mater. 15 (**1999**), 426–433
[9] T. Kosmač, Č. Oblak, P. Jevnikar, N. Funduk, L. Marion: J. Biomed. Materi. Res., 53 (**2000**), 304–313
[10] R. C. Garvie, P. S. Nicholson: J. Am. Ceram. Soc., 55 (**1972**), 303–305
[11] T. Kosmač, R. Wagner, N. Claussen: J. Am. Ceram. Soc., 64 (**1981**), C72–C73
[12] J. B. Wachtman, W. Capps, J. Mandel: J. Mater. Sci., 7 (**1972**), 188–194
[13] F. Guiberteau, N. P. Padture, B. R. Lawn: J. Am. Ceram. Soc., 77 (**1994**), 1825–1831
[14] B. R. Lawn: Fracture of brittle solids, 2nd ed. Cambridge, Cambridge University Press, UK, 1993
[15] H. K. K. Xu, S. Jahanmir, L. K. Ives: Mach. Sci. Tech., 1 (**1997**), 49–66

UDK 669.35:620.179.1
Original scientific article/Izvirni znanstveni članek

ISSN 1580-2949
MTAEC9, 41(5)243(2007)

POVRŠINA ZLITINE Cu-Sn-Zn-Pb PO OBSEVANJU Z ULTRAVIJOLIČNIM DUŠIKOVIM LASERJEM

SURFACE OF Cu-Sn-Zn-Pb ALLOY IRRADIATED WITH ULTRAVIOLET NITROGEN LASER

Franc Zupanič[1], Tonica Bončina[1], Davor Pipić[2], Višnja Henč - Bartolić[2]

[1] Univerza v Mariboru, Fakulteta za strojništvo, Smetanova 17, SI-2000 Maribor, Slovenija
[2] Sveučilište u Zagrebu, Fakultet elektrotehnike i računarstva, Zavod za primijenjenu fiziku, Unska 3, 10 000 Zagreb, Hrvaška
franc.zupanic@uni-mb.si

Prejem rokopisa – received: 2007-05-07; sprejem za objavo – accepted for publication: 2007-07-09

Površino zlitine Cu-Sn-Zn-Pb smo obsevali z laserskimi impulzi dušikovega laserja (valovna dolžina 337 nm). Pri tem sta se spremenila tako topografija površine kot tudi mikrostruktura pod njo. Ker je s klasičnimi metalografskimi metodami zelo težko primerno pripraviti obsevano površino za mikroskopsko opazovanje, smo kot temeljno orodje za metalografsko preiskavo uporabili fokusirani ionski curek (FIB), kajti FIB lahko odstranjuje material na specifičnih mestih v mikro- in nanoobmočju in odkrije mikrostrukturo brez prejšnje metalografske priprave. To nam je omogočilo, da smo raziskali vpliv obsevanja z laserjem na spremembo oblike površine, ugotovili profil kraterjev ter mikrostrukturne spremembe v območju toplotnega vpliva.

Ključne besede: laserska ablacija, bakrova zlitina, fokusirani ionski curek (FIB), mikrostruktura, topografija površine

Surface of a Cu-Sn-Zn-Pb alloy was irradiated by ultraviolet nitrogen laser pulses (wavelength 337 nm). As a result both surface topography and microstructure beneath the surface changed. Since it is very difficult to adequately prepare the damaged regions for microscopical observations using classical metallographic methods, we used a focussed ion beam (FIB) as the main tool for microstructural characterisation. Namely, FIB can remove material at specific sites in micro- and nanoregions and reveal microstructure without any previous metallographic preparation. This allowed us to investigate the influence of laser pulses on change of surface topography and subsurface microstructure.

Key words: laser ablation, copper alloy, focussed ion beam, microstructure, surface topography

1 UVOD

Obdelava površin kovinskih gradiv z laserjem se hitro razvija. Laserski žarki krajevno segrejejo površino materiala na zelo visoko temperaturo in učinkujejo do globine 10–100 μm. V odvisnosti od energije laserski žarki segrevajo, talijo ali uparjajo snov oziroma ustvarjajo plazmo. Trajanje energijskega impulza je lahko 1 ns ali manj. Kasnejše ohlajanje lahko vodi do ponovnega strjevanja z drobnozrnato mikrostrukturo, v jeklih se lahko pojavi tudi premena avstenit/martenzit. Pri nekaterih zlitinah je lahko ohlajanje dovolj hitro, da se tvori steklasta faza.[1]

Pri laserski ablaciji uparjamo snov s površine materiala. Postopek med drugim uporabljamo za kemijsko analizo [2] ter za nanašanje tankih prevlek [3]. (V Slovarju slovenskega knjižnega jezika [4] pojem laserska ablacija ni opredeljen, najbolj soroden pomen besede "ablacija" je definiran v geologiji: odnašanje sipkega zemeljskega materiala z dežjem, odplakovanjem.)

Fokusirani ionski curek (FIB), ki navadno uporablja galijeve ione, ima premer od 5 nm do nekaj mikrometrov. Ko deluje kot mikroskop, je njegova ločljivost nekoliko manjša, kot je ločljivost vrstičnega elektronskega mikroskopa, vendar ima bistveno boljši orientacijski kontrast. Z njim lahko odvzemamo ali nanašamo material na izbranih mestih z natančnostjo vsaj 100 nm. Ta značilnost omogoča, da se uporablja v najrazličnejše namene, od popravila elektronskih vezij, preko 3D-mikroskopije, do izdelave najrazličnejših 3D-objektov v nano- in mikrometrskem območju. Kombinacija fokusiranega ionskega curka in vrstičnega elektronskega mikroskopa bistveno izboljša zmogljivosti obeh. [5,6]

Glavni cilj tega dela je prikazati uporabnost fokusiranega ionskega curka pri opredelitvi vpliva obsevanja z laserskimi žarki na spremembo topografije površine in mikrostrukture pod površino.

2 INTERAKCIJA LASERJA S POVRŠINAMI KOVIN

Pri laserski ablaciji s pulzirajočo ultravijolično svetlobo potekajo številni kompleksni procesi [7]. Kadar kratek laserski pulz osvetli površino kovine, lasersko energijo takoj absorbirajo prosti elektroni, pri procesu, ki je nasproten zavornemu sevanju. Absorbirana energija se takoj spremeni v gibanje mreže v obliki elektronskih in fononskih nihanj v obdobju nekaj pikosekund, kar povzroči segrevanje površine. Porazdelitev temperature v materialu po laserskem impulzu lahko izračunamo z enačbo za prenos toplote. Ko obsevalna doza preseže ablacijski prag, se snov na osvetljeni površini najprej stali, nato pa začne izparevati. S tem začne površina oddajati delce – poteka ablacija kovinske tarče. Blizu ablacijskega praga je para tako razredčena, da lahko

zanemarimo njeno interakcijo z lasersko svetlobo. Pri večjih dozah je prehod snovi iz pregrete površine zelo hiter (tudi z eksplozivnim izparevanjem), tako da nastane plinski oblak z veliko gostoto, v katerem je del delcev tudi ioniziran. Pojavi se tudi interakcija med oblakom in laserskimi žarki, v kateri se porabi večina intenzitete laserskega žarka. Tako se delež energije, ki doseže kovinsko površino, močno zmanjša. Po drugi strani absorbirana energija segreva plinski oblak in inducira nastanek plazme. Plazma močno absorbira laserske žarke z inverznim zavornim sevanjem in loči laserski impulz od površine; plazma dejansko ščiti površino, tako da le malo laserskega žarka doseže površino kovine. Poleg tega plazma loči zrak od ablacijske površine in omeji površinsko reakcijo, čeprav je temperatura površine dovolj visoka. Tako ima povečanje doze majhen vpliv na kemijsko sestavo v kraterju zaradi zaščitnega učinka plazme (senčenja).

Pri dušikovem laserju je navadno gostota energije v goriščni točki neenakomerna, kar povzroči na ožarčeni površini velike temperaturne gradiente [8]. V središču laserske točke se material upari in tudi ionizira ter ima veliko težnjo, da se širi v vzdolžni in prečni smeri. Sosednja območja, ki so se samo stalila, so zato izpostavljena velikemu tlaku v prečni smeri, ki ga povzroča plinski oblak med širjenjem. Rezultat je poškodba površine; nastane krater z dvignjenim robom, na sosednjo površino pa lahko izvrže kapljice tekoče snovi. Pri pulzirajočem delovanju laserja se obsevano območje izmenično segreva in ohlaja, kar vodi do spremembe površine kot tudi mikrostrukture pod njo.

3 EKSPERIMENTALNO DELO

Za preiskavo smo uporabili vzorec rdeče litine (Cu-Sn-Zn-Pb), ki je imel naslednjo kemijsko sestavo: 6,12 % Sn, 5,75 % Zn, 3,06 % Pb, 0,52 % Ni, 0,31 % Fe, drugo Cu.

Površino vzorca smo obsevali s kratkimi impulzi (trajanje 6 ns, frekvenca 1 Hz) ultravijolične svetlobe dušikovega laserja, ki je imela valovno dolžino 337,1 nm. Povprečna energija laserskega impulza je bila 3×10^{-3} J, obsevano območje na vzorcu pa je bilo veliko 0,75 mm^2. Obsevali smo tri območja, in to z desetimi, dvajsetimi in stotimi impulzi. Energijska gostota ni bila enaka po celotni obsevani površini, kar je značilno za to vrsto laserja [8]. S spektroskopskimi meritvami (monokromator SPEX) smo ugotovili, da je bila elektronska temperatura plazme neposredno nad kraterjem ≈ 14 000 K.

Površino obsevanega območja smo opazovali z vrstičnima elektronskima mikroskopoma Quanta 200 3D in Sirion 400 NC (oba Fei Company). Za mikrokemično analizo EDS smo uporabili sistem INCA 350 (Oxford Analytical). Glavno delo je potekalo s fokusiranim ionskim curkom (FIB), ki je sestavni del mikroskopa Quanta 200 3D. Z elektronsko mikroskopijo smo najprej poiskali območja, ki so bila obsevana z lasersko svetlobo. Nato smo vzorec nagnili za 52°, tako da je ionski curek padal na površino pod kotom 90°. Za ionsko mikroskopijo smo uporabili majhne toke ionov (navadno 10 pA), medtem ko smo za grobo odvzemanje materiala uporabili tokove 3–20 nA, za srednje grobo odvzemanje tokove 0,5–1 nA in za glajenje prerezanih površin 0,1–0,5 nA.

4 REZULTATI IN DISKUSIJA

Mikrostrukturo zlitine Cu-Sn-Zn-Pb sestavljata trdna raztopina na osnovi bakra (α_{Cu}) in evtektični otočki ($\alpha_{Cu} + \beta_{Pb}$). Svinec je namreč malo topen v bakru in se razmeša že v tekočem stanju [9], medtem ko sta Sn in Zn precej bolj topna [10,11] in se substitucijsko vgradita v trdno raztopino α_{Cu}. Površina zlitine je bila pred obdelavo z laserjem stružena, sledovi so delno opazni na desni strani **slike 1**. Zato je bila plast pod površino močno deformirana, le na površini je bila tanka plast po vsej verjetnosti dinamično rekristaliziranih enakoosnih kristalnih zrn. **Slika 1** prikazuje površino, kjer je bila vroča točka laserske svetlobe. Pri obsevanju se je talina segrela nad vrelišče, zato je na tistem mestu nastal krater (K). Njegov rob (R) je dvignjen nad površino, vidni so učinki hitrega segrevanja in ohlajanja. Z večanjem števila impulzov so postajali kraterji večji in globlji. Po desetih impulzih je bila velikost kraterja 40 μm × 20 μm, globina 15 μm; po dvajsetih impulzih: 42 μm × 20 μm, globina 15 μm ter po stotih impulzih: 50 μm × 40 μm, globina 30 μm.

V okolici kraterja so na nekaterih mestih vidne kapljice (D), ki jih je razširjajoč plinski oblak v vroči točki razpršil naokoli. V drugih območjih se je površina segrela le nad temperaturo likvidus, nastala je kapilarna valovitost (KV), katere valovna dolžina je okoli 5 μm.

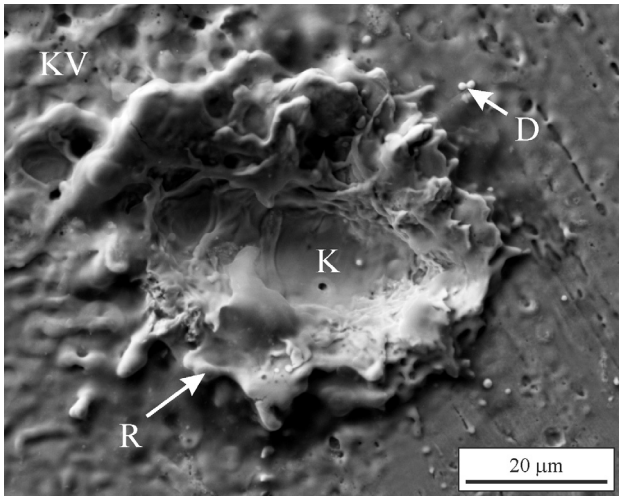

K – krater (crater), R – rob kraterja (crater edge), KV – kapilarna valovitost (capilary vawes), D – kapljica (droplet)

Slika 1: Krater po dvajsetih laserskih impulzih (SEM, sekundarni elektroni)

Figure 1: Crater after twenty laser pulses (SEM, secondary electrons)

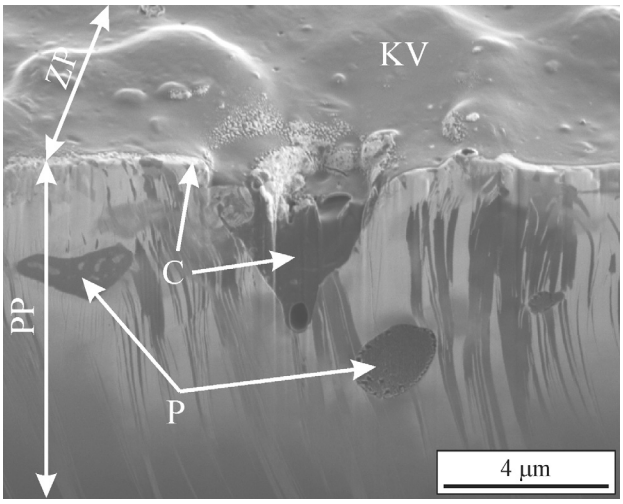

P – evtektik $\alpha_{Cu} + \beta_{Pb}$ (eutectic $\alpha_{Cu} + \beta_{Pb}$), C – snov, bogata z ogljikom (carbon-rich substance), KV – kapilarna valovitost (capilary vawes), ZP – zgornja površina (upper surface), PP – prečni prerez FIB (FIB cross-section)

Slika 2: Mikrostruktura na mestu, obsevanem z manjšo energijsko gostoto (slika s sekundarnimi elektroni, ki so jih inducirali ioni, število laserskim impulzov: 20)

Figure 2: Microstructure of the alloy at a site irradiated with lower energy density (secondary electrons induced by ion beam, number of pulses 20)

Dodatne informacije na tem mestu smo dobili, ko smo s FIB naredili prečni rez. Mikroposnetek (**slika 2**) razkriva reliefnost površine; relativna višinska razlika med vrhovi in dolinami je nekaj mikrometrov. Na njih so še manjše izbokline, ki merijo v višino nekaj desetink mikrometra, med njimi pa je površina gladka. Mikroposnetek tudi razkriva, da je površina prekrita s približno 100 nm debelo sivo plastjo (C), z njo pa so napolnjene tudi površinske vdolbine. Analiza EDS je pokazala, da je v glavnem iz ogljika. Njeno navzočnosti si lahko pojasnimo le s tem, da je bila površina pred obdelavo kontaminirana s snovjo, ki vsebuje ogljik. Pod površino je okoli 8 μm debela plast usmerjenih kristalnih zrn α_{Cu}, ki v prečni smeri merijo od nekaj desetink mikrometra do enega mikrometra. (Razdalje v vodoravni smeri lahko dobimo neposredno z merjenjem na osnovi črtice, medtem ko moramo v navpični smeri vsako razdaljo deliti s cos 52°, kajti ionski curek je bil nagnjen za 52° proti površini prečnega prereza.) Najverjetnejša razlaga za njihovo navzočnost je, da se je ≈ 8 μm debela zunanja plast zlitine stalila, pri strjevanju pa so kristalna zrna rasla v smeri pravokotno na površino zaradi hitrega odvoda toplote v nasprotni smeri. V tej plasti sta opazna tudi dva otočka evtektika ($\alpha_{Cu} + \beta_{Pb}$), ki sta označena s P. Poudariti moramo, da kontrast med kristalnimi zrni α_{Cu} izvira iz različne kristalografske orientacije kristalnih zrn glede na smer ionskega curka. Velja namreč, da so kristalna zrna, ki imajo smeri z majhnimi vrednostmi Millerjevih indeksov vzporedne z ionskim curkom, temna, druga pa so svetlejša. Razlog za to je, da ioni v smereh z majhnimi Millerjevimi indeksi zaradi kanalskega pojava prodrejo globoko v material, pri tem pa na površini inducirajo le malo sekundarnih elektronov [6]. Pod to plastjo je območje, ki ima enakomeren meglen videz; to je gotovo začetna hladno deformirana mikrostruktura, ki se pri obsevanju ni spremenila.

Slika 3 prikazuje prečni prerez kraterja, ki je nastal po obsevanju z desetimi laserskimi impulzi. Prečni prerez poteka skozi ravnino, v kateri je krater najdaljši in najgloblji. Dobro je viden zelo razgiban relief površine v okolici kraterja. Sam krater meri v dolžino približno 40 μm in sega okoli 15 μm pod začetno površino. Na robu kraterja je del materiala izvržen nad začetno površino – to je bil material, ki je bil staljen in hitro ohlajen. **Slika 3a** je posnetek z odbitimi elektroni, ki dajejo *Z*-kontrast; območja z večjim vrstnim številom Z so svetlejša. Na

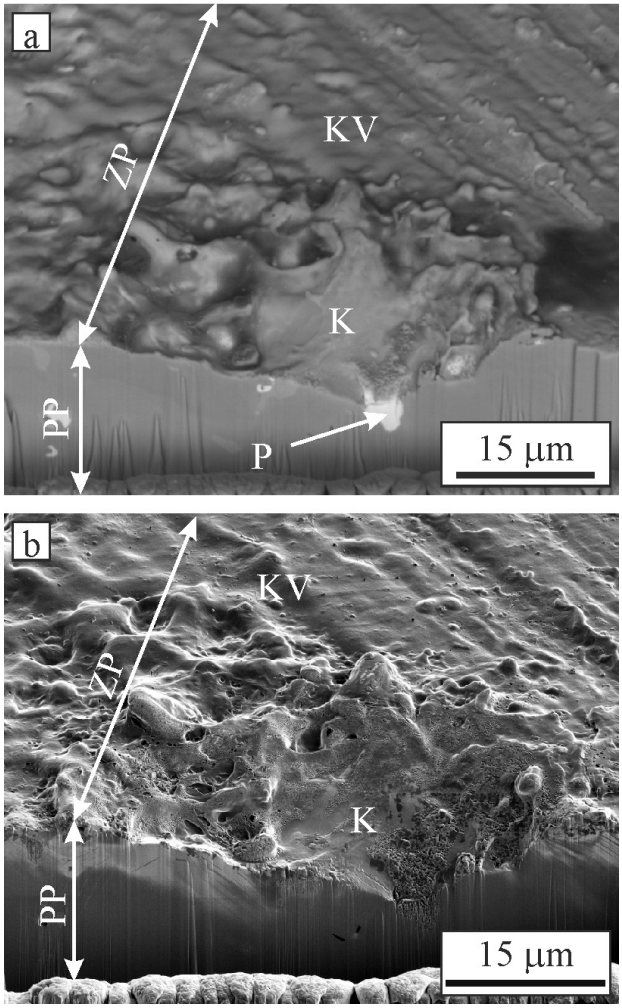

K – krater (crater), KV – kapilarna valovitost (capilary vawes), ZP – zgornja površina (upper surface), PP – prečni prerez FIB (FIB cross-section), P – evtektik $\alpha_{Cu} + \beta_{Pb}$ (eutectic $\alpha_{Cu} + \beta_{Pb}$)

Slika 3: Mikroposnetka območja na mestu z največjo energijsko gostoto pri številu laserskih impulzov N = 10 po rezanju s FIB: a) slika z odbitimi elektroni, b) slika s sekundarnimi elektroni, ki so jih inducirali ioni.

Figure 3: Micrographs of the site irradiated with the high-energy density after 10 laser pulses. a) secondary electron image, b) FIB-induced secondary electron image.

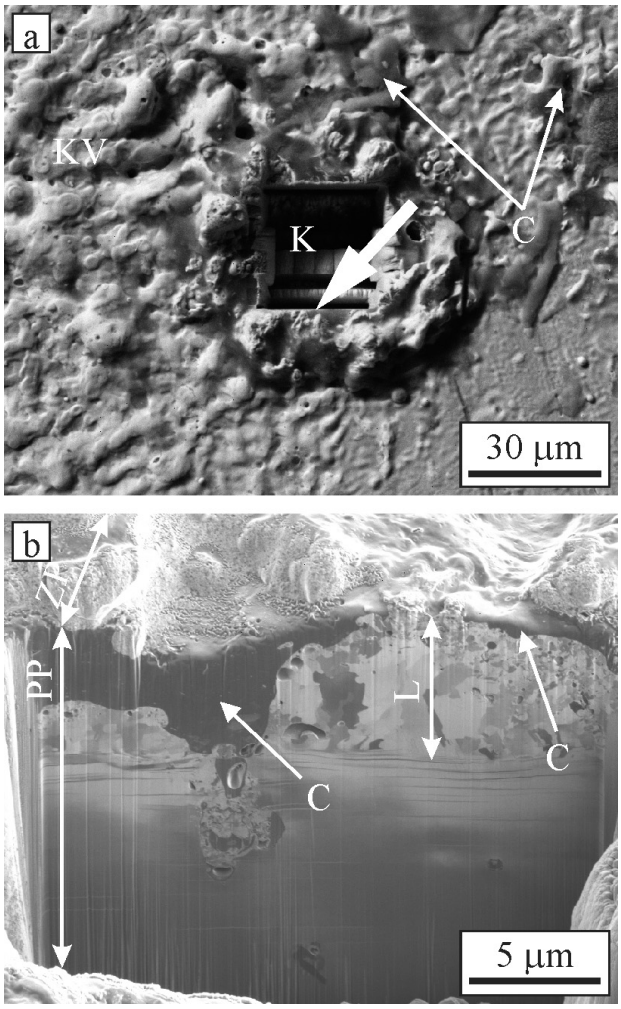

K – krater (crater), KV – kapilarna valovitost (capilary vawes), ZP – zgornja površina (upper surface), PP – prečni prerez FIB (FIB cross-section), L – pretaljena plast (melted and resolidified layer), C – snov bogata z ogljikom (carbon-rich substance)

Slika 4: Mikroposnetka območja na mestu z največjo energijsko gostoto pri številu laserskih impulzov $N = 100$: a) slika s sekundarnimi elektroni (pogled od zgoraj), b) prečni prerez (sekundarni elektroni, ki so jih inducirali ioni).

Figure 4: Micrographs of a site irradiated with the highest energy density after 100 laser pulses. a) secondary electron image (top view), b) FIB-induced secondary electron image (FIB cross-section).

sliki lahko opazimo območja s tremi različnimi odtenki. Zelo svetla območja so bogata s svincem (P), na temnih mestih zunaj kraterja ter tudi na površini kraterja je snov bogata z ogljikom ter sivkasta območja zlitinske osnove. Slika s sekundarnimi elektroni, ki so jih inducirali ioni (**slika 3b**), nima tako dobrega faznega kontrasta, so pa zelo poudarjene topološke značilnosti, delno pa se že razkrije mikrostruktura v prečnem prerezu. Mikrostruktura je spremenjena približno do 5 mikrometrov pod dnom kraterja, kjer so opazni trakovi kristalnih zrn, pod tem območjem pa v mikrostrukturi ne opazimo posebnih značilnosti, razen por, ki so večinoma v stiku z območji, ki so bogata s svincem.

Krater in njegova okolica sta bila po stotih impulzih že v večjem obsegu prekrita s snovjo, bogato z ogljikom (oznaka C, **slika 4a**). **Slika 4b** prikazuje dno kraterja. Vidno je, da staljena plast ni bistveno debelejša kot na drugih mestih (8-10 μm). Novonastala kristalna zrna so različnih velikosti; nekatera merijo le nekaj desetink mikrometra, druga pa tudi do 2 μm. Kristalna zrna so večinoma enakoosna, kar verjetno pomeni, da se je po večkratnem obsevanju segrela tudi podlaga, zato se odvod toplote v smeri pravokotno na površino zmanjša. Pod plastjo enakoosnih kristalnih zrn je prav tako enakomerno sivo, deformirano območje. Morda se je dodatno deformiralo tudi zaradi udarnega delovanja plinske faze, ki nastane pri obsevanju z laserjem. Da bi to dokazali, bi bilo treba spremeniti začetno stanje površine. Najbolj smiselno se zdi, da bi z žarjenjem dosegli povsod enako velika enakoosna kristalna zrna α_{Cu}, da bi lahko po obdelavi z laserjem laže ugotovili, kaj se je dogajalo med obsevanjem.

5 SKLEPI

Neenakomerna energijska gostota ultravijolične laserske svetlobe dušikovega laserja je povzročila spremembo površinske topografije in mikrostrukture pod površino. Zaradi površinske kontaminacije je bilo območje, obsevano z laserjem, prekrito s tanko plastjo snovi, bogate z ogljikom. Pod njo je okoli 5–10 μm debela staljena in hitro strjena plast, v njej pa so v odvisnosti od števila impulzov ter energijske gostote usmerjena in/ali enakoosna kristalna zrna. V vroči točki laserskega žarka je nastal krater, ki je v odvisnosti od števila impulzov segal v globino 10–20 μm; staljen in izvržen material pa je tvoril rob kraterja, ki se je dvigal nekaj mikrometrov nad začetno površino.

Fokusirani ionski curek se je pri raziskavi topografije površine in mikrostrukture zlitine Cu-Sn-Zn-Pb v območju, ki je bilo obsevano s kratkimi impulzi dušikovega laserja, pokazal kot zelo primerno orodje za odvzemanje materiala in metalografsko preiskavo. Poleg tega je mogoče na prečnih prerezih, izdelanih s FIB-om, izvesti tudi analizo EDS, s katero dobimo še dodatne informacije o kemijski sestavi pod prosto površino raziskanega materiala.

Zahvala

Avtorji se zahvaljujejo doc. dr. Lidiji Ćurković (Sveučilište u Zagrebu, Fakultet za strojarstvo i brodogradnju) za kemijsko analizo preiskovane zlitine.

6 LITERATURA

[1] R. E. Smallman: Modern physical metallurgy and materials engineering : science, process, applications, 6th ed., Oxford, Butterworth Heinemann, 1999

[2] O. V. Borisov, X. L. Mao, A. Fernandez, M. Caetano, R. E. Russo: Spectrochimica Acta Part B 54 (**1999**), 1351–1365

[3] N. Patel, G. Guella, A. Kale, A. Miotello, B. Patton, C. Zanchetta, L. Mirenghi, P. Rotolo: Applied Catalysis A: General 323 (**2007**) 18–24
[4] Slovar slovenskega knjižnega jezika, Ljubljana DZS, 1994, str. 2
[5] F. Zupanič: Vakuumist 26 (**2006**), 4–9
[6] J. Orloff, M. Utlant, L. Swanson: High Resolution Focused Ion Beams, FIB and Its Applications, Kluwer Academic/Plenum Publishers, New York, 2003
[7] D. W. Zeng, K. C. Yung, C. S. Xie: Applied Surface Science 217 (**2003**), 170–180
[8] Z. Andreić, V. Henč - Bartolić, D. Gracin, M. Stubičar: Applied Surface Science 136 (**1998**), 73–80
[9] D. J. Chakrabarti, D. E. Laughlin (Cu-Pb) in T. B. Massalski (Ed.), Binary Alloy Phase Diagrams, Second Edition, ASM International, 1990, 1452–1454
[10] N. Saunders, A. P. Miodownik (Cu-Sn) in T. B. Massalski (Ed.), Binary Alloy Phase Diagrams, Second Edition, ASM International, 1990, 1481–1483
[11] A. P. Miodownik (Cu-Zn), in: T. B. Massalski (Ed.), Binary Alloy Phase Diagrams, Second Edition, ASM International, 1990, 1508–1510

UDK 539.44
Original scientific article/Izvirni znanstveni članek

ISSN 1580-2949
MTAEC9, 41(5)249(2007)

A PRELIMINARY S-N CURVE FOR THE TYPICAL STIFFENED-PLATE PANELS OF SHIPBUILDING STRUCTURES

PRELIMINARNA KRIVULJA S-N ZA TOGE PLOŠČATE PANELE ZA LADJEDELNIŠKE STRUKTURE

Luljeta Gusha[1], Skender Lufi[2], Marenglen Gjonaj[2]

[1]Technological University "I. Q. Vlora", Marine Faculty, Naval Engineering Department, Lagja: Pavaresia, Rruga: Sadik Zataj, Vlora-Albania
[2]Politechnical University of Tirana, Mechanical Faculty, Mechanical Department, Sheshi: Nene Tereza, Tirana-Albania
gusha@aul.com.al

Prejem rokopisa – received: 2006-05-17; sprejem za objavo – accepted for publication: 2007-07-10

This paper presents the results of a preliminary study focused on the structural behavior of typical stiffened plate panels used for shipbuilding structures and their fatigue strength under a lateral load. The investigated panels are thin plates, welded with longitudinal bulb stiffeners through alternate welding seams. This makes the panel a composite structural element with a complex strength behavior. The aim of the research was to obtain data about the failure conditions of the panels. Testing covers the bending tests carried out on the real-size panels of shipbuilding structures. A reliable definition of a fatigue design curve was not possible due to the limited number of specimens, although a tentative S-N curve was drawn on the basis of the test data.

Key words: shipbuilding panels, fatigue, real-size testing, S-N data

Članek predstavlja rezultate preliminarne študije ciljane na strukturno vedenje tipičnih togih ladijskih panelov in utrujenostno trdnost pri bočni obremenitvi. Paneli so tanke plošče zvarjene z podolžnimi rebri za preprečenje izbočenja z alternativnimi spoji. Taki paneli so kompozitni strukturni elementi s kompleksnim trdnostnim vedenjem. Cilj raziskave je bil opredeliti podatke o pogojih za nastanek preloma panelov. Preizkusi so obsegali upogib panelov realne velikosti za ladijske strukture. Zanesljiva opredelitev krivulje S-N ni bila mogoča zaradi omejenega števila preizkusnih panelov. Zato je bila določena le poizkusna krivulja S-N na podlagi rezultatov preizkusov.

Ključne besede: ladjedelniški paneli, utrujenost, preizkušanje v realni velikosti, podatki S-N

1 INTRODUCTION

Stiffened plate panels are the basic structural components of a ship's structure. Fatigue constitutes a major source of local damage in ships and other marine structures, since the most important loading on the structure, the wave-inducted loading, consists of large numbers of load cycles of alternating sign. The prevention of fatigue failure in ship structures is strongly dependent on proper attention to the design and fabrication of structural details. Much of the quantitative information on fatigue obtained by experiments and S-N fatigue design curves is drawn on the basis of test data.

With the test results, and based on Wöhler's diagram, a tentative attempt is made to construct an S-N curve for the stiffened panels, where the thin plates are welded with longitudinal bulb stiffeners through alternate welding seams.

According to IIW documents, more than 15 specimens are in general necessary to establish the fatigue limit and more than 25 for the S-N curve, using static analysis methods (e.g., the staircase method) [8].

2 EXPERIMENTAL

The experimental measurements were made at the DINAV of the Naval Structural Laboratory of Università degli Studi di Genova.

2.1 Data on the panel and model description

As a model for the experimental test, a stiffened plate panel of real size, simply supported, was considered. The effects of stress and initial distortion were not considered.

Panel-type stiffeners were welded in the span between the transversal T-beams, using alternate welding seams with a length of 50 mm and a step of 200 mm. It is worth pointing out that at a 50-mm interval the stiffeners are welded to the plate, alternatively on one or the other. The panels were built according to standard fabrication practice using semi-automatic arc welding. The welding parameters are as follows:
Wire: FRO Fluxofil 19, d = 1 mm
Voltage: 23/24 V, Current: 140/150 A
Welding speed: 50 cm/min
Throat: 3.5 mm

Table 1: Geometrical characteristics of the panel
Tabela 1: Geometrijske značilnosti panelov

Plate dimensions	(1800 × 2600 × 5) mm
Stiffeners(HP80X6)	I_x = 39.0 cm^4 W_{min} = 8.15 cm^3
Effective plate width included (s = 500 mm)	I_x = 155 cm^4 W_{min} = 21 cm^3
Transversal beams	(180 × 90 × 5 × 8) mm (180 × 5; 90 × 8) mm

Reference standard: MM-042F-331
Welding on unpainted surfaces

Table 2: Characteristics of materials
Tabela 2: Lastnosti materiala

Yield stress	σ_y = 355 N/mm^2
Yield load (s = 500 mm)	P_y = 49.7 MPa
Young's modulus	$E_x = 2 \cdot 10^5$ MPa
Shear modulus	$G_{xy} = 0.793 \cdot 10^5$ MPa
Poisson's modulus	$\nu = 0.33$
Density of the material	$d = 7.9 \cdot 10^{-5}$ kg/mm^3

All the panels were manufactured from the same material. The panel is modeled as shown in **Figure 1**, and is considered to be supported on two T-beams along both its longest sides (2600 mm) and along two other free sides (**Figure 2**).

The assumed failure criteria are:

- A crack propagation over the section of the bulb,
- A number of cycles $N = 1.0 \times 10^6$

2.2 Procedure and experimental tests

The bending was achieved with a transversal beam along the whole panel width. The loading beam had an "I" section with two large flanks of size (1800 × 200) mm and a thickness of 20 mm [1,12]. Its inertia moment is large enough to ensure a constant distribution of the load along the beam. Between the flat and the panel surface, a thick rubber strip was interposed during the tests in order to prevent damage to the surface. The strip had a width of 200 mm and this should be regarded as the area of the 200 MPa load application. The load jack is hinged to a frame and acts vertically downward, as shown in **Figures 2 and 3**. It was selected on the basis of the predicted limit load of 10 t. A load cell was interposed between the jack and the loading beam [3,12]. Seven linear strain gauges for each panel and one load cell (200 MPa max. load), as in **Figure 3**, were applied for each test. Two rows of linear strain gauges were placed near the loading "*I*" beam (**Figure 3**). These strain gauges measure the strain in the longitudinal direction of the bulb after each loading sequence. The panels were tested in the range of about 0.7 yield stress with a sinusoidal pulsating load. The maximum stress during the fatigue test did not exceed the yield stress [7,8,9,10]. The load and strain were continuously monitored. The tests were monitored with strain-gauge measurements and visual inspections. The signals were stored in the data files in millivolts and converted into the real physical quantities by means of a calibration (**Figure 4**). The displacement transducers were placed in their position and then calibrated "in situ" with mechanical gauges.

The acquisition program was run for every test at a sampling rate of 1.4–1.5 Hz [1,8] for a predetermined period of time. For each acquisition the maximum, minimum, mean and range values were evaluated and subsequently converted into stress and the acting force.

The range versus cycles and the maximum range versus cycle plots are presented in **Figure 5 and 6**.

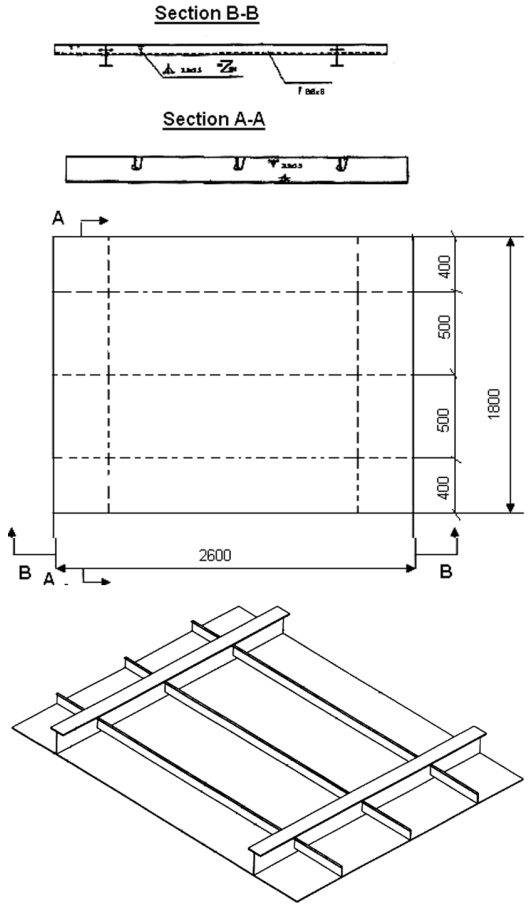

Figure 1: Sketch (a) and isometric (b) view of the tested panel
Slika 1: Skica (a) in izometričen (b) pogled preizkusnega panela

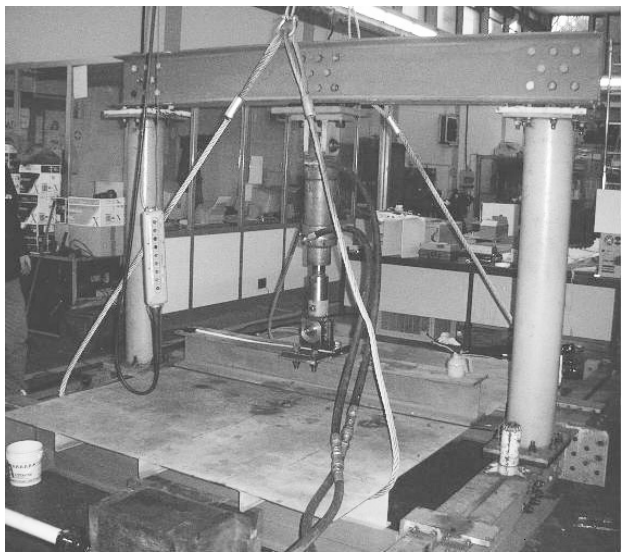

Figure 2: View of the testing device
Slika 2: Preizkusna naprava

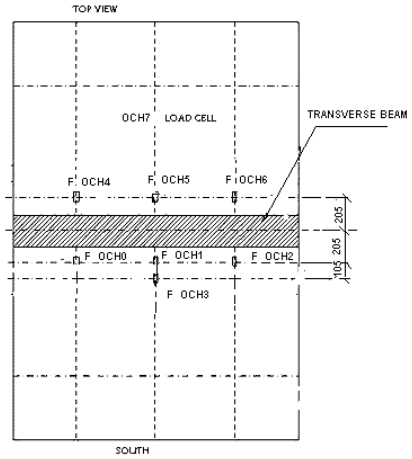

Figure 3: View of the position of the strain gauges
Slika 3: Položaji merilnih doz

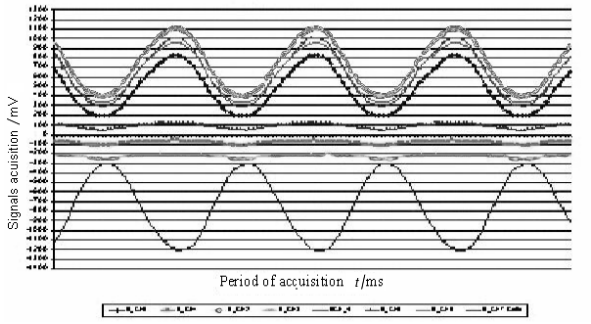

Figure 4: Gauges and load-cell measurements at the end of the test after about 1.45×10^6 cycles
Slika 4: Doze in meritve obremenitvenih celic pri koncu preizkusa pri $1{,}45 \cdot 10^6$ amplitudah

2.3 Results and discussion

The results are shown in graphical form in **Figures 5, 6 and 7**. The panel was loaded with a pulsating sinusoidal loading wave with a range of about 41 MPa, at a mean level of about 25 MPa for 10^6 cycles (stress ratio $R \approx 0.1$). No cracks were found.

The range load was then increased up to 52 MPa, at a mean level of 33 MPa (stress range $R \approx 0.1$) for 1.35×10^6 cycles. Then another 10^6 cycles were applied at 46.5 MPa, at the same mean level. No cracks were detected

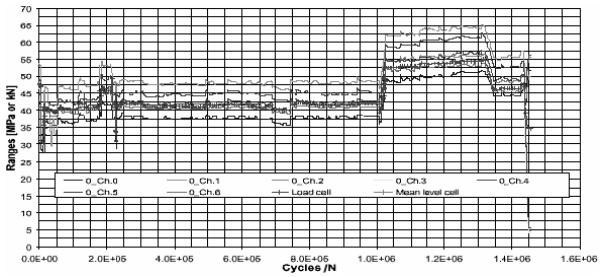

Figure 5:. Test measurements plot: range vs. cycles.
Slika 5: Rezultati meritev obremenitev v odvisnosti od števila amplitud

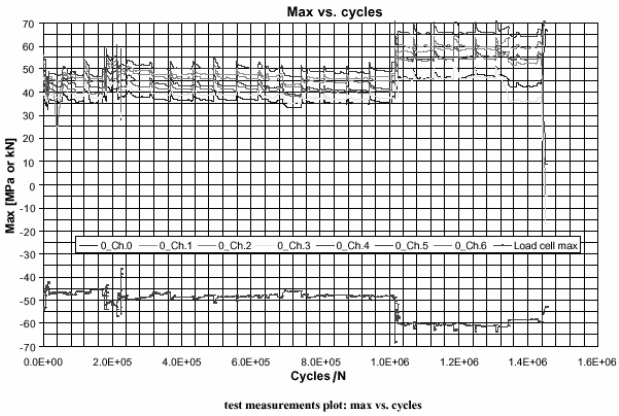

Figure 6: Test measurements plot: max vs. cycles
Slika 6: Rezultati meritev obremenitev v odvisnosti od števila amplitud

Figure 7: Cracks in the central stiffener, both sides and the lateral stiffener (after panel dismantling)
Slika 7: Razpok v centralnem rebru, obe strani in bočna utrditev (po demontaži panela)

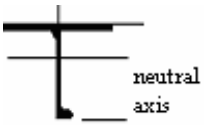

Figure 8: Composite cross-section of beam
Slika 8: Prečni prerez rebra

with a visual examination and strain-gauges signal analysis.

At about 1.45×10^6 cycles a crack started from the head of the central bulb stiffener about the span middle and propagated up to the plating, while a second crack started in the west side bulb stiffener in the same position and propagated up to the stiffener web. From the analysis of the gauge measurements, it is concluded that the crack propagated for about 10^4 cycles.

The boundary conditions of the panel are considered as simply supported, the load is applied in the center of the panel and the panel is in a positive bending moment condition with the maximum of the bending moment in the center of the panel.

According to the elastic beam theory, in this case, the neutral axis is near the plate, as in **Figure 8**, so the maximum stress is achieved at the head of the bulb.

In the preliminary assessment using the finite-element method, for these panels [11] and in static loading, three critical areas of the panels' collapse were identified:

a) The region including the plate area between the stiffeners (in compression);
b) The region including the plate area around the stiffeners (in compression);
c) The region including the head area of the stiffeners (in tension)

The specific stress-strain situation in each of these regions defines the type of collapse that can occur in them. The expected collapse in the region (a) is generally of a static nature, while in the regions (b) and (c) it is generally of a fatigue type. In this case, since the region (b) is in compression, the region (c) is expected to collapse in fatigue [2,4,10,11]. The finite-element analysis showed the region (c) as the hottest stress area between the (b) and (c) regions.

3 PRELIMINARY S-N CURVE

Due to the limited number of specimens it was not possible to obtain a curve. For this reason, a preliminary S-N curve was drawn on the basis of the test data. According to the IIW documents, more than 15 specimens are necessary to establish a reliable fatigue limit and more than 25 for the S-N curve, using static analysis methods (e.g., the staircase method) [8]. To construct the S-N curve, we relied on Wohler's curve. The shape of this curve is shown in **Figure 9** [1,2,3,4,5,6,10].

Where:

- S is the upper point, static resistance σ_r vs. 10^3 cycles.
- G is the point of the fatigue limit $\sigma_{a\infty}$ vs. 2×10^6 cycles (or an endurance limit).
- In the lg σ_a – lg N diagram the curve slope is a constant k.

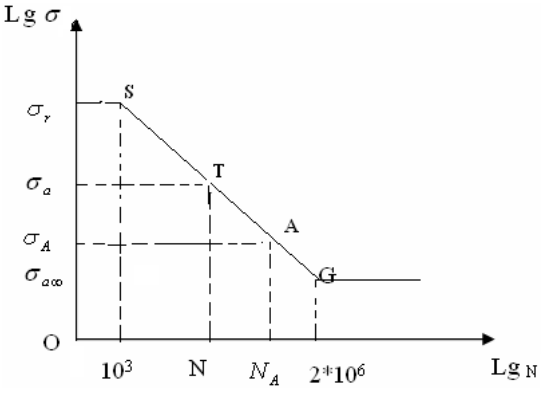

Figure 9: Typical S-N curve for a mild steel
Slika 9: Tipična krivulja S-N za konstrukcijsko jeklo

- The point A is the point of the conventional reference, N_A, σ_A

$$N\sigma_a^k = N_A \sigma_A^k \tag{1}$$

$$k = \frac{lg_{10} \frac{N_A}{N}}{lg_{10} \frac{\sigma_a}{\sigma_A}} \tag{2}$$

A typical value of $k = 3$ is given in several references [1,2,3,13].

In our case, since the load is a sinusoidal pulsing load: $r \approx 0.1$, $\Delta\sigma_E \cong \sigma_y = 355$ N/mm^2 (see HSS $\Delta\sigma_E$ = 330 –360 N/mm^2), where $\Delta\sigma_E = \sigma_{a\infty}$, and σ_y is the stress at the S point. The coordinates of the point G are $1.5 \cdot 10^5$ and 330, and the panel is loaded with 42 MPa at 10^6 cycles and with 52 MPa at $0.45 \cdot 10^6$ cycles.

From the De Saint Venant relation, $\sigma = \frac{M_b y}{I_{xx}}$, it is deducted:

At 10^6 cycles, $P = 42$ MPa, $\sigma_A = 278.8$ N/mm^2 and at $0.45 \cdot 10^6$ cycles, $P = 52$ MPa, $\sigma_T = 278.8$ N/mm^2.

The proof of the service fatigue strength on the basis of the damage is the accumulation rule according to Miner:

$$D = \sum_{j=1}^{n} \frac{N_j}{N_{fj}} \tag{3}$$

$$D \leq D_{per} \text{ where } D_{per} = 0.5 - 1.0 \tag{4}$$

where D is the total damage, D_{per} is the permissible total damage, ΔN_j is the number of cycles on level j, N_{fj} is the number of cycles of failure on the level j according to the allowed stress S–N curve, j is the number of the stress level and n is the total number of stress levels .

- Let us now deduce the value of k:

$$1 = \frac{N_1}{N_{f1}} + \frac{N_2}{N_{f2}} \tag{5}$$

$$N_{f1}\sigma_1^k = N_{f2}\sigma_2^k \tag{6}$$

Starting from the conventional point S(10^3, σ_y) with $\sigma_y = 355$ N/mm^2 it is possible to write:

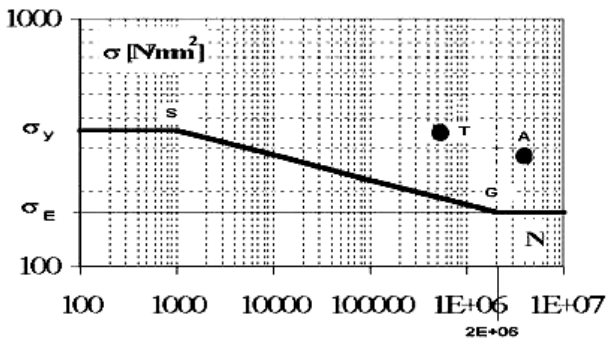

Figure 10: Wöhler curve for the panels
Slika 10: Wöhlerjeva krivulja za panele

$$10^3\left(\frac{\sigma_y}{\sigma_2}\right)^k = N_1\left(\frac{\sigma_1}{\sigma_2}\right)^k + N_2 \quad (7)$$

where, $\sigma_1 = \sigma_A = 278.8$ N/mm^2, $\sigma_2 = \sigma_T = 345.2$ N/mm^2

From the three mentioned equations a tentative value of $k = 10$ is deduced. This is in agreement with NAFEMS [3], because the crack propagated in the bulb head, without weld seams and the material behaves as if it is unwelded [2].

From equations 5,6 N_{f1}, N_{f2} we deduced:

$$\begin{cases} N_{f1} = 4810000 \\ N_{f2} = 568091 \end{cases}$$

In this step it is necessary to verify that $\sigma_{a\infty} = \sigma_E$, assuming a known number of cycles corresponding to the endurance limit $\sigma_{a\infty} = \sigma_E$ at $2 \cdot 10^6$.

From the relation $N\sigma_a^k = N\sigma_A^k$ we can write:

$N_{f1}\sigma_1^k = N_{fE}\sigma_E^k \Rightarrow \sigma_E = 166.006$ N/mm^2

Finally, it is possible to construct the preliminary S–N curve for the panel shown in **Figure 10**.

The S-N curve with these characteristic points, based on the damage-accumulation rule according to Miner and the curve of Wohler, has the following coordinates.

A(N_{f1}, σ_1) = A(4810000, 278.8)

T(N_{f2}, σ_2) = T(568091 ,345.2)

G(N_E, σ_E) = G($2 \cdot 10^6$, 166.006)

S(10^3, σ_Y) = S(10^3, 166.006)

4 CONCLUSIONS

From the experimental point of view, it is evident that the points A and T are situated in the safety zone. The value of the curve's slope is $k = 10$, and it can increased up to $k = 14$ (the results can be in a scatter band with the value of "k" from 10 up to 14).

Future results will permit a further revision and implementation with the aim to obtain good agreement between the Wöhler curve and the experimental data.

5 REFERENCES

[1] G. Sines, J. L. Waisman, Metal fatigue, London, (1959)

[2] S. J. Maddox, Fatigue strength of welded structure, England, 1991

[3] B. P. Atzori, Introduzione alla progettazione a fatica, *NNAMFES*, Italy, 2001

[4] O. Hughes, Ship structural design, Sydney, 1983

[5] O. Hughes, J. B. Caldwell, Marine structures selected topics, examples and problems, Sydney, 1991

[6] J. J. Jensen, Load and global response of ships, Denmark, 2000

[7] I. S. O. Standarted proposal. Fatigue testing of welded components, France, 1996

[8] H. P. Lieurade, I. Huther, IIW Fatigue Testing Standard and Effect of Quality and Weld Improvement Methods WRC Proceeding IIW, 1996

[9] International Institute of Welding, IIW Recomendation on large scale fatigue testing of welded components, Germany, 1999

[10] D. Radaj, C. M. Sonsino, Fatigue assessment of welded joints by local approaches, England, 1998

[11] L. Gusha, S. Lufi, Strain-stress analysis of stiffened plate panels of shipbuilding structures, ACTA Universitatis Pontica Euxinus, Rumania 5 (**2005**), 2

[12] L. Gusha, Typical stiffened plate panels in shipbuilding – ultimate and fatigue strength. Universita degli Studi di Genova DINAV, Genova (Internal Report 03CRI04), 2003

[13] M. Gjonaj, F. Pejani, Detale Makinash. Kritere Kryesore te Llogaritjes se Detaleve te Makinave, Tirana, Albania, 1987